Nitrogen cycling in the northern Benguela Upwelling System based on the $\delta^{15}N$ of chlorophyll pigment

Dissertation

Zur Erlangung des Doktorgrades der Naturwissenschaften im

Fachbereich Geowissenschaften der Universität Hamburg

vorgelegt von

Yu XIN

aus

(Shan Dong, P.R. China)

Hamburg

(2015)

Als Dissertation angenommen

vom Fachbereich Geowissenschaften der Universität Hamburg

Auf Grund der Gutachten von Prof. Dr. Kay-Christian Emeis

und Dr. Richard Seifert

Hamburg, den

Prof. Dr. C. Betzler

Leiter des Fachbetreichs Geowissenschaften

Summary

Coastal upwelling ecosystems account for only 7% of the Earth surface, but sustain 25 % of global biological productivity, and serve as the major regions for CO_2 exchange between atmosphere and ocean. The global climate warming has invoked significant pressure on the development of coastal upwelling systems since the mid-20th century. The climate-driven fluctuations in ocean circulation imprint the thermocline through wind stress and heat fluxes, and modify its depth and strength that both govern the communication between intermediate waters and upper layer waters at coastal margins. As a result, the nutrient and oxygen concentrations in the upwelled waters vary and together influence the cycling of nitrogen, one of the key elements to primary production in coastal upwelling systems.

The Benguela Upwelling System (BUS) belongs to the Eastern Boundary Upwelling Systems (EBUSs), and has the highest primary productivity while it suffers massive nitrogen loss in association with a severe Oxygen Minimum Zone (OMZ). The upwelled nitrate is one of the most important nutrient species to local primary production, and its inventory in shelf waters is governed prominently by the upwelling intensity as a major source, and the nitrogen loss (N-loss) in OMZs and plankton assimilation as major sinks. The isotopic signature of the nitrate pool is imprinted on planktonic biomass via nitrate assimilation, a process through which chlorophyll-a (Chl-a) is produced with the assimilated nitrate. The nitrogen atoms embedded in Chl-a molecular skeleton thus link the $\delta^{15}N$ of nitrate with the biological production by recording the isotopic fractionations that are associated with various nitrogen cycling (N-cycling) processes in shelf waters. The perennial low oxygen conditions in shelf waters of the BUS assist the preservation of Chl-a in the surface and core sediment, which makes the $\delta^{15}N$ of Chl-a a suitable isotope marker to track the N-source, utilization, and N-sink processes by recording the $\delta^{15}N$ signals of N-nutrients.

This thesis focuses on the spatial and temporal variations of N-cycling in association with upwelling intensity in the northern BUS. For this goal, I firstly develop the

HPLC method to acquire purified chlorophyll pigment and the analytical method to measure its $\delta^{15}N$. Then, I analyzed the $\delta^{15}N$ of chlorophyll pigment in the surficial sediment and in one dated sediment core of the northern BUS to investigate the spatial pattern of N-cycling and the past response of N-loss to upwelling variation in the northern BUS. The results are presented in three chapters.

In the first chapter, I find that the recrystallized $K_2S_2O_8$ that is used as oxidization reagent has a low N-content but a depleted ^{15}N background of -15‰. The ^{15}N background of $K_2S_2O_8$ would cause -1- -2‰ deviation on the $\delta^{15}N$ of sample that contains nanomolar level N. This finding requires examining the $\delta^{15}N$ of recrystallized $K_2S_2O_8$ when it is used to oxidize reductive N-samples. The method that is established in this work is reliable for $\delta^{15}N_{pigment}$ measurement and has an average analytical precision better than ±0.5‰ (1σ).

In the second chapter, I focus on the spatial pattern of nitrate sources and sinks in the coastal waters of the northern BUS. The spatial $\delta^{15}N_{Chl-a}$ distribution helps to demarcate the northern BUS into two sectors: in the northern sector, the nitrate of fresh South Atlantic Central Water (SACW) origin is removed mainly by plankton assimilation in coastal waters, while in the southern sector, the prominent OMZ invokes denitrification as the major nitrate sink. The upwelling dynamics over the shelf play a major role in governing the spatial pattern of nitrate supply, OMZ state and denitrification intensity, which are partially constrained by the local shelf topography.

The third chapter is aimed at investigating the past N-loss variation in response to the upwelling intensity in the northern BUS. The $\delta^{15}N_{Chl-a}$ record reveals that the N-loss intensity in the northern BUS varied considerably over the past two centuries, and inversely tracked the upwelling intensity as shown by a significant inverse correlation with a U_{37}^{K} -SST record (unsaturated alkenone ratio based surface seawater temperature). This result suggests that the $\delta^{15}N_{Chl-a}$ can be applied together with U_{37}^{K} -SST to link the variation of N-loss with upwelling intensity at other Eastern Boundary Upwelling Systems (EBUSs).

II

IV

1 Introduction

1.1 Benguela Upwelling System and its environmental settings

The Benguela Upwelling System (BUS, Fig. 1.1) belongs to the Eastern Boundary Upwelling Systems (EUBSs), and it extends from Angola (~15-17°S) along the west coast of Namibia to South Africa (~36 °S). Two boundaries, the northern boundary of the Angola-Benguela Frontal Zone (ABFZ) and the southern boundary to the Agulhas Current, surround the BUS with a steep shelf. In the middle part, a wide shallow shelf receives upwelled waters that are rich in nutrients and deficient in oxygen. While maintaining the highest productivity of all the EUBSs (Carr and Kearns 2003), the BUS is experiencing intensive N-loss associated with the existence of a perennial Oxygen Minimum Zone (OMZ) situated on the shelf (Brüchert et al., 2006, Brüchert et al., 2009, Nagel et al., 2013).
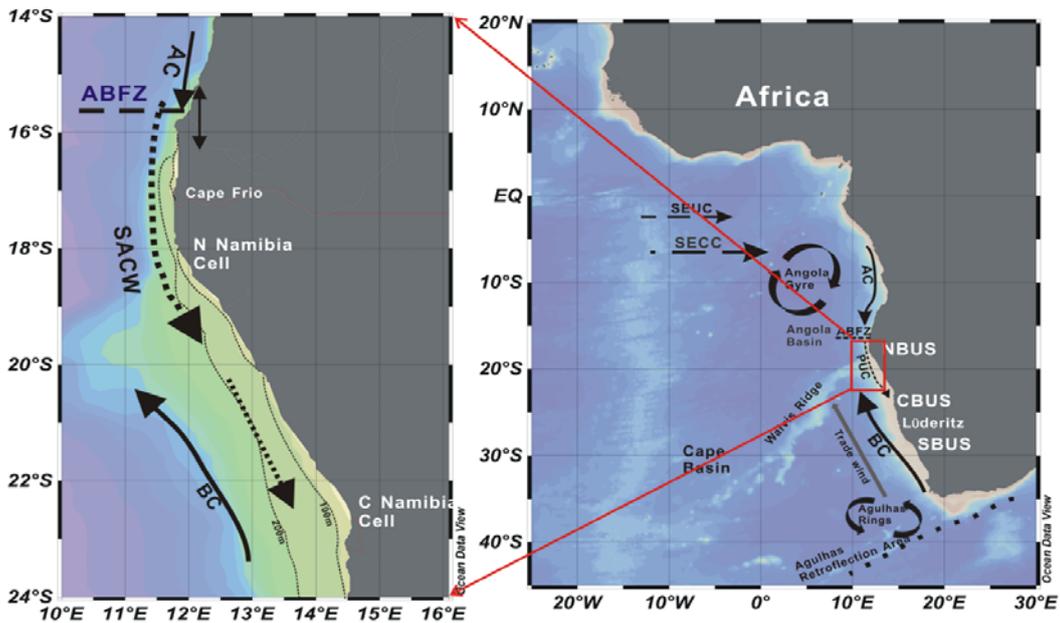
Fig. 1.1 Left panel is the studied area: the northern Benguela Upwelling System (BUS). Dashed line denotes depth contours. Right panel depicts the currents system surrounding BUS: arrows show surface (solid) and subsurface (dashed) hydrographic features: NBUS=northern BUS, BUS=central BUS, SBUS=southern BUS, ABF= Angola-Benguela Front, BC= Benguela Current, AC = Angola Current, PUC = Poleward Undercurrent, SEUC=South Equatorial Under Current, SECC=South Equatorial Counter Current (Arhan et al., 2003, Mercier et al., 2003).

1.1.1 Hydrological features

The South Atlantic central water (SACW) and the Eastern SACW (ESACW) are the two major intermediate water masses found over the shelves of BUS (Mohrholz et al., 2001, Shillington et al., 2006). The SACW is transported via the equatorial current system and the subtropical gyres into the Angola Basin. Continuous re-mineralization of organic matter along its pathway reduces the oxygen concentration (Table 1.1) while raising its nutrient content (Lass et al., 2000). The thermocline water from the Angola Gyre transports the modified SACW southwards via the Angola Current (AC) (Lass et al., 2000, Mohrholz et al., 2001), and eventually, it is advected across the ABFZ into the northern BUS. The ESACW is formed in the Cape Basin and comprises a mixture of SACW from the subtropical gyre and Indian central water (ICW). Typically oxygen-rich (~300 $\mu mol \cdot l^{-1}$) and nutrient-depleted (Mohrholz et al., 2001), the ESACW is injected into the South Atlantic through the Agulhas Current and transported northward via Benguela Current (BC) parallel to the coast of the BUS.

Table1.1 Characteristics of water masses at BUS

Parameter	SACW (Angola Gyre type, northern BUS type) (Mohrholz et al., 2008)		SACW (Hagen and Schemainda 1987)	ESACW (Poole and Tomczak 1999) (Mohrholz et al., 2008)	
Temperature (℃)	8	16	8	5.9559	14.4067
Salinity	34.7201	35.6366	34.7	34.4069	35.3016
Oxygen ($\mu molL^{-1}$)	22.4342	68.4832	–	300.0553	249.3363
Nitrate ($\mu molL^{-1}$)	37.8611	21.9115	–	11.7672	0
Phosphate ($\mu molL^{-1}$)	2.7056	1.5029	–	1.3083	0.236
Silicate ($\mu molL^{-1}$)	19.5903	6.5066	–	7.0952	3.6276

Upwelling activity in the BUS shows a clear seasonal cycle with a maximum in the northern BUS that occurs during late austral winter to spring (Chapman and Shannon

1987, Mohrholz et al., 2008). The variation of upwelling intensity in the BUS is controlled remotely by tropical Atlantic climate variability (Lübbecke et al., 2010) and locally by south easterly trade wind stress (Richter et al., 2010, Fennel et al., 2012), together determining the spatial variation of upwelling intensity at annual and multi-decadal scales.

1.1.2 Shelf Topography

The coastal margin of BUS is characterized by a narrow and steep shelf at the northern Kunene (~17°S) and southern Baker Bay (~28°S), and a wide shelf with low-angle slope extending from Cape Frio to Lüderitz (~18.5-28°S) (Rogers and Bremner 1991). In the northern BUS, the shelf break is in the vicinity of 200 m from Kunene (~17°S) to Sand Table Hill (~20°S) (Table 1.2). From Sand Table Hill to Sylvia Hill (~25°S), there is an inner shelf break at ~200m, and the main outer shelf break is at about 400 m. In the Walvis Bay region (~23°S), pronounced double shelf breaks occur at depths of 140 and 400 m, respectively, which is very unique among all the EBUSs.

Table 1.2 Average morphological parameters of the continental margin (Bremner 1981)

	Kunene Margin	Walvis Ridge Abutment	Walvis Margin
Shelf break depth (meter)			
inner	—	140	155
outer	196	305	361
Shelf width (km)			
inner	—	46	67
outer	44	78	119
Shelf Gradient (degree)	0.31	0.23	0.16
Upper slope gradient(degree)	2.06	0.8	1.27

1.1.3 Oxygen minimum zones in the shelf waters

Shelf waters of the northern BUS exhibit an annual oxygen deficit (< 90 $\mu mol \cdot l^{-1}$)

with strong seasonal variations (Chapman and Shannon 1987, Bailey and Chapman 1991, Monteiro and van der Plas 2006). Oxygen levels generally drop from hypoxic (< 90 $\mu mol \cdot l^{-1}$) to anoxic (< 20 $\mu mol \cdot l^{-1}$) during late austral summer to autumn, developing severe OMZs in shelf waters. Oxygen ventilation occurs during the late winter to spring when fresh ESACW invades the shelf, and weakens the OMZ intensity (Mohrholz et al., 2008).

One characteristic of the OMZ in the northern BUS is the existence of a zonal low-oxygen gradient in the bottom layer of shelf waters along the Namibian coast (Brüchert et al., 2006). This is caused by a gradual decrease in dissolved oxygen concentration in the SACW when it advects southward and experiences remineralization processes that continuously consume the dissolved oxygen. A stagnant bottom water layer of up to 30 m thickness, spreading from ABFZ to the south, was observed by a 8-month mooring observation at the mud belt off Walvis Bay (Brüchert et al., 2006). The stagnancy of the bottom layer will specifically enhance the oxygen consumption and generate the thoroughly anoxic and finally sulfidic conditions on the shelf (Struck et al., 2002, Emeis et al., 2004, Brüchert et al., 2009, Lavik et al., 2009).

1.2 Nitrogen cycling in the northern BUS

The overall nitrogen cycle is composed of nitrogen sources, sinks and internal cycling (Fig. 1.2). The nitrogen cycling in the northern BUS is governed significantly by the upwelling dynamics: the on-shelf upwelling dynamics determines nitrate inputs (source) and the nitrate delivery to phytoplankton assimilation; the OMZ intensity governs the removal of reactive nitrogen (sink) via anaerobic processes. For each process in N-cycling, a fractionation factor (ε) in per mil (‰) is associated to indicate the discriminating effect against ^{15}N. A positive ε means an enrichment of ^{15}N in the reactant and a concomitant depletion of ^{15}N in the product.

1.2.1 Nitrogen sources

The nitrogen sources in the northern BUS consist of atmospheric deposition (wet/dry),

4

riverine inputs, N-fixation and N-nutrient fluxes delivered by upwelling currents. The atmospheric deposition is mainly in the form of dust that is an important source of bio-available iron for phytoplankton in southeastern Atlantic (Vink and Measures 2001, Sarthou et al., 2003). But there is no good estimate on either air-borne nitrogen flux or riverine inputs to the northern BUS. The N_2 fixation is also undetectable in our study area (Sohm et al., 2011). Thus, I consider the upwelled nitrate of SACW origin as the major N-source to the northern BUS.
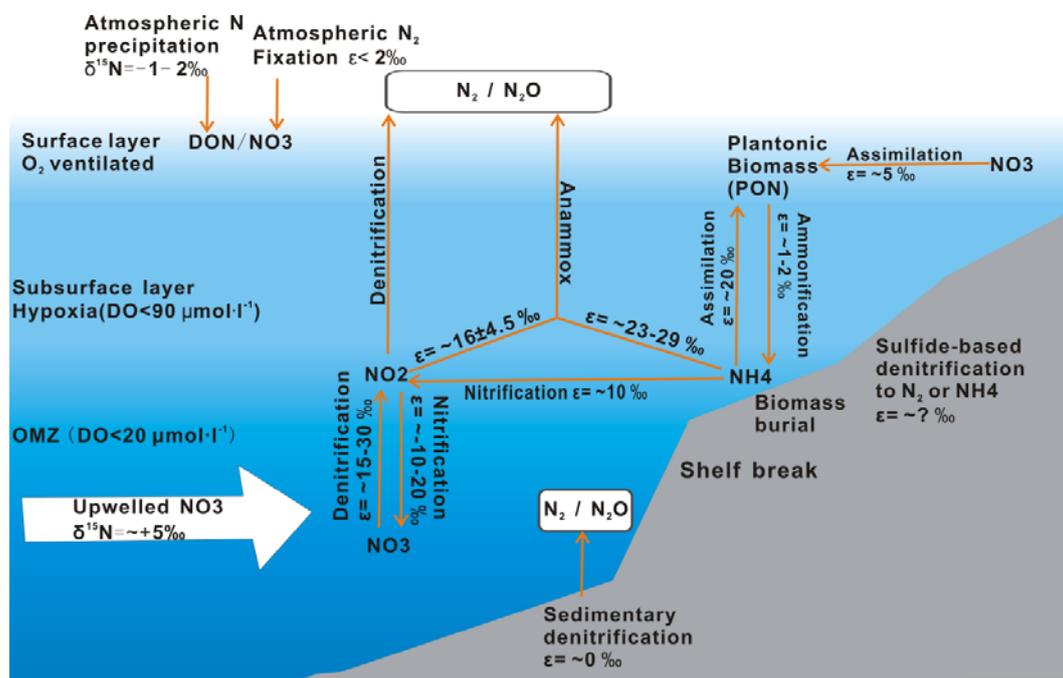
Fig.1.2 Main nitrogen cycling processes occurring at OMZ in shelf waters of a coastal upwelling system. Solid orange arrows indicate the turnover processes among different forms of nitrogen. An isotopic fractionation factor (ε) is associated with each N-cycling process (Granger et al., 2004, Sigman et al., 2009, Kritee et al., 2012, Dähnke and Thamdrup 2013, Möbius 2013, Karsh et al., 2014).

1.2.2 Nitrogen sinks

Phytoplankton assimilation and nitrogen loss (denitrification and anammox) are the two most prominent biogeochemical processes to remove the upwelled nitrate from shelf waters in the northern BUS.

Phytoplankton assimilation

Phytoplankton assimilates reactive nitrogen in various forms and preferentially

consumes ^{14}N relative to [15]N (Karsh et al., 2014). Diatoms are the most abundant primary producers in coastal waters of the northern BUS and assimilate the upwelled nitrate as the main N-source (Wasmund et al., 2014). The strongest ^{15}N fractionation happens during the 1st step of nitrate reduction inside the cell nitrate pool, which has an estimated isotope effect of 26.6‰ (Karsh et al., 2014). There is insignificant fractionation during the intracellular transportation of nitrate through the cell membrane (Needoba et al., 2003, Granger et al., 2004). The fractionation effect differs depending on N-species, with ε of 5.2±0.2‰ for nitrate, and 20±1‰ for ammonium (Waser et al., 1998). Nutrient-limitation, iron availability, light and physiological conditions of plankton are important environmental parameters that all play a role in the fractionation effect of nitrate assimilation. The light limitation incurs a more significant isotope effect than other parameters on the ambient nitrate pool (Needoba et al., 2003).

Nitrogen loss processes

Denitrification strongly discriminates against the heavier ^{15}N and progressively enriches the remaining nitrate pool with [15]N (Codispoti et al., 2001). Culture studies of denitrifying bacteria suggest a fractionation factor of ~10–30‰ (Sigman et al., 2001, Casciotti et al., 2002, Kritee et al., 2012). In OMZs of the northern BUS, water column denitrification causes a significant elevation in the $\delta^{15}N$ of nitrate (Emeis et al., 2009, Nagel et al., 2013).

Another mechanism leading to fixed-N loss is the ANaerobic AMMonium OXidation (anammox) process by chemoautotrophic anammox bacteria (Güven et al., 2005, den Camp et al., 2006). Anammox has been reported to dominate in the bottom waters over the Namibian shelf (Kuypers et al., 2005), Arabian OMZ (Schmid et al., 2007), and Peru/Chile shelf waters (Thamdrup et al., 2006). The fractionation effects of anammox on ^{15}N depend on the sources of nitrite and ammonium that react, and the extent to which they are consumed, respectively (Casciotti 2009). Recently, a fractionation effect of 23.5-29.1‰ against NH_4 and 16.0±4.5‰ against NO_2 has been reported (Brunner et al., 2013).

6

1.2.3 The competition between denitrification and anammox

There is no consensus on the dominance of anammox or denitrification as the dominant N-loss pathway in the major OMZs, suck as Black Sea (Kuypers et al., 2003, Jensen et al., 2008), Arabian Sea (Ward et al., 2009, Bulow et al., 2010), the coastal upwelling regions of Peru (Lam et al., 2009) and Chile (Thamdrup et al., 2006), or in the northern and central BUS (Kuypers et al., 2005, Emeis et al., 2009, Nagel et al., 2013). Anammox and denitrification often co-exist (Wenk et al., 2013) due to the overlapping oxygen threshold for the occurrence of anaerobic activity (Kalvelage et al., 2011), but the relative contribution vary in a very dynamical way in time and space (Bohlen et al., 2011).

Besides oxygen sensitivity, trace metal availability also limits the two N-loss processes (Godfrey and Glass 2011). The denitrification to N_2 is a Cu-limited process, especially in sulfidic environments (Buick 2007). The anammox bacterium requires only Fe for the reaction, but in high quotas (Kuenen 2008). The lack of a Cu requirement enables anammox to overwhelm denitrification under Cu-limitation conditions (Hannig et al., 2007, Godfrey and Glass 2011). In the northern BUS where OMZ state varies significantly in space and the field data of trace metal (Cu, Fe) in shelf waters is scarce, it is very difficult to segregate the two N-loss processes, and an N-loss budget that is based simply on one specific process is likely to be wrong.

1.3 Chlorophyll pigment as a compound specific ^{15}N marker to track N-cycling

Chlorophyll-a (Chl-a) is the most abundant chlorophyll pigment that is produced by marine phytoplankton community (Wright and Jeffrey 1997, Wright et al., 2005). It is synthesized through a phototrophic process that utilizes the carbon and N-nutrients assimilated by phytoplankton. Upon the death of phytoplankton, Chl-a loses the magnesium atom and turns into the pheophytin-a. The pheophytin-a is the richest degradation product that originates from Chl-a, especially under anoxic conditions (Ming-Yi et al., 1993). The pheophytin-a deposits together with planktonic biomass and is buried in the sediment (Fig. 1.3).
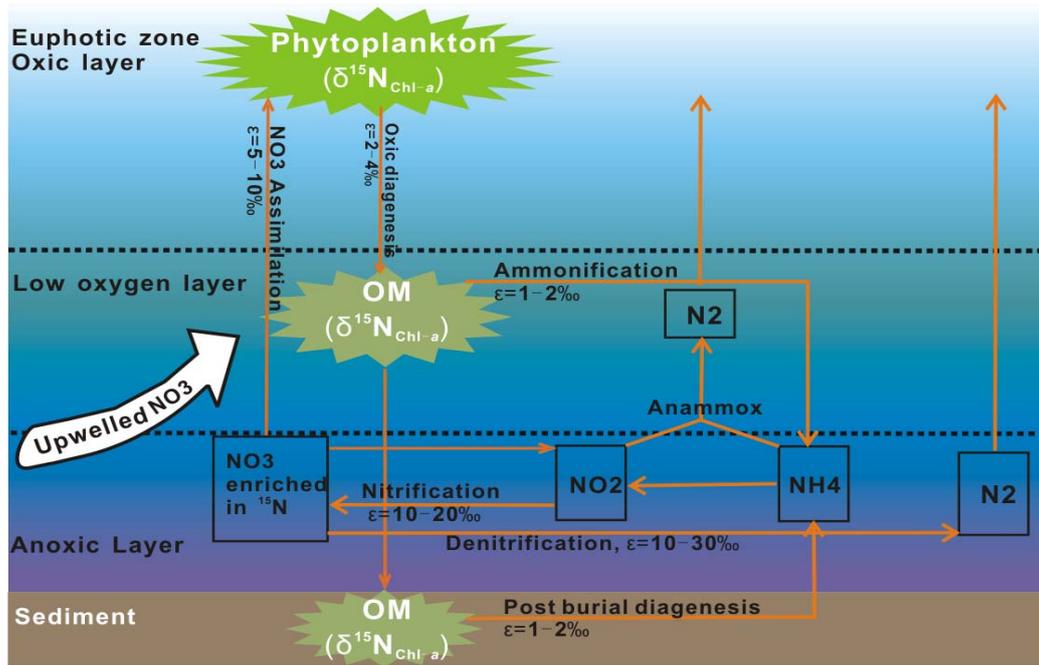
Fig.1.3 The major N-turnover processes (in orange arrows) under low oxygen concentrations. The fractionation factor (**ε**) is associated with each process (Needoba et al., 2003, Granger et al., 2004, Sigman et al., 2009, Robinson et al., 2012, Möbius 2013, Karsh et al., 2014). OM: organic matter of planktonic biomass; the light green color in euphotic zone indicates the freshly born planktonic biomass, and the grey green color in the sediment indicates the post-deposition plantonic biomass.

The isotopic fractionation of nitrogen occurs during nitrate assimilation and its utilization to synthesize Chl-a (Needoba et al. 2003). Therefore, the nitrogen atoms bound in the tetrapyrrole skeleton of Chl-a bear the isotope signature of both the nitrate sources and the nitrate assimilation. The $\delta^{15}N$ of Chl-a is thus affected by denitrification occurring in the oxygen minimum zone (OMZ) via the residual nitrate isotopic ratio (Fig.3). The isotopic integrity of N-atoms in Chl-a is maintained until the tetrapyrrole skeleton of Chl-a is broken and the N-atoms embedded are exposed to reactions that induce kinetic isotopic fractionation. This property indicates that the $\delta^{15}N_{Chl-a}$ is a suitable and robust marker to record variations in N-loss associated with the OMZ intensity in the shelf waters of the northern BUS.

There have been a few studies (Sachs and Repeta 2000, Junium 2010, Tyler et al., 2010, Fulton et al., 2012) that analyzed the $\delta^{15}N$ of chlorophyll pigment to investigate the N-loss variation during the Holocene (Fulton et al., 2012) and the last glacial-interglacial transition (Tyler et al., 2010). But all these studies used methods

8

that require a large amount of sediment samples (10~100g dry sediment) to meet the quantity and purity demand of Chl-a for $\delta^{15}N$ measurement by EA-IRMS, which limits $\delta^{15}N_{Chl-a}$ analysis at low pigment concentrations.

The "denitrifier method" (Sigman et al., 2001) makes it possible to measure the $\delta^{15}N$ of aqueous nitrate accurately at nano-molar N concentrations, which is merely ~1/100 of the quantity needed by EA-IRMS. This advancement facilitates the application of $\delta^{15}N_{Chl-a}$ as a compound-specific ^{15}N-marker in terms of applications to a wide range of environments from coastal settings to the pelagic ocean, and longer time-periods from the present back to the Holocene. Based on the "denitrifier method", Higgins et al measured the $\delta^{15}N$ of porphyrin (2008) and the $\delta^{15}N$ of chlorins extracted from sediments of the Eastern Mediterranean Sea (Higgins et al., 2010).

As stated above, with the favorable properties and analytical methods that are available, the $\delta^{15}N$ of Chl-a is a tool to analyze the past variations in the nitrate isotopic composition during Chl-a synthesis and integrates all the isotopic effects incurred by various N-cycling processes in the shelf waters.

1.4 The development of N-cycling in the BUS

1.4.1 BUS under global climate warming

Bakun (1990, 2010) hypothesized a strengthening of coastal upwelling in response to global climate warming. But quite a few recent investigations have argued the existence of non-uniform variations in upwelling intensity in the EBUSs. Field observations supporting this hypothesis has been found in the geoproxies records at the northern west Africa (McGregor et al., 2007), the Lüderitz upwelling cell off Namibia (Narayan et al., 2010), and the California and Peru upwelling systems by field observations (Gutiérrez et al., 2011). However, a general warming trend is found in all the EBUSs over 1910-2009 (Chavez et al., 2011); the Peru region also shows a weakening in upwelling intensity that was accompanied by a slight warming in surface water within the period 1948−2009 (Pardo et al., 2011).

Even within one upwelling system like BUS, the same non-uniform evolution of

upwelling has occurred. Monteiro et al (2006, 2008, 2011) found a strong warming trend of ~0.6°C (SST) over the period of 1982-2006 at the ABFZ, as well as in the offshore of Namibia. Similarly, Rouault et al (2007) observed an increase of 0.3-0.4℃ per decade at the boundaries of ABFZ and Agulhas Bank. In spite of the reported warming trend, Pardo et al (2011) showed an increase of the upwelling index I_w (Bakun 1973) in the central Benguela with a synchronous slight warming trend in surface waters; while at the northern and southern boundary the surface warming was associated with a decrease in upwelling intensity. Emeis et al (2009) found different trends in upwelling variation in the northern BUS that were reconstructed from proxies in sediment multicores. How such a non-uniform variation pattern in upwelling intensity and boundary warming events has impacted the N-cycling in the northern BUS ecosystem remains unknown.

1.4.2 The N-cycling variations in the northern BUS

The climate-driven fluctuations prompt changes in ocean circulation by modulating the depth and strength of the thermocline / nutricline (Chavez et al., 2011), and the communication between intermediate waters and upper layer waters thus varies in response (García‐Reyes and Largier 2012). Significant surface warming has been registered in the tropical Atlantic (Levitus et al., 2005, Levitus et al., 2009) and locally in the northern boundary of ABFZ (Rouault et al., 2007), which may induce upwelling variation in the northern BUS and changes in the N-nutrient inventory, oxygen flux and biological productivity, all acting together to re-organize the location and severity of the OMZ and to alter the intensity of the anaerobic N-loss processes. This calls for a re-investigation on the spatial and temporal variation pattern of N-nutrient sources and sinks in the northern BUS, and the mechanism that drives such variation.

Several key questions related to N-cycling in the northern BUS are addressed in this thesis:

i. How has the upwelling intensity varied in the northern BUS in response to the warming registered at the boundary to the ABFZ?

10

ii. What is the present-day spatial pattern of the N-source (upwelled nitrate input) and N-sink (nitrate removal) in shelf waters of the northern BUS?

iii. How have these two patterns varied in association with OMZ development during the past few hundreds of years?

1.5 Hypotheses and research objectives

This thesis investigates the long-term variations of N-cycling in association with upwelling intensity in the northern BUS under the influence of gradual warming now seen at the northern boundary (ABFZ), by examining the following 3 hypotheses:

i. Long-term variations of upwelling intensity occurred in the major upwelling zones of the northern BUS in the past, and were registered on the unsaturated alkenone-derived sea surface temperature ($U_{37}^{K'}$- SST) in a sediment core from the inner shelf.

ii. The nitrate flux to the northern BUS fluctuates in association with the variation in upwelling intensity; the nitrate isotopic signal images the nitrate source either of the pristine nitrate reservoir of the Angola Gyre, or of the nitrate pool that is modified by N-cycling processes, such as assimilation and denitrification. The resulting nitrate isotopic signal is recorded in chlorophyll-a through process of phytoplankton assimilation.

iii. The variation in oxygen flux via the upwelling current and the oxygen demand by biogenic organic matter diagenesis govern the formation and intensity of OMZ over the shelf, and the nitrate isotopic signal mirrors this OMZ development. The variation of OMZ-associated N-loss is encoded in the δ15N of chlorophyll-a in surface sediments and in sediment records.

Based on the above hypotheses, this study focuses on the following **research objectives**:

i. To track upwelling variation near the northern boundary of the ABFZ by analyzing $U_{37}^{K'}$- SST in one high-resolution sediment cores (21ºS, inner shelf). Published $U_{37}^{K'}$-SST records are integrated to analyze the upwelling variation pattern

in the northern BUS.

ii.   To track the nitrate inputs and sinks from the ABFZ to the central BUS (17-23ºS) by analyzing $\delta^{15}N_{Chl-a}$ of surface sediment; to describe the along-shelf and cross-shelf distribution pattern and to explore its connection with on-shelf upwelling dynamics, biological activities, and the OMZ distribution on the shelf.

iii.   To reconstruct the long-term variation of the $\delta^{15}N$ signal of nitrate imported to the northern BUS through $\delta^{15}N_{Chl-a}$ of a sediment core located between the northern boundary and the central part of BUS; to explore how the past denitrification intensity varied in response to upwelling development.

1.6 Thesis outline

In this thesis, I report HPLC procedures to separate chlorophyll pigments that are extracted from sediment and methods to measure the $\delta^{15}N$ of chlorophyll pigment accurately (Chapter 2). Then, surficial sediment samples of 27 stations (Chapter 3) and one dated sediment core (Chapter 4) are analyzed for the $\delta^{15}N$ of chlorophyll pigment and other proxies of environmental conditions. Chapter 3 focuses on the spatial variation pattern of nitrate sources and sinks in association with on-shelf upwelling dynamics, while chapter 4 reconstructs the temporal variation of N-loss in response to upwelling intensity variations over the past 180 years. Cruise data of M76-2 and a historical dataset "Namibian collection of Bottle" are integrated into the analyses.

The following three chapters are written in article format, and are to be submitted to peer-reviewed journals:

Chapter 2: A two-step HPLC separation of chlorophyll pigment from coastal sediment and its $\delta^{15}N$ measurement

In this part of work, a two-step HPLC method has been established for separation of pheophytin-a, which is extracted from sediment sample. The N-background and the isotopic background in the entire sequence of experimental steps are examined thoroughly. The procedures for $\delta^{15}N$ of pheophytin-a measurement using the "denitrifier method" are established and evaluated for repeatability. The recrystallized $K_2S_2O_8$ that is used as oxidization reagent has a low N-content of 1.4 nmol·ml^{-1}, and a $\delta^{15}N$ background of -15‰. The overall measurement of $\delta^{15}N_{pigment}$ is reliable and has an average analytical precision of less than ±0.5‰ (1σ).

My contribution to this chapter is:

All the experimental work of N-blank examination has been performed by XIN Yu.

$\delta^{15}N_{pigment}$ measurement procedures are designed by Dr. Kirstin Dähnke and XIN Yu, and all the measurements have been performed by XIN Yu at Helmholtz Zentrum Geesthacht.

Status: elaboration of the manuscript.

Chapter 3: Spatial distribution of $\delta^{15}N_{Chlorophyll-a}$ in northern Benguela Upwelling System

In order to study the spatial patterns of nitrogen cycling in coastal upwelling system, we analyzed the $\delta^{15}N$ of chlorophyll-a (Chl-a) in surface sediments of the northern Benguela Upwelling System (BUS), which is characterized of high primary productivity in surface waters and massive nitrogen loss in the subsurface oxygen minimum zone (OMZ). Upwelled nitrate is the major source of reactive nitrogen to the northern BUS, and is mainly removed through processes of denitrification and phytoplankton assimilation. Both processes gradually enrich the residual nitrate pool in ^{15}N that is subsequently assimilated to synthesize Chl-a. The $\delta^{15}N_{Chl-a}$ distribution

in surficial sediment should thus image the combined effects of denitrification and biological assimilation on δ^{15}N of nitrate in the overlying shelf waters. Our results show that the distribution of δ^{15}N$_{Chl-a}$ in surface sediment captures the spatial patterns of denitrification and nitrate assimilation, respectively, in the northern BUS, and their relative contributions to the nitrate sink.

My contribution to this chapter is:

Conceptual design came from XIN Yu and Prof. Emeis.

All the pigment extractions, separation, and δ^{15}N$_{Chl-a}$ measurements were done by XIN Yu.

One part of the δ^{15}N$_{sed}$ analysis was done by XIN Yu. Other bulk geochemical proxies, like TOC and TN content (%) were analyzed by project group members.

Status: elaboration of the manuscript.

Chapter 4: Temporal variations of Nitrogen-loss intensity in the northern Benguela Upwelling System based on the δ^{15}N$_{Chlorophyll-a}$ records in a sediment core

Significant warming has been registered in the sea surface at the northern boundary between the northern BUS and the adjacent Atlantic subtropical system. It signals the re-arrangement in the relative SACW proportions in the northern BUS that determine the extent of the OMZ and the associated reactive nitrogen loss via denitrification. To examine the N-loss intensity in response to upwelling fluctuations in the past, we analyzed the alkenone-derived sea surface temperatures and δ^{15}N of chlorophyll pigment in a dated sediment core located in the core OMZ of the northern BUS. We find out that the N-loss intensity in the northern BUS varied significantly over the past two centuries, and inversely tracked the upwelling intensity. The decreasing trend of δ^{15}N$_{Chl-a}$ along with the increasing U_{37}^{K}-SST since 1990 AD suggests that the OMZ is currently weakening in response to upwelling relaxation. It seems that the regional changes as reflected in OMZ weakening and upwelling relaxation in the

northern BUS contradict the expected trend of upwelling intensification. Our work suggests that a combined application of $\delta^{15}N_{Chl-a}$ and U^{K}_{37}-SST could interpret the regional variations of N-loss with upwelling intensity at other Eastern Boundary Upwelling Systems (EBUSs).

My contribution to this chapter is:

Conceptual design came from XIN Yu and Prof. Emeis

All the pigment extractions, separation, and $\delta^{15}N_{Chlorophyll-a}$ measurements were performed by XIN Yu

Analysis of $\delta^{15}N_{sed}$, water content (%) and bulk dry density of whole core slices were done by XIN Yu; the other bulk geochemical proxies TOC and TN content (%) were done by project group members.

Core dating was done by Dr. Jana Friedrich and colleagues at Helmholtz Zentrum Geesthacht.

Status: elaboration of the manuscript

2 A two-step HPLC separation of chlorophyll pigment in sediments and the δ^{15}N measurement

Abstract

Chlorophyll-a is the most abundant chlorophyll pigment produced by marine phytoplankton, and it bears the isotope signature of the nitrate source assimilated in the N-atoms that are embedded in its porphyrin ring. In the northern Benguela Upwelling System, the perennial hypoxia in the water column and in sediments assists the preservation of pheophytin-a, the first degradation product of chlorophyll-a, in the shelf sediment. An accurate measurement of the δ^{15}N of pheophytin-a provides information that characterizes the sources and sinks of nitrate in the coastal upwelling system. For this purpose, a two-step HPLC method was established for separation of pheophytin-a that is extracted from sediment sample. The N-background and the isotopic background in the entire sequence of experimental steps are examined thoroughly. The procedures for δ^{15}N of pheophytin-a measurement by using "denitrifier method" are established and evaluated for repeatability. Critical for precision and accuracy of the measurements are the N-content in acetone and $K_2S_2O_8$, because they constitute the majority of the exogenic N contamination in a pigment sample, and result in an oxidization efficiency yield of over 100%. In my method, the recrystallized $K_2S_2O_8$ that is used as oxidization reagent has a low N-content of 1.4 nmol·ml^{-1}, and a δ^{15}N background of -15‰, which is established by continuous examinations over a period of two months. This ^{15}N background of $K_2S_2O_8$ would cause -1- -2‰ deviation on the δ^{15}N of sample that contains nanomolar level N, and highlight the need to examine the δ^{15}N of recrystallized $K_2S_2O_8$ when it is used to oxidize samples containing N. The overall measurement of $\delta^{15}N_{pigment}$ is reliable and has an average analytical precision better than ±0.5‰ (1σ).

Keywords: nitrogen isotopes, chlorophyll pigments, isotope background, potassium persulfate, isotope spiking method

2.1 Introduction

Chlorophyll-a (Chl-a) is the most abundant chlorophyll pigment that is produced by the marine phytoplankton community (Wright and Jeffrey 1997, Wright et al., 2005). It is synthesized through a phototrophic process that utilizes the carbon and N-nutrients assimilated from the ambient nitrate. When the phytoplankton dies, Chl-a loses the Mg-atom in the first degradation step and becomes into pheophytin-a, which is the most abundant degradation product especially under anoxic conditions (Ming-Yi et al., 1993). The pheophytin-a is preserved in sinking organic matter, deposits at the sea floor and is buried in the marine sediment.

Isotopic fractionation creates differences in 15N/14N relative abundance in the nitrate source. When nitrate is transported through the cell membrane, the isotopic fractionation effect is comparatively insignificant (<2‰) (Granger et al., 2004, Karsh et al., 2014). The most intensive ^{15}N fractionation (ε= 26.6‰) occurs in the first reduction step of nitrate to nitrite (Granger et al., 2004, Karsh et al., 2012). Another process that may cause ^{15}N fractionation, but which has not been reported so far, is the synthesis of glutamic acid by using ammonium and porphobilinogen, the precursor of the tetrapyrrole skeleton of chlorophyll pigment (Grimm et al., 2006). Thus, the isotope signature of both the nitrate sources and assimilation fractionation during biosynthesis and Chl-a produced are imprinted on the nitrogen atoms that are bound in the tetrapyrrole skeleton of Chl-a (Fig. 2.1). In the case of water column denitrification that substantially enriches the dissolved nitrate pool with ^{15}N (Casciotti et al., 2002, Sigman et al., 2009), the $\delta^{15}N$ of Chl-a is concomitantly imprinted with the signal of denitrification that is significantly driven by the oxygen minimum zone (OMZ) intensity. The ^{15}N of Chl-a is undoubtedly a suitable marker to track the N-cycling in coastal upwelling zones with denitrification in the water column.
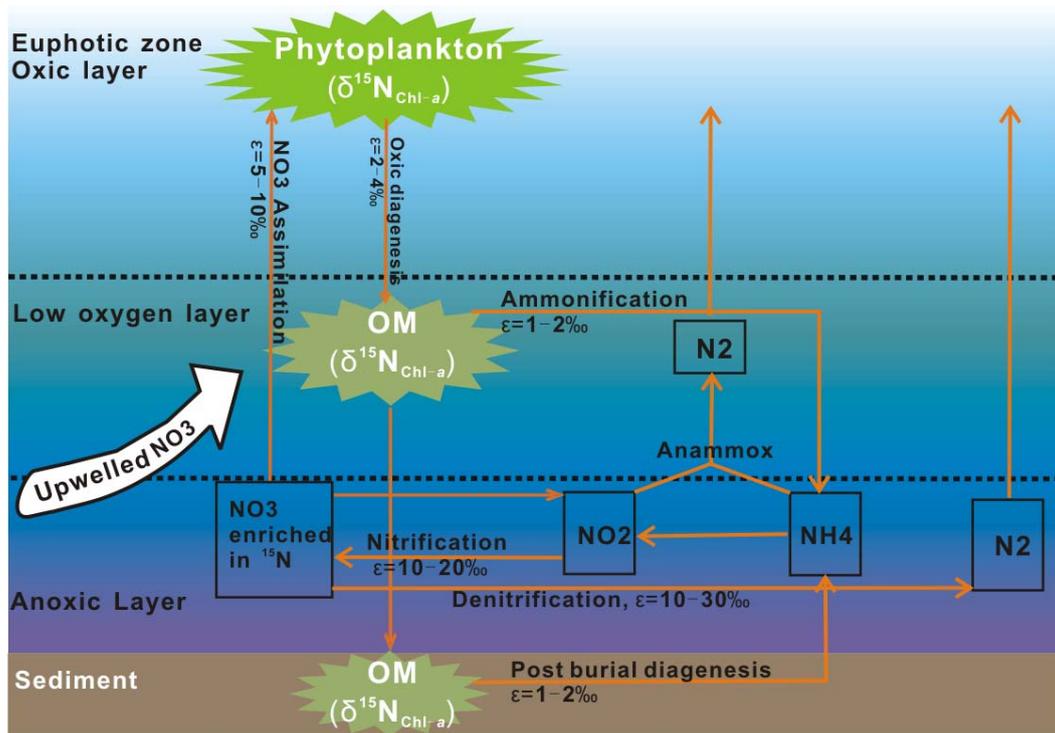
Fig.2.1 The major N-turnover processes (in orange arrows) under low oxygen concentration. The fractionation factor (ε) is noted with each process (Needoba et al., 2003, Granger et al., 2004, Sigman et al., 2009, Robinson et al., 2012, Möbius 2013, Karsh et al., 2014). OM: organic matter of planktonic biomass; the light to grey green color images the relative aging of plantonic biomass.

The $\delta^{15}N$ of bulk sedimentary ($\delta^{15}N_{sed}$) is another means that has been used widely to track the utilization of nitrate (Altabet and Francois 1994, Altabet et al., 1999, Higginson et al., 2003) and denitrification in the ocean (Altabet 2007, Emeis et al., 2009, Meisel et al., 2011, Deutsch et al., 2014) . But when $\delta^{15}N_{sed}$ is used to establish isotopic linkage between nitrate sources and sinks, large deviations are created by two main processes: the mixing of allochthonous N-containing organic matter and the diagenetic processes in water column and sediment. The isotope composition of bulk sediment is easily modified by being mixed with organic matter of a different ^{15}N source, i.e. microbial biomass (Macko and Estep 1984). The $\delta^{15}N_{sed}$ is also subject to isotope fractionating effects of various diagenetic processes (Sachs et al., 1999, Lehmann et al., 2002, Gaye-Haake et al., 2005, Robinson et al., 2012, Möbius 2013). In contrast, the tetrapyrrole skeleton of chlorophyll-a isolates the N-atoms until it is broken and the N-atoms embedded are exposed to reactions that create kinetic

isotopic fractionation. This indicates that the $\delta^{15}N_{Chl-a}$ is a more robust ^{15}N-marker to capture N-cycling processes than $\delta^{15}N_{sed}$, and that an accurate $\delta^{15}N$ measurement of Chl-a in the sediment can avoid the ambiguity imprinted by various processes on $\delta^{15}N$ of bulk sediment.

Bidigare et al. (1991) first used HPLC to separate and purify Chl-a/b, and proved that the N-isotope integrity of pigment was maintained during the steps of purification. Sachs and Repeta (2000) measured the $\delta^{15}N_{Chl-a}$ and an isotopic deviation of N in Chl-a relative to total algal nitrogen showed a robust value of 5.1±1.1‰. These studies (Sachs and Repeta 2000, Higgins et al., 2010, Tyler et al., 2010) require a large amount of sediment samples (10~100g dry sediment) to meet the quantity and purity demand of Chl-a for ^{15}N measurement by EA-IRMS, which limits the possibilities to analyze $\delta^{15}N_{Chl-a}$ in sample with low pigment content.

The recently-developed "denitrifier method" (Sigman et al., 2001) makes it possible to measure the $\delta^{15}N$ of aqueous nitrate accurately at nano-molar level, which is merely ~1/100 of the quantity needed for EA-IRMS. Based on the "denitrifier method", Higgins et al. (2008) measured the $\delta^{15}N$ of porphyrin and the $\delta^{15}N$ of chlorin extracted from sediment core in the Eastern Mediterranean Sea (Higgins et al., 2010).

The "denitrifier method" facilitates the application of $\delta^{15}N_{Chl-a}$ as a compound-specific $\delta^{15}N$-marker in terms of applications to a wide range of environments from coastal settings to the pelagic ocean, and longer time-periods from the present back to the Holocene (Fulton et al., 2012). However, the nano-molar level N-content of Chl-a in the sample also makes it quite vulnerable to external-N contaminations that are induced during experimental steps. A thorough examination of the N-blanks as well as the ^{15}N background concentration and $\delta^{15}N$ in the entire experimental steps is therefore a prerequisite for an accurate $\delta^{15}N_{Chl-a}$ measurement.

This study is aimed at developing methods and procedures for accurate measurements of $\delta^{15}N_{Chl-a}$. It is composed of 3 parts: 1) to establish a HPLC method for a qualified separation of chlorophyll pigments; 2) to thoroughly examine the N-blank and isotope background in experimental steps; 3) to examine the repeatability of the entire

measurement.

2.2 Materials and methods

2.2.1 Chlorophyll pigments extraction and separation

2.2.1.1 Chlorophyll pigments extraction

Chlorophyll pigments are extracted from sediment samples with a mixture of dichloride methane and methanol (9:1) in an ASE 200 under highly pure N_2 (Accelerated Solvent Extraction System, Thermo Fisher Scientific Inc., temperature is set at 80℃, and pressure at 1000 psi). After two extractions, the solution is concentrated, removed for sulfide or sulfur, and concentrated again to 200 μl for HPLC separation. The exposure of pigments to light and air was avoided.

2.2.1.2 Pigments separation and purification

A two-step HPLC method to separate and purify pigment is developed in this study based on those by Sachs et al. (1999), Higgins et al. (2010) and Roy et al. (2011). A Shimadzu HPLC system equipped with one reverse-phase semi-preparative column (LiChrospher RP-18, 9.4 mm x 250 mm, 10 μm, Merck KGaA) and three consecutive reverse phase analytical columns (LiChrospher RP-18e, 4.0 mm x 250 mm, 5 um, Merck KGaA) was used. The wavelength is set at 660 nm to monitor the separation (Wright et al., 2005). In the first step of separation, the semi-preparative column is used and mobile A is methanol: acetone (7:3), mobile B is methanol: ethyl acetate: acetone (5:3:2) at a flow rate of 2.24 ml·min^{-1}. In the second step of separation, 3 analytical columns are used and mobile A is changed to methanol: acetone (9:1) while mobile B remains the same at a flow rate of 0.75 ml·min^{-1}. The fraction of chlorophyll pigments is collected within the time window of 10-15 minutes during the first step. The fraction of target pigment (pheophytin-a) is collected from 16.7 to 17.7 min during the second step. The HPLC separation can be processed at a rate of 2-3 injections per day. All the pigment fractions are preserved at -20 ℃ in the dark.

2.2.2 N-blank and the $\delta^{15}N$ background

The N-phases in organic solvents, the HPLC columns, and $K_2S_2O_8$ are firstly transformed into aqueous nitrate by POR, and then measured by a UV-Vis based method (Roman et al., 1991, Mack and Bolton 1999) in this study (Fig. A2.1 & 2.2). The isotopic effect of this two-step HPLC separation is examined by analyzing Chl-a standard. The fractionated Chl-a is then transformed into aqueous nitrate and its $\delta^{15}N$ is measured by the "denitrifier method".

2.2.3 Pigment oxidization

Oxidizing reagent preparation

Potassium persulfate (ACS reagent, Sigma-Aldrich Co.) is recrystallized four times before dissolving it in highly pure sodium hydroxide (Semi-conductive, Sigma-Aldrich Co.) aqueous solution (Milli-Q, 0.15 $mol·l^{-1}$), to reach a final concentration of 0.05 $mol·l^{-1}$. This alkaline solution of the oxidization reagent is named "POR" hereafter (Higgins et al., 2008).

Oxidization settings and efficiency

Oxidization is an essential step to convert nitrogen atoms in pigment to aqueous nitrate for the next step of $\delta^{15}N_{NO3}$ measurement. Autoclave is set at 121 ℃, 30 minutes (Higgins et al., 2008) with Milli-Q water steaming. A Chl-a standard (>95% purity, Sigma-Aldrich Co.) is used for oxidization efficiency assessment.

2.2.4 $\delta^{15}N_{NO3}$ determination

$\delta^{15}N$ of nitrate is determined using the "denitrifier method" (Sigman et al., 2001, Casciotti et al., 2002). The sample solutions are injected into a suspension of *Pseudomonas aureofaciens* (ATCC#13985). The dissolved nitrate in the samples is quantitatively converted to N_2O gas, which is stripped from the vials by purging with helium, concentrated and purified on a Gas-Bench II, and analyzed on a Delta V mass spectrometer (Thermo Finnigan). Replicate measurements are performed, and two international standards IAEA-N3 ($\delta^{15}N = +4.7‰$) and USGS 34 ($\delta^{15}N = -1.8‰$,), are

measured with each batch of samples. For quality assurance of the results, we use an internal potassium nitrate standard that is measured with each batch of samples. Isotope values are corrected using the "bracketing scheme" (Sigman et al., 2009) for the two-point correction referring to IAEA-N3 and USGS34 for $\delta^{15}N_{NO3}$. To evaluate the isotopic background of the whole separation and oxidization process, a Chl-a standard (Sigma-Aldrich Co. purity > 95%) is used as an internal standard. The standard deviation for international and in-house standards is 0.3‰ for $\delta^{15}N$ (n = 6), deviations for replicate samples are within the same range.

2.2.5 The $\delta^{15}N$ background of the POR solution

A spiking method was developed to measure the $\delta^{15}N$ of POR solution ($\delta^{15}N_{POR}$). Briefly, 5.0 ml autoclaved POR is spiked with 10 μl of 5.0 mM KNO_3 standard (noted as KBI) to make the final NO_3 concentration ~10 μmol·l^{-1}. Then, $\delta^{15}N$ of spiked POR solution ($\delta^{15}N_{POR(spiked)}$) and KBI ($\delta^{15}N_{KBI}$) is separately measured. With the volume and nitrate concentration of POR ($C_{NO3-POR}$), KBI ($C_{NO3-KBI}$) and spiked POR solution ($C_{NO3-POR(spiked)}$), the $\delta^{15}N_{POR}$ is calculated based on the isotopic mass balance. The same spiking procedure is performed with IAEA-N3 (5 mM) and USGS (5 mM) as well. The spiking of KBI with POR solution is taken as an example below:

$$\delta^{15}N_{POR} \times (C_{NO3-POR} \times V_{POR}) + \delta^{15}N_{KBI} \times (C_{NO3-KBI} \times V_{KBI}) = \delta^{15}N_{POR(spiked)} \times (C_{NO3-POR(spiked)} \times V_{POR(spiked)})$$

The V_{POR}, V_{KBI} and $V_{POR(spiked)}$ refer to the volumes of POR and KBI solutions, and the volume of POR after spiking, respectively.

2.3 Results and discussions

2.3.1 Pigment extraction, separation and purification

The recommended solvent in JGOFS protocols (Joint Global Ocean Flux Study) for chlorophyll pigment extraction is acetone aqueous solution (90%) and sonication in an ice bath (Wright and Jeffrey 1997, Wright et al., 2005). Another frequently used solution is dimethylformamide (Wright et al., 2005). But neither of them is used in this study due to either their N-blank as a potential contamination, or the toxicity. The ion-pair reagents ($NH_4C_2O_2H_3$ aqueous solution or pyridine) are widely used in mobile gradients in HPLC systems for thorough separation of pigments. But the N– containing ion-pair reagent is a possible N-contamination to pigment samples, and not employed in separation, because of its unknown $\delta^{15}N$ signature. Besides, the removal steps of the ion-pair reagent will unnecessarily expose the pigment sample to air and light.

A baseline-resolution separation of the target pigment (pheophytin-a) is achieved (Fig. 2.2b) by the two-step HPLC separation used here. Q_y/Q_{Soret} ratio of the peak (R_t=6.14 min) is 3.8, and the insignificant peak at the Soret band (Fig. A2.3) is chlorophyllone (Aydin et al., 2003). For the peak at R_t=17.14 min, the Q_y/Q_{Soret} ratio is 1.27. These spectrum features (3 small bumps at 500-600 nm) indicate that the peak (R_t=17.14 min) belongs to the phaeopigments. With reference to self-made pheophytin-a standard, the HPLC spectrum of the target pigment identifies it as pheophytin-a.


23
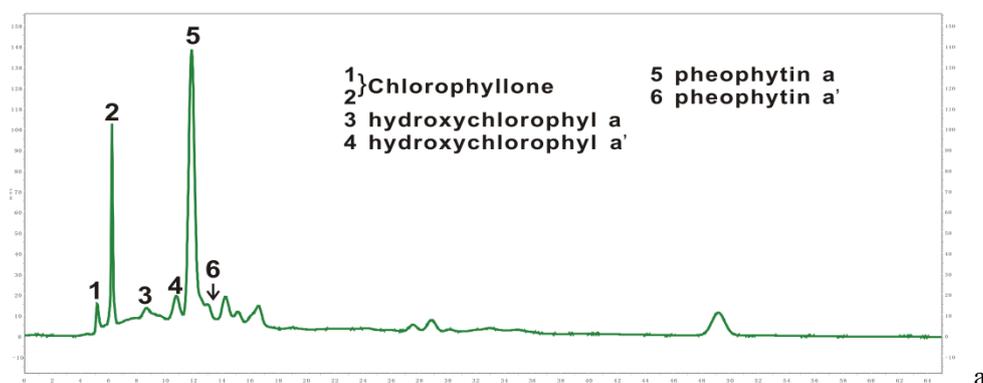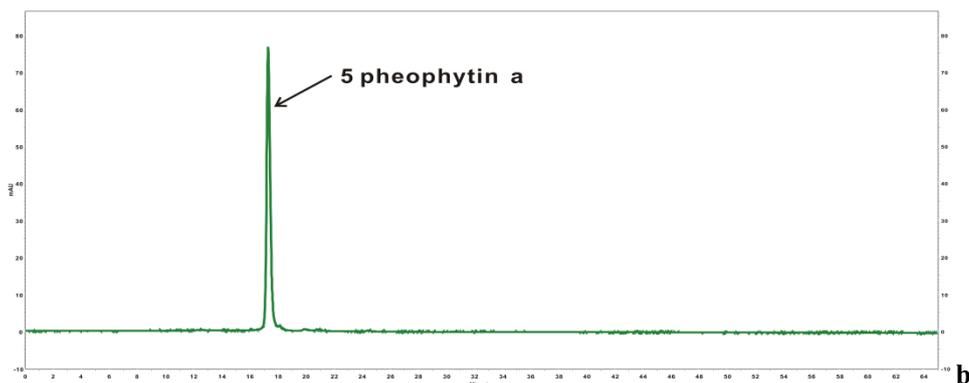
Fig.2.2 Separation and purification of pigment by HPLC (a, 1st step of separation by semi-preparative HPLC; b, pheophytin-a fractionated by 2nd step of separation on analytical RP columns in HPLC)

Further purification by normal phase column is not performed for several reasons: 1) the chromatogram of normal phase HPLC (Lichrospher Si-60, 5 μm, 4.6 mm×250 mm, Merck KGaA) has yielded no other peak than the peak of the target pigment (pheophytin-a); 2) the recovery efficiency of normal phase HPLC separation is ~ 66% so that there would be one third loss of the target pigment, and results in insufficient sample for "denitrifier method". 3) another round of HPLC separation would expose the samples again to air and light that might result in degradation of pigment.

2.3.2 N-blanks and ö^{15}N backgrounds of the organic solvent and the HPLC system

2.3.2.1 The N-blanks

Higgins et al. (2008) reported a very low N-blank (< 0.2 nmol·ml^{-1}) in methanol, dichloromethane, ethyl acetate, but comparatively high N-contents in acetone (~2 nmol·ml^{-1}). Our analyses show that the re-distillation procedure substantially reduces the N-content in organic solvent: there is only trace-level N-content (~0.2 nmol·ml^{-1}) in the re-distilled ACE, while the N-content of the other solvents are below detection limit (Table A2.3). Acetone is recommended for pigment extraction by Jeffrey and Wright (1997, 2005). When 20 ml re-distilled acetone is used for pigment extraction, the N-content of acetone can result in an enrichment of ~4.0 nmol N in pigment extractions. Apparently, the N-content in acetone could bias the δ^{15}N of pigment due

to the unknown $\delta^{15}N$ of acetone. For this reason, acetone is used as sparingly as possible in separation steps. A qualified re-distillation is strongly recommended as a standard procedure for pigment separation. Unlike the report by Higgins et al. (2008), our results suggest negligible N release from either the NP or RP columns during the HPLC separation. Nevertheless, thorough column washing is required repeatedly before and after each round of sample separation.

2.3.2.2 The $\delta^{15}N$ background in HPLC separation

The two-step HPLC separation alters the $\delta^{15}N$ of Chl-a standard by creating an offset of -0.5±0.48‰ (Table 2.1). As no N is released from the HPLC columns, the N contained in acetone is suspected to cause the negative ^{15}N deviation to offset the $\delta^{15}N_{Chl-a}$.

Table 2.1. The $\delta^{15}N$ of Chl-a standard after two-step HPLC separation

Sample ID	$\delta^{15}N$(‰) Dupl.1	$\delta^{15}N$(‰) Dupl.2	AVG	
Chl-a-FRC1	12.40	12.39	12.40	
Chl-a-FRC2	12.94	13.14	13.04	Chl-a-FRC stands for the Chl-a standard after 2-step HPLC separation
Chl-a-FRC3	12.88	12.94	12.91	
Chl-a-FRC4	13.94	13.53	13.74	
Average	13.13	13.00	13.07	
St. deviation	0.65	0.41	0.48	
Chl-a (EA-IrMS)			13.6	

The $\delta^{15}N_{ACE}$ measurement is not an option in our study, because it requires enrichment of a large quantity of re-distilled acetone to meet the quantity demands for "denitrifier method" (M.B. Higgins, personal comm., 29th Nov. 2011). The isotopic bias that is produced by HPLC separation is in the following not corrected in the $\delta^{15}N$ of pigment samples reported.

2.3.3 Oxidization efficiency


$$R^2\ 0.998$$
$$Y=0.36+1.04X$$
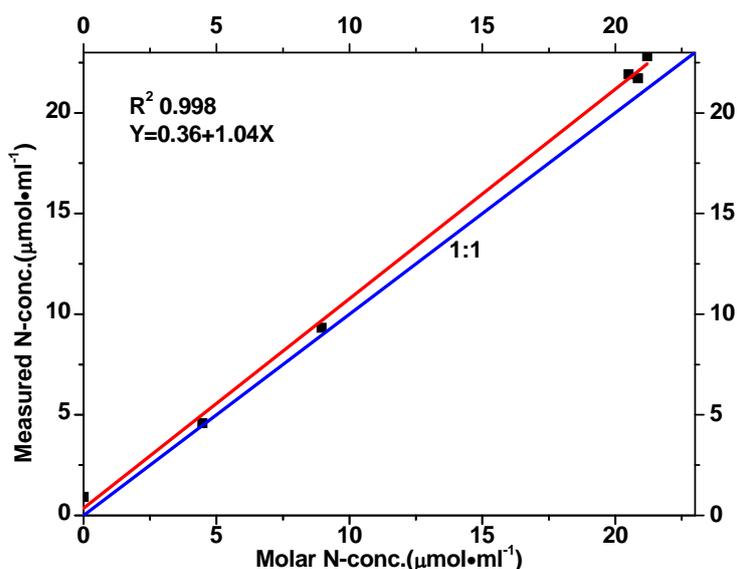
Fig.2.3a The oxidization yield of Chl-a standard into aqueous nitrate (blue line stands for 1:1 yield; red line is the regression fitting; nitrate concentration is measured by Bran&Lübbe AA3 with error bar included).
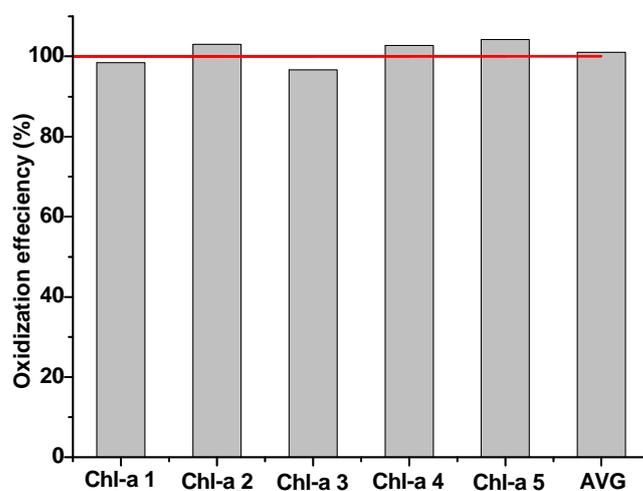

Fig.2.3b Oxidization efficiency of the Chl-a standard (5 replicates; nitrate concentration is measured by UV-Vis method).

The >1:1 yield of Chl-a standard to nitrate (Fig. 2.3a) probably results from the N-blank in the acetone. An analysis by spectrometric methods (Bran&Lübbe AA3) shows that there is neither nitrite nor ammonium in the sample solutions after oxidization, which indicates a thorough turnover. However, silicate reaches 140-190

$\mu mol \cdot ml^{-1}$, and white flecks on inner wall of the glass tubes suggest that severe corrosion of glass has occurred during autoclave treatment. A quartz tube was much less corroded and was therefore selected for sample oxidization. The oxidization efficiency based on UV-Vis measurements was estimated to an average of 101% ($\pm 3.3\%$), and is in good agreement with the results of $\sim 104.1 \pm 3.1\%$ measured by an auto-analyzer method (Fig. 2.3b). The comparable results by two methods indicate the consistency and suitability of the oxidization treatment employed here and the reliability of the UV-Vis method for determining nitrate concentrations after oxidization.

2.3.4 $\delta^{15}N$ background of POR solution

The impact of sample solution acidity or alkalinity on the digestion efficiency of the denitrifying bacteria is unknown yet (Sigman et al., 2001). The bacterial culture is composed of a strong buffering system (KH_2PO_4, $(NH_4)_2SO_4$, low nutrients seawater) and could neutralize the weak acidity or alkalinity of sample solution. Nevertheless, given that the nitrate digestion by the starving denitrifying bacteria occurs immediately upon the sample injection, it is advised to adjust the sample solution to pH 7.0 before injection (D. Sigman, personal comm., 28th Aug. 2012). The oxidized sample usually shows strongly alkaline (pH >14) that results from the amount of NaOH in POR. Therefore, pH adjustment is performed on each oxidized sample with 10% H_2SO_4 (ACS reagent, Sigma-Aldrich Co.). Generally, a small fraction ($\sim 50 \mu l$) of the sample solution is replaced for pH adjustment to 7.0 ± 0.5.

The N in potassium persulfate ($K_2S_2O_8$) crystals exists mainly in form of ammonium (Nydahl 1978), and could compromise both the N content and isotopic composition of pigment samples. Although multiply recrystallized $K_2S_2O_8$ makes the POR solution contain only $\sim 1-2$ nmol N per ml, the isotopic effect of POR on pigment sample cannot be overlooked. The $\delta^{15}N$ of the Chl-a standard (Sigma-Aldrich Co. >95%) analyzed by the denitrifier method shows an average $11.6 \pm 0.3\permil$ (6 duplicates), about 2‰ lower than the $\delta^{15}N$ of $13.6 \pm 0.2\permil$ measured by EA-IRMS. Incomplete oxidization could produce the ^{15}N depleted NO_3 from Chl-a, based on a Rayleigh

27

fractionation model (Higgins et al., 2008), but our oxidization yield averages 100% and the nutrient analysis indicates a thorough and quantitative transformation of pigment-N to NO_3. Since the same stock of Chl-a standard is used, the only difference is the involvement of POR, suggesting that the deviation on $\delta^{15}N_{Chl-a}$ is caused by the $\delta^{15}N$ background of the POR solution.

There is no earlier report on the $\delta^{15}N$ background of POR. We first tried direct measurement and then developed a spiking method. The direct measurement of $\delta^{15}N_{POR}$ by the "denitrifier method" gives a value of -6.5±0.01‰ (n=2), proving the existence of a low $\delta^{15}N$ background of the POR solution as expected. But the peak signal (1.35±0.05, n=2) on the IRMS is too small to support the robustness of the $\delta^{15}N$ data (Table 2.2). In order to increase the signal on the IRMS, 5.0 ml post-autoclave POR containing ~7-9 nmol nitrate is injected. This attempt failed to give a satisfactory result, probably due to the dilution effects on the denitrifier bacteria or other unknown reasons.

Table 2.2 $\delta^{15}N_{POR}$ measurement by direct measuring method and spiking method

Sample ID	Signal on IrMS ((in arbitrary unit)	$\delta^{15}N$(‰) direct measurement	$\delta^{15}N_{POR}$(‰) spiking method	Signal on IrMS (in arbitrary unit)	$\delta^{15}N$(‰) direct measurement	$\delta^{15}N_{POR}$(‰) spiking method	Annotation
	Mesurement on 23rd Oct.2012			Mesurement on 25th Oct.2012			
POR-1	1.35	- 6.50					The POR is made of
POR-2	1.45	- 6.49					recrystallized $K_2S_2O_8$
POR+KBI II-1	33.03	6.35	-15.60	10.33	4.27	-14.42	POR solution spiked
POR+KBI II-2	33.06	6.38	-14.81	9.81	4.17	-16.74	with KNO_3 standard
POR+KBI II-3	33.21	6.32	-15.68	10.24	4.32	-14.33	(40 $\mu mol \cdot l^{-1}$), 5
POR+KBI II-4	33.02	6.46	-13.22	10.31	4.37	-13.77	replicate
POR+KBI II-5	33.62	6.30	-14.18	10.26	4.38	-13.89	measurements
AVG+STD	33.19±0.25	6.36±0.06	-14.70±0.92	10.19±0.21	4.30±0.09	-14.63±1.21	
No-POR1	4.25	3.90					No-POR means the
No-POR2	4.23	3.62					POR made of not
No-POR3	4.52	4.15					recrystallized
No-POR4	4.31	3.69					$K_2S_2O_8$
AVG+STD	4.33±0.13	3.84±0.24					

The N-content in not re-crystallized $K_2S_2O_8$ is almost 3 times as high as that of recrystallized $K_2S_2O_8$. The positive $\delta^{15}N$ of not re-crystallized $K_2S_2O_8$ suggests that its isotopic background could cause a $\delta^{15}N$ deviation of ~+1‰ on a sample containing 10 nmol N. But after 4 times of recrystallization, the POR becomes depleted in ^{15}N and the $\delta^{15}N$ decreases to around -14.7‰ (Table 2.2). Although less concentrated in the recrystallized $K_2S_2O_8$, the residual N is able to compromise the $\delta^{15}N$ of samples with its $\delta^{15}N$. It is very necessary to measure the $\delta^{15}N$ of POR solution accurately before it is used to oxidize samples of nanomolar N concentrations. The direct measurement cannot produce reliable data, but the spiking method gives satisfactory results.

In order to examine the long-term variance of $\delta^{15}N_{POR}$, random measurements of the $\delta^{15}N$ of POR solution were carried out from October to November 2012 (Table 2.3). A comparatively constant $\delta^{15}N_{POR}$, averaging -15‰ is obtained on the same stock of recrystallized $K_2S_2O_8$.

Table 2.3, Two-month measurement of $\delta^{15}N_{POR}$ by spiking method

$\delta^{15}N$ standard	9th Nov.2012			12th Nov.2012			29th Nov.2012		
	IAEA	KBI-II	USGS	IAEA	KBI	USGS	IAEA	KBI	USGS
Replicate 1	-14.95	-14.73	-14.80	-14.33	-16.47	-15.14	-11.66	-16.20	Data
Replicate 2	-13.13	-15.83	-14.50	-13.45	-13.34	-15.44	-16.55	-15.32	unavailable
Replicate 3	-14.28	-16.40	-13.35	-15.46	-14.71	-14.06	-14.31	-14.93	
AVG	-14.41	-14.84	-14.78	-14.12	-15.66	-14.22	-15.43	-15.48	
STD	1.00	1.24	0.72	0.92	0.85	0.76	1.58	0.65	

The spiking method with USGS failed on 29th Nov. 2012 and gave no qualified data.

This quantitative examination of $\delta^{15}N_{POR}$ identifies the isotopic bias of POR on the $\delta^{15}N$ of samples. The two-month measurements prove the robustness of the spiking method. We believe that the isotopic deviation caused by $\delta^{15}N_{POR}$ has significant impact on samples that contain nitrogen at nano-molar levels when POR is used in the oxidization step to transfer reduced nitrogen to nitrate. It is recommended from this

study that the same stock of recrystallized $K_2S_2O_8$ should be used in each round of pigment sample oxidization, and that the $\delta^{15}N_{POR}$ should be measured along with each batch of samples to correct the $\delta^{15}N_{pigment}$.

2.3.5 Repeatability of $\delta^{15}N_{pigment}$ measurements

The repeatability of the $\delta^{15}N_{pigment}$ measurement steps is evaluated by measuring $\delta^{15}N$ of Chl-a standard in replicates. The 95% confidence zone ($\pm 1\sigma$, Fig. 2.4 a/b) indicates a consistent performance of the entire measurement sequence, with a standard deviation of ± 0.32‰ and ± 0.26‰, as given by two separate examinations.
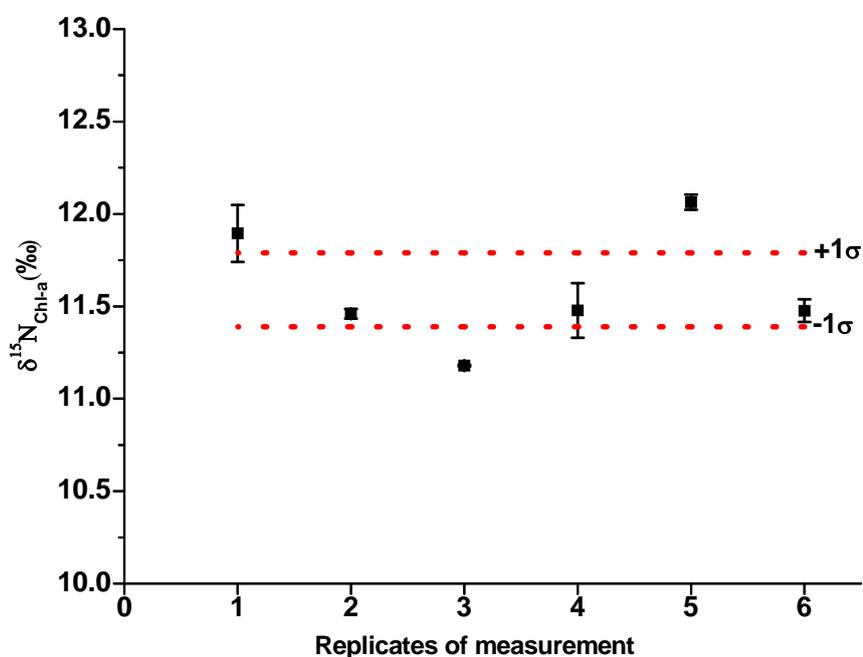
Fig.2.4a $\delta^{15}N$ of Chl-a standard by the denitrifier method (purchased in Aug, 2012), dashed lines mark the 95% confidence zone ($\pm 1\sigma$), error bars are for duplicate measurements.
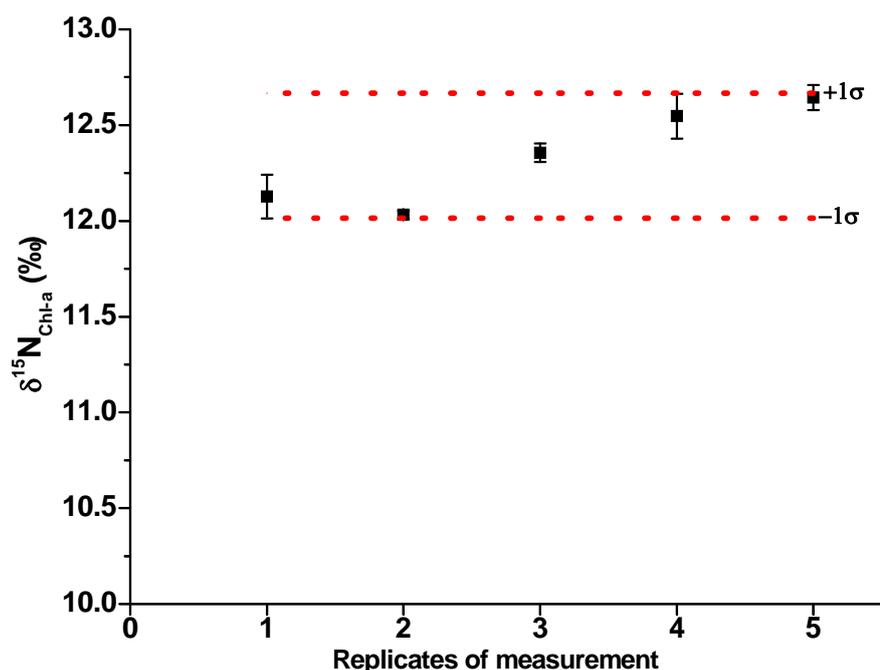
Fig.2.4b $\delta^{15}N$ of Chl-a standard by the denitrifier method (purchased in Dec. 2012), dashed lines mark the 95% confidence zone ($\pm 1\sigma$) error bars are for duplicate measurements.

2.4 Summary and conclusions

A two-step HPLC method was established in this study for thorough separation of chlorophyll pigments that were extracted from the shelf sediments in the northern Benguela Upwelling System. In order to accurately measure the $\delta^{15}N$ of chlorophyll pigment, the N-blank and the ö^{15}N background are examined in the entire experimental sequences. The exogenic N that contaminates pigment samples originates mainly from the N contained in acetone and in POR solution made of $K_2S_2O_8$. The oxidization efficiency of pigment is around 101-104% and this >100% yield is attributed to the N in acetone used as organic solvent. The POR solution made of 4×re-crystallized $K_2S_2O_8$ has a low N-content of 1.4 nmol·ml^{-1} and is low in $\delta^{15}N$. An average $\delta^{15}N$ of -15‰ is observed during a 2 months examination by using a spiking method. This $\delta^{15}N$ background of the POR solution would cause a shift by -1 - -2‰ in the $\delta^{15}N$ of samples that contain 10-20 nanomolar reduced N, and requires that the $\delta^{15}N$ of recrystallized $K_2S_2O_8$ should be examined along with sample

oxidization. The overall measurement of the $\delta^{15}N_{pigment}$ shows a consistent performance with an average analytical precision better than ±0.5‰ (1σ).

3 Spatial distribution of $\delta^{15}N_{cholorophyll-a}$ in surface sediment of the northern Benguela Upwelling System

Abstract

We analyze the $\delta^{15}N$ of chlorophyll-a (Chl-a) in surface sediments of the northern Benguela Upwelling System (BUS), a coastal upwelling system with high primary productivity in surface waters and intensive denitrification in the subsurface oxygen minimum zone (OMZ). Upwelled nitrate is the major N-input to the northern BUS, and is mainly removed through processes of denitrification and phytoplankton assimilation. Both processes gradually enrich the residual nitrate pool in ^{15}N that is assimilated to synthesize chlorophyll a (Chl-a). The $\delta^{15}N_{Chl-a}$ distribution in surficial sediment should thus characterize the combined effects of denitrification and biological assimilation on $\delta^{15}N$ of nitrate in the overlying shelf waters, and should image the spatial patterns of denitrification and nitrate assimilation, respectively, in the northern BUS.

Paired $\delta^{15}N_{Chl-a}$ and bulk sediment $\delta^{15}N$ ($\delta^{15}N_{sed}$) data of 27 surface sediment samples lack a significant correlation (R^2 0.19, P<0.02). This insignificant correlation and the spatial discrepancies between $\delta^{15}N_{sed}$ and $\delta^{15}N_{Chl-a}$ suggest a varying post-depositional bias of diagenetic processes on the $\delta^{15}N_{sed}$. The onshore-offshore difference (Δ) of $\delta^{15}N_{Chl-a}$ in the northern sector of the studied area (17°-19°S,11°–14°E) is created mainly by fractionation effects of progressive plankton assimilation, because the OMZ is weak and water-column denitrification is insignificant. In the southern sector (19°-23°S, 11°–14°E) where the OMZ is prominent, additional nitrate loss through denitrification causes most of the onshore-offshore difference (Δ) of $\delta^{15}N_{Chl-a}$. Along the inner shelf (17°-23°S), the $\delta^{15}N_{Chl-a}$ correlates significantly with both salinity (R^2=0.76, P<0.01) and temperature (R^2=0.82, P<0.01) at 10m water depth. The southward increase of $\delta^{15}N_{Chl-a}$ along the inner shelf mirrors an increase of $\delta^{15}N_{NO3}$ from 17°S to 23°S, from which an annual denitrification rate of ~0.6 Tg yr^{-1} is calculated based on the south-north difference in $\delta^{15}N_{Chl-a}$ of 11.3‰. In coastal upwelling zones where OMZ intensity is coupled to the upwelling dynamics over the

shelf, the $\delta^{15}N_{Chl\text{-}a}$ in surface sediment captures the spatial patterns of integrated N-loss intensity.

35

3.1 Introduction

The Benguela Upwelling System (BUS, Fig. 3.1) is one of the four major Eastern Boundary Upwelling Systems (EBUSs) and has the highest primary productivity of all these systems (Carr and Kearns 2003). The upwelling hydrodynamics subdivide the BUS roughly into a northern (17°S - 26°S) and a southern part (26°S-34°S). The northern BUS has a higher primary productivity and more severe oxygen-deficient conditions than the southern BUS (Brüchert et al., 2006, Monteiro et al., 2006). The upwelling water in the northern BUS (Fig. 3.1, right panel) is mainly composed of two water masses: (i) nutrient-rich and oxygen-depleted South Atlantic Central Water (SACW) and (ii) nutrient-poor but well-oxygenated Eastern SACW (ESACW) (Mohrholz et al., 2008). The SACW supplies most of the reactive N in form of nitrate to the northern BUS.
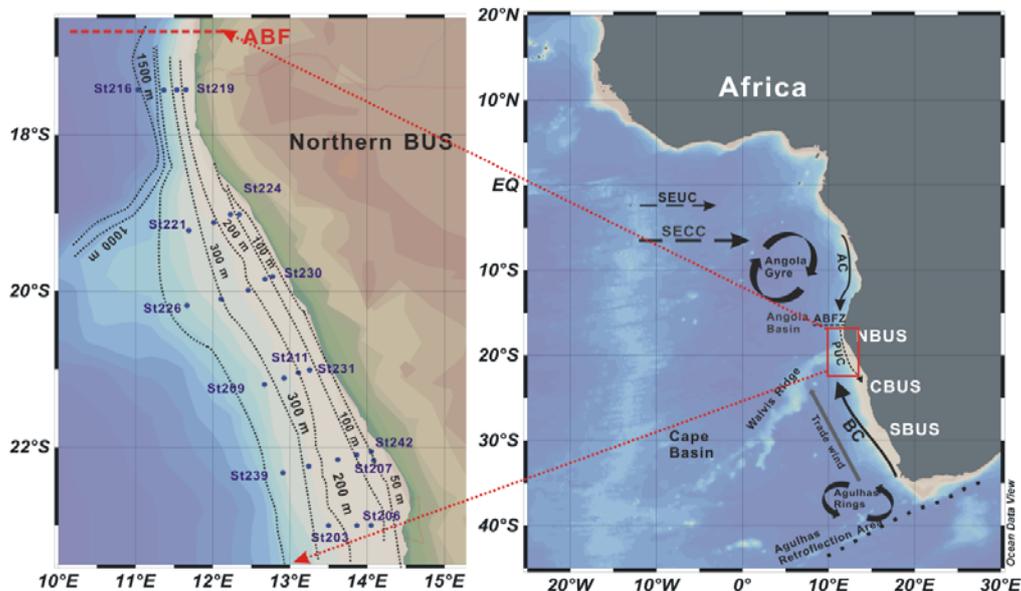
Fig.3.1 M76-2 surface sediment sampling stations: in left panel, the dashed lines denote depth contours; right panel: Arrows show surface (solid) and subsurface (dashed) hydrographic features: NBUS=northern BUS, BUS=central BUS, SBUS=southern BUS, ABF= Angola-Benguela Front, BC= Benguela Current, AC = Angola Current, PUC = Poleward Undercurrent, SEUC=South Equatorial Under Current, SECC=South Equatorial Counter Current (Arhan et al., 2003, Mercier et al., 2003).

The two most prominent biochemical processes to remove the nitrate from the

upwelling waters are planktonic nitrate assimilation and denitrification. The first turnover step in planktonic nitrate assimilation ($NO_3 \rightarrow NO_2$) is similar to denitrification and enriches the residual nitrate pool in ^{15}N (Granger et al., 2004, Karsh et al., 2012, Karsh et al., 2014). After uptake from ambient water, NO_3 is stepwise reduced to NH_4^+, and then is used in the synthesis of chlorophyll pigments (Grimm et al., 2006). The assimilation of nitrate by marine plankton is associated with a per mil fractionation factor (ε) of 4-10‰ (Waser et al., 1998, Needoba et al., 2003, Granger et al., 2004), so that the $\delta^{15}N$ of both total biomass and Chl-a is lower than that of the assimilated nitrate (York et al., 2007, Higgins et al., 2010, Higgins. et al., 2011).

Heterotrophic denitrification, occurring at oxygen concentration <20 $\mu mol \cdot l^{-1}$ (Kalvelage et al., 2011), is the other nitrate removal pathway that is as well associated with an ε of 10-30‰ (Sigman et al., 2009, Kritee et al., 2012). After the upwelled nitrate is consumed by denitrification in suboxic water column intervals, the residual nitrate pool enriched in ^{15}N is upwelled to the euphotic zone and is assimilated by phytoplankton. The denitrification effect raises the $\delta^{15}N_{Chl-a}$ and offsets the negative fractionation effect caused by assimilation. The local nitrate pool is also replenished by nitrification, a stepwise oxidization of ammonium that is released via ammonification of organic matter (Granger et al., 2011, Gaye et al., 2013). Thus, the $\delta^{15}N_{Chl-a}$ integrates isotopic signatures of nitrate affected by specific sources, sinks, and diverse conversion processes in the nitrate pool, and characterizes the sum of major nitrate cycling processes.

The same is assumed for $\delta^{15}N_{sed}$, but the isotopic composition in bulk biomass (the precursor of sediment) is vulnerable to isotopic biases during early diagenesis and remineralization (Lehmann et al., 2002, Gaye-Haake et al., 2005). Differing from that, $\delta^{15}N_{Chl-a}$ is barely affected by the diagenetic processes (Sachs et al., 1999), because the N-atoms of chlorophyll are tightly embedded in the molecular skeleton of the porphyrin structure and are not exchanged unless the porphyrin ring is broken.

The spatial distribution of $\delta^{15}N_{Chl-a}$ in surface sediments on the upwelling shelf could

answer the following two questions:

i. How are denitrification and nitrate assimilation processes coupled to upwelling dynamics at different shelf locations?

ii. What are the spatial patterns of denitrification and nitrate assimilation, respectively, in the northern BUS? And what are their relative contributions to the loss of nitrate?

Here we present $\delta^{15}N$ data for both bulk surface sediment and Chl-a contained in the same samples in the northern BUS, along with marine cruise (M76-2) CTD data to picture upwelling dynamics and OMZ, and other proxies related to export production. We will firstly compare the paired $\delta^{15}N$ proxies ($\delta^{15}N_{Chl-a}$, $\delta^{15}N_{sed}$), and interpret their differences in spatial distribution in surface sediment. We further characterize the spatial distribution of $\delta^{15}N_{Chl-a}$ and attempt to segregate the effects of phytoplankton assimilation and denitrification on $\delta^{15}N_{Chl-a}$. Finally, we discuss the biogeochemical implications of $\delta^{15}N_{Chl-a}$ for N-cycling in the northern BUS.

Study Area

Coastal upwelling

The upwelling dynamics over the shelf distinguish 2 sectors in the studied area (Fig.2) (Muller et al., 2014). The northern sector stretches from 17-19ºS and the southern sector from 19-23ºS, which are denoted here as northern and southern sector. The two sectors significantly differ in water mass composition during the upwelling seasons. The northern sector is dominated by waters of the meridional Polarward Under Current (PUC) that carries pristine SACW southward close to the coastline (Mohrholz, 2008, Veitch, 2010). The southern sector is a mixing zone where the southward flowing SACW and waters of the northward flowing ESACW meet. Significant differences of upwelling dynamics also exist between the inner shelf (first shelf break) and the outer shelf waters (beyond the first shelf break). The inner shelf is entirely filled with either the SACW during a spring-summer upwelling season, or the ESCAW during a late-autumn to winter of upwelling weakening period. By contrast, the water masses compositions at the outer shelf vary dynamically with latitudes and

seasons. The outer shelf of the southern sector (19-23ºS) is dominated by the ESACW, but the subsurface layer over the outer shelf of the northern sector (17-19ºS) is dominated on an annual average by the SACW (Muller et al, 2014). The differences in shelf upwelling dynamics in the northern BUS causes the nitrate input of the SACW source to vary considerably in space.

Nitrate dynamics

The spatial inhomogeneity in hydrodynamics determines that the upwelling delivery of nitrate varies over our studied area (Fig. 3.2). The nitrate distribution at 20m water depth pictures a narrow nitrate-rich band hugging the coast along the inner shelf, while a band of low nitrate concentrations extends southward to 23ºS over the outer shelf.
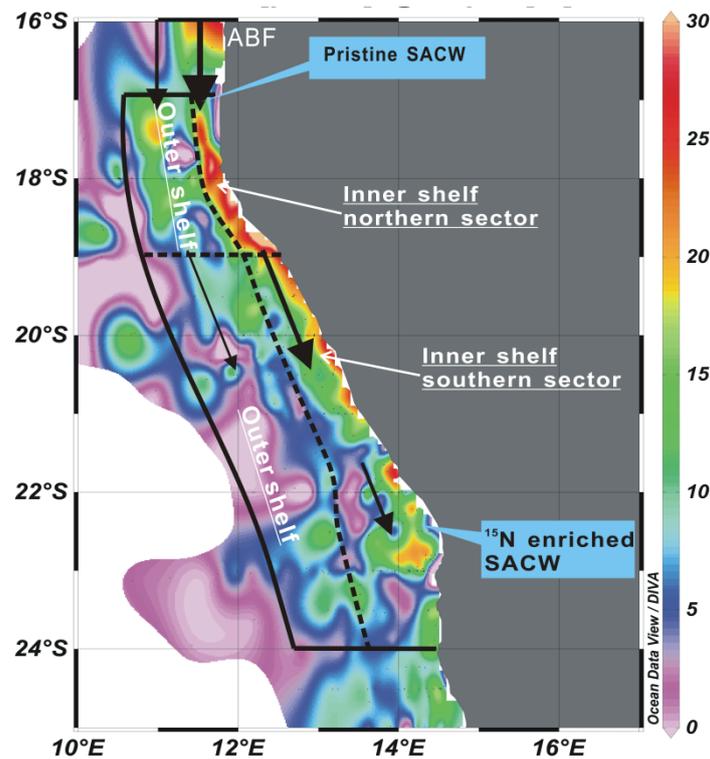
Fig.3.2 The nitrate distribution at the depth of 20m in the studied area, with color bar indicating the concentration (μmol·l^{-1}). Black solid line marks the boundary of the study area 17-24ºS. The two dashed lines split the study area into 4 sectors: the meridional dashed line marks the 200m depth contour line, the latitudinal dashed line at 19ºS marks the boundary between the northern and southern sub-areas. Arrows refer to the advection of SACW, and the thickness of arrows roughly matches the nitrate concentration. This figure is based on the Namibian Collection of Bottle dataset.

Over the inner shelf from 17 ºS to 23 ºS, nitrate concentrations vary within 35-20 μmol·l^{-1} at the bottom of the euphotic zone, while over the outer shelf at 17°S, nitrate is only 10-15 μmol·l^{-1}, suggesting that only a small fraction of the nitrate carried by pristine SACW is available to plankton assimilation. In contrast, a larger proportion of nitrate (>20 μmol·l^{-1}) enters the euphotic layer over the outer shelf at 23 °S. The inner shelf receives abundant nitrate from the upwelled SACW, but the deeper depth of both the thermocline and surface mixed layer over the outer shelf prevents the upward advection and diffusion of the nitrate to the euphotic zone (Monteiro et al., 2005, Jacox and Edwards 2011). The inhomogeneity in the nitrate concentrations in shelf waters governs the primary production, and causes the OMZ and denitrification intensity to vary across the northern BUS.

3.2 Materials and methods

3.2.1 Sediment sampling and processing

27 surface sediment samples (Fig. 1, left panel) were taken during the cruise M76-2 (May, 2008). Upon retrieval, the surface sediment samples were kept in evacuated and sealed polyethylene bags and were stored at -20 ℃, until they were freeze-dried (-20℃), ground, and kept in air-tight glass bottles in the dark for further analyses. General sediment properties are summarized in Table 1 of the supplementary material.

3.2.2 Elemental and isotopic analyses

Total nitrogen (TN, in wt%) and total organic carbon (TOC, in wt%) were measured in duplicate by a Carlo Erba 1500 CNS Analyser (Milan, Italy).

($\delta^{15}N = \frac{Rsample - Rstandard}{Rstandard} \times 1000$ [‰]; with $R = \frac{^{15}N}{^{14}N}$ and $R_{standard}$ being the $\frac{^{15}N}{^{14}N}$ ratio of the reference standards, atmospheric N_2 used as the reference)

Bulk $\delta^{15}N$ were determined using a Finnigan MAT 252 gas isotope mass spectrometer connected with a Carlo Erba NA-2500 elemental analyzer. Pure tank N_2 calibrated against the reference standards IAEA-N-1 and IAEA-N-2 of the International Atomic Energy Agency and a sediment standard were used as working standards. A

round-robin experiment over a wide range of sample types from diverse depositional environments revealed a mean standard deviation of 0.31‰ (Bahlmann et al., 2010).

3.2.3 Chlorophyll pigments extraction and $\delta^{15}N_{Chl-a}$ measurement

The chlorophyll pigments were extracted from sediment with a mixture of dichloromethane (DCM) and methanol (9:1) in an ASE 200 (Accelerated Solvent Extraction System, Thermo Fisher Scientific Inc.). Highly pure N_2 gas is used throughout the extraction to prevent the degradation or oxidization of chlorophyll pigments. Chlorophyll pigments were separated by a HPLC procedure modified from Sachs and Repeta (Sachs and Repeta 2000) and Higgins et al (2008, 2011). The separated pigments were identified by chromatography spectra with reference to Chl-a/b standards (Sigma-Aldrich Co.) and cross-checked with published spectra of chlorophyll pigments (Grimm et al., 2006, Roy et al., 2011).

Pigment oxidization

Potassium persulfate ($K_2S_2O_8$) was crystallized 4 times before being dissolved in a NaOH (Semi-conductor grade, Sigma-Aldrich Co.) solution (0.15 mol·l^{-1}) to reach a final concentration of 0.05 mol·l^{-1} (referred to as POR). The purified pigment fraction was dried under a gentle N_2 gas flow in a screw-top quartz tube with a Teflon-lined cap, and 2 ml of POR were added. The quartz tube was sealed and autoclaved at 121℃ for 30 minutes. Then the autoclaved solution was neutralized with H_2SO_4 (10% standard solution, Sigma-Aldrich Co.) to pH 7.0±0.5 for the next step of $\delta^{15}N_{NO3}$ measurement.

Measurement of $\delta^{15}N_{NO3}$

$\delta^{15}N$ of nitrate was determined using the "denitrifier method" (Sigman et al., 2001, Casciotti et al., 2002). The sample solutions were injected into a suspension of *Pseudomonas* a*ureofaciens* (ATCC#13985). The dissolved nitrate in the samples was quantitatively converted to N_2O gas, which was stripped from the vials by purging with helium, concentrated and purified on a Gas-Bench II, and analyzed on a Delta V mass spectrometer (Thermo Finnigan). Replicate measurements were performed, and

two international standards IAEA-N3 ($\delta^{15}N$ = +4.7‰) and USGS 34 ($\delta^{15}N$ = −1.8‰,), were measured with each batch of samples. For quality assurance of the results, we used an internal potassium nitrate standard that was measured with each batch of samples. Isotope values were corrected using the "bracketing scheme" (Sigman et al., 2009) for the two-point correction referring to IAEA-N3 and USGS34 for $\delta^{15}N_{NO3}$. The standard deviation for international and in-house standards was 0.3‰ for $\delta^{15}N$ (n = 6), deviations for replicate samples were within the same range.

3.3 Results

3.3.1 Surface sediment
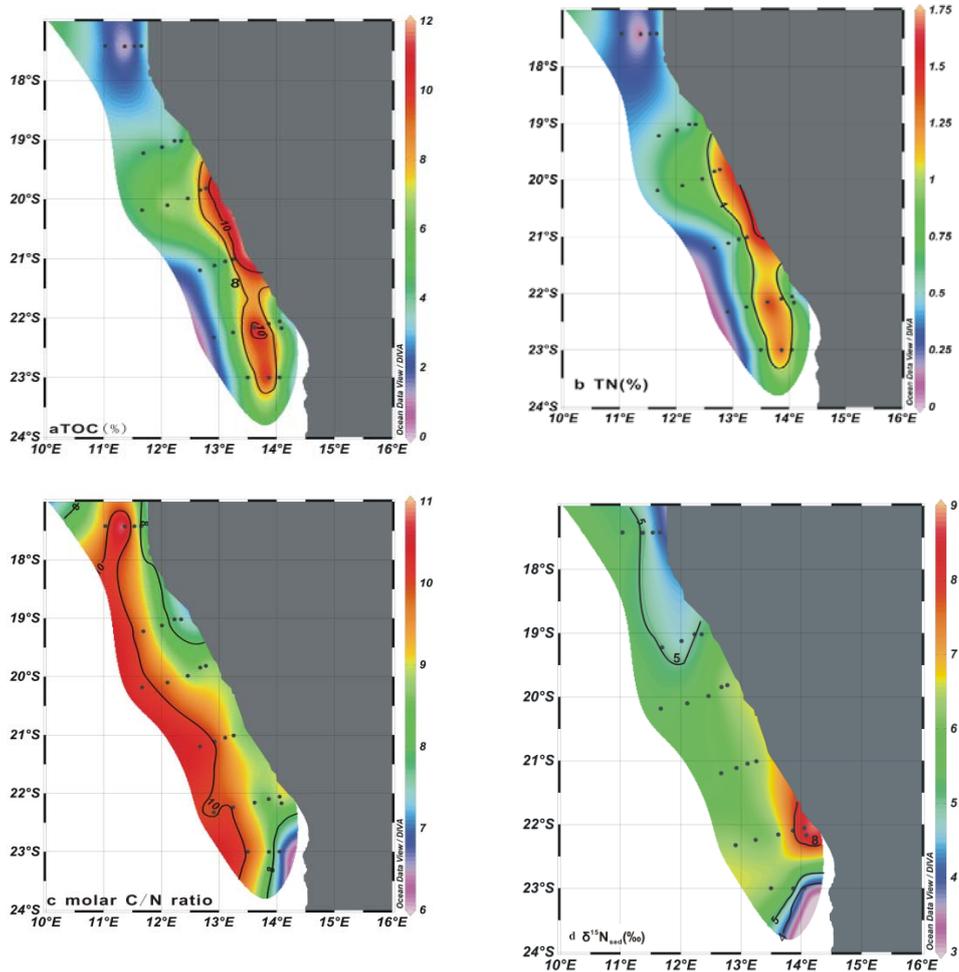
Fig.3.3 (a) TOC (%) in surface sediment samples; (b) TN (%) in surface sediment samples; (c) Molar ratio of TOC and TN in surface sediment samples; (d) $\delta^{15}N_{sed}$ (‰) in surface sediment samples

The TOC content (Fig. 3.3a) was between 0.72% (ST 217, 17.4°S) and 12.12% (ST 205, 23°S). The belt of richest TOC (8-12%) was found along the coast line from 19.5°S ~ 23°S at water depths of 100-150m. The TN (Fig. 3.3b) distribution pattern follows that of TOC, with highest concentrations measured at ST 241 (1.56%, ~22°S) and lowest at ST 217 (0.07%, 17.4°S). The 1% contour line of TN roughly envelopes the shelf area shallower than 200 m. The TOC:TN molar ratio (C/N, Fig. 3.3c) varies from 6.7 (ST206, 23°S) to 11.75 (ST217, 17.4°S), decreasing landward from the

upper continental slope. The $\delta^{15}N_{sed}$ (Fig. 3.3d) shows an increasing trend from ~17°S to 23°S along the coast with the highest value at ST 207 (8.89‰, water depth 70 m, 22.2°S) and lowest at ST 219 (4.04‰, water depth 93m, 17.4°S) and ST 206 (3.46‰, water depth 130.7m, 23°S), producing a north-south difference of ~5‰.

3.3.2 The spatial distribution of $\delta^{15}N_{Chl-a}$
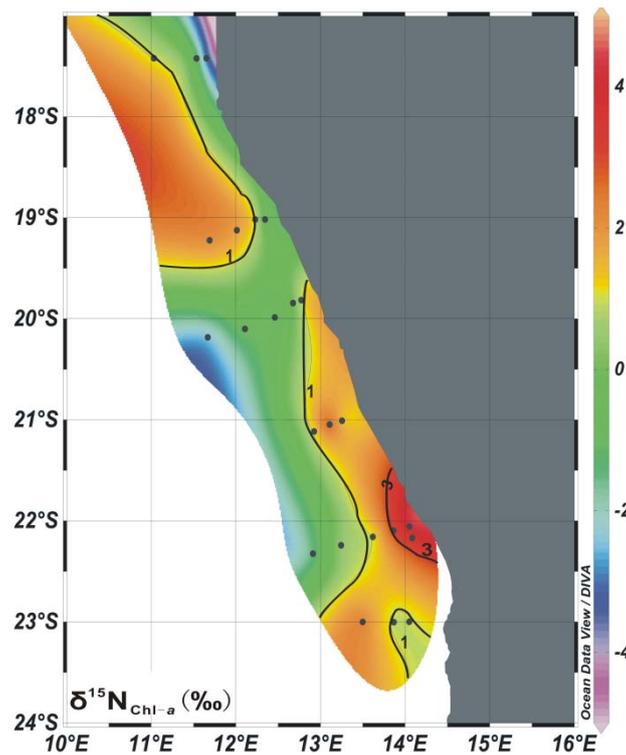
Fig.3.4 Distribution of $\delta^{15}N_{Chl\,a}$ (‰) in surface sediment stations
(M76-2, May 2008)

A high value $\delta^{15}N_{Chl\,a}$ of 4.54‰ was measured at 22°-22.5°S (ST242, Fig. 3.4) and a low value of -4.50‰ at 17°S (ST219, Fig. 3.4), producing a range in $\delta^{15}N_{Chl-a}$ of ~9‰. Similar to $\delta^{15}N_{sed}$, the $\delta^{15}N_{Chl-a}$ also shows a southward increase along the inner coast, while an offshore decrease is observed across the shelf in the 20°-23°S sector of the shelf and upper continental slope. Another comparatively high $\delta^{15}N_{Chl-a}$ area (>2‰) corresponds to the offshore sector (18°-20°S, bottom depth ~ 400m), from where $\delta^{15}N_{Chl-a}$ decreases to -1‰ towards the coast.

3.4 Discussion

The $\delta^{15}N_{Chl-a}$ depends on the $\delta^{15}N_{nitrate}$ that is coined by various N-cycling processes occurring in association with planktonic assimilation of nitrate upwelled into the euphotic zone and suboxic processes consuming nitrate in the OMZ on the shelf and upper slope of the northern BUS. Both are directly driven by over-shelf upwelling dynamics that determine nitrate abundance and OMZ state. In the following sections, we firstly compare the differences in spatial patterns of $\delta^{15}N_{sed}$ and $\delta^{15}N_{Chl-a}$, and discuss the impacts of major biogeochemical processes on the spatial pattern of $\delta^{15}N_{sed}$ (3.4.1). Then, we separately examine how plankton assimilation (3.4.2) and denitrification (3.4.3) imprint on the spatial distribution patterns of $\delta^{15}N_{Chl-a}$, and link them to the nitrate dynamics and OMZ locations over the shelf. Comparing the patterns in the northern sector (with weak OMZs) with those in the southern sector (with intensive OMZs), we can further segregate the effects of plankton assimilation and denitrification on the $\delta^{15}N_{Chl-a}$ (3.4.4). Lastly, we explore the implications of the spatial $\delta^{15}N_{Chl-a}$ distribution for N-cycling processes in the northern BUS (3.4.5).

3.4.1 Comparison of $\delta^{15}N_{sed}$ and $\delta^{15}N_{Chl-a}$

The process of nitrate assimilation has a strong fractionation effect on ^{15}N (Waser et al., 1998, Needoba et al., 2003) and thus on the $\delta^{15}N$ of planktonic biomass, the precursor of $\delta^{15}N_{sed}$. As a result, a spatial co-variation is expected between the $\delta^{15}N_{sed}$ and the nitrate concentration in the surface layer, which means a higher $\delta^{15}N_{sed}$ corresponds to a lower nitrate concentration that is caused by progressive nitrate asslimilation (Altabet and Francois 1994, Altabet et al., 1999). But this co-variation is not recognized from the spatial distributions of $\delta^{15}N_{sed}$ (Fig. 3.3d) and nitrate concentration at the depth of 20m in the studied area (Fig. 3.2). At the inner shelf, the gradient of southward increasing $\delta^{15}N_{sed}$ can not be explained by the effect of progressive nitrate assimilation since it unlikely happens within the nitrate rich band that closely hugs the coast from 17^0S to 23^0S. In the north (17-19^0S) and south parts (21-23^0S) of the studied area, the two different onshore gradients of $\delta^{15}N_{sed}$, as well,

can not be simply attributed to the effect of nitrate assimilation, because the nitrate concentration shows a spatially-unified onshore increaseing trend. The surficial distribution of $\delta^{15}N_{sed}$ suggests that the nitrate assimilation is not the only process that impacts its distribution pattern in the northern BUS.
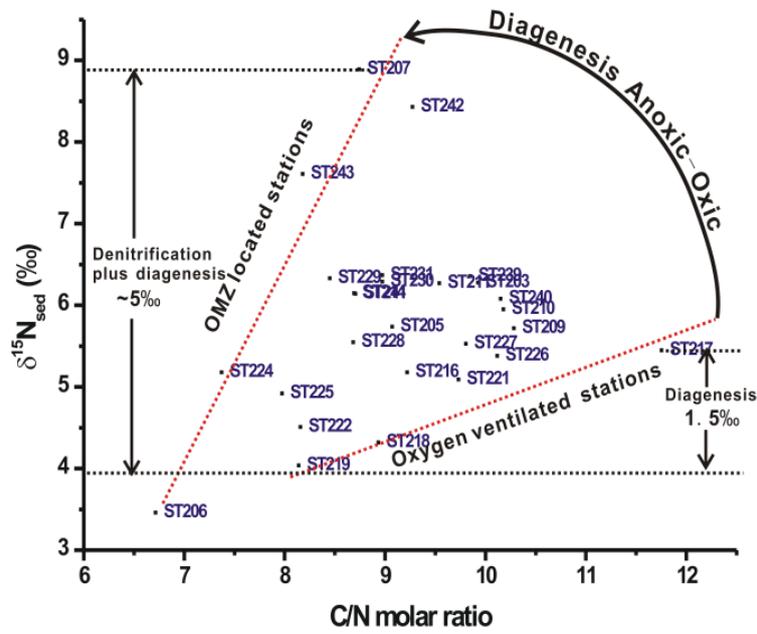
Fig.3.5 The variation of the $\delta^{15}N_{sed}$ with C/N ratio at shelf stations (the upper and lower black dashed line respectively notes the highest and lowest $\delta^{15}N_{sed}$; red dashed lines mark the oxic-anoxic boundaries in the studied area.)

The nitrate assimilation effect aside, the $\delta^{15}N_{sed}$-signals could as well be interpreted in terms of diagenesis, denitrification or a combination of both. The plot of $\delta^{15}N_{sed}$ and C/N (Fig. 3.5) indicates that both diagenesis and denitrification are affecting the spatial pattern of $\delta^{15}N_{sed}$, and highlights a coastward shift from diagenesis to denitrification as the dominant process. Freshly produced planktonic biomass in the northern BUS has a C/N ratio of ~7 that is close to the Redfield ratio (Holmes et al., 2002, Meisel et al., 2011). The comparatively low C/N ratio (~8-9) in tandem with high $\delta^{15}N_{sed}$ (6-9‰) at the inner shelf stations (stations that are close to the red dashed line in the left) apparently do not bear the effect of oxic diagenesis that usually produces high C/N (~10-12) in association with high $\delta^{15}N_{sed}$ (Gaye-Haake et al., 2005). A reasonable explanation is that the anoxic conditions in shelf waters promote

denifitrication that raises $\delta^{15}N_{sed}$ while proventing the C/N ratios from being elevated. On the contrary, the higher C/N ratios (10-12) associated with low $\delta^{15}N_{sed}$ (4-6‰) at outer shelf stations correspond to the $\delta^{15}N$ signal of pristine SACW-sourced nitrate that does not undergo denitrification, but overprinted by oxic diagenesis. For instance, the station 219 receives prestine SACW nitrate resulting in a $\delta^{15}N_{sed}$ value of ~4‰, while the intensive denitrification at the station 207/242 (22.5ºS) produces a $\delta^{15}N_{sed}$ value of ~9‰, a zonal $\delta^{15}N_{sed}$ gradient of ~5‰. By contrast, the laditudinal gradient in $\delta^{15}N_{sed}$ at the 17ºS transect shows a seaward increase by only ~1.5‰ suggesting that the increasing exposure time to oxygen in offshore direction leads to a stronger diagenetic effect on $\delta^{15}N_{sed}$, and that the increase of ~1.5‰ on $\delta^{15}N_{sed}$ is attributed to oxic diagnesis (Robinson et al., 2012).

The spatial $\delta^{15}N_{sed}$ gradients suggest that the denitrification modifies the $\delta^{15}N_{sed}$ twice as strong as the oxic diagenesis (~5‰ vs 1.5‰), and overwhelms both diagenesis and nitrate utilization effects on the inner shelf of the northern BUS. The $\delta^{15}N_{sed}$ and C/N on the one hand demarcate the boundaries for the occurrence of oxic diagenesis and denitrification in association with OMZ, on the other hand, they cannot segregate the effects of dentrification and diagenesis under anoxic conditions.
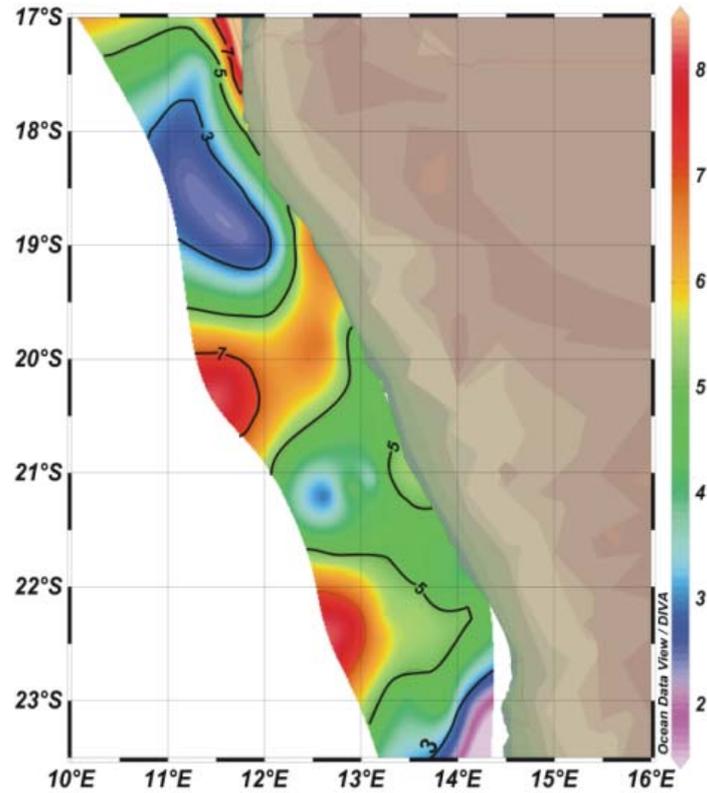
Fig.3.6 The spatial pattern of the $\Delta(\delta^{15}N_{sed} - \delta^{15}N_{chla})$, color bar unit is in per mil (‰).

The sedimentary organic matter and chlorophyll pigment both orginate from the biomass that are imprinted with the $\delta^{15}N$ signal of the nitrate pool assimilated by phytoplanton. As reported by Sachs et al (2000), the $\delta^{15}N$ of fresh biomass shows a consistent and higher value of 5.1±1.1‰ than the $\delta^{15}N$ of Chl-a. But in the 27 surface samples in this study, an unexpectedly weak correlation between the $\delta^{15}N_{sed}$ and $\delta^{15}N_{Chl-a}$ is observed (R^2=0.19, P=0.012). In our interpretation, the diagenesis occurring in the water column and in the surface sediment is responsible for such a mismatch by altering $\delta^{15}N_{sed}$ and thus erasing the consistency with $\delta^{15}N_{Chl-a}$. Either oxic or anoxic diagenesis, or a combination of both, could overprint the $\delta^{15}N_{sed}$, but to different extents. It is widely accepted that an alteration by +1 - +5‰ on the $\delta^{15}N$ of organic matter is due to the fractionation effect of oxic degradation (Robinson et al., 2012). The effect of anoxic diagenesis on $\delta^{15}N$ of organic matter is much smaller (<2‰) than that of oxic degradation (Meisel and Struck 2011, Möbius 2013), or even negative (-1- -3‰) (Lehmann et al., 2002).

The $\delta^{15}N_{sed}$ is affected by diagenesis at locations whereas the $\delta^{15}N_{Chl-a}$ retains the signal of precursor biomass. The difference (Δ) between $\delta^{15}N_{sed}$ and $\delta^{15}N_{Chl-a}$ should thus cancel out the signal of denitrification contained in both, and thus reflect the diagenesis intensity either under oxic or anoxic conditions in the water column and surface sediment (Fig. 3.6). The redox conditions in water column and at the sediment-water interface govern the alterations imposed on the N-isotope composition of bulk biomass through oxic-anoxic diagenesis (Lehmann et al., 2002). This implies that the the OMZ percentage in water column should co-vary significantly with diagenetic intensity as identified by $\Delta(\delta^{15}N_{sed}-\delta^{15}N_{Chl-a})$. The OMZ is defined as the dissolved oxygen concentration is below 20 $\mu mol \cdot l^{-1}$. The OMZ percentage (%) in the water column is calculated by the thickness of the OMZ interval divided by the bottom depth of sampling station (dataset of dissolved oxygen concentration is from marine cruise M76-2). The correlation between OMZ percentage and the $\Delta(\delta^{15}N_{sed}-\delta^{15}N_{Chl-a})$ (R^2=0.5, P=0.009, Fig. A3.1) just indicates that it is the spatial variance of relative OMZ intensity that drives the denitrification and diagenesis to modify $\delta^{15}N$ of bulk sediment and establishes the distribution pattern of $\Delta(\delta^{15}N_{sed} -\delta^{15}N_{Chl-a})$ over the shelf. The correlation is not as significant as expected, which we believe mainly orginate from the different time periods that are represented: the $\Delta(\delta^{15}N_{sed} -\delta^{15}N_{Chl-a})$ depicts sedimentation during an estimated period of 1-3 yrs, while the OMZ proportions are calculated based on the in-situ measurement during a cruise situation when upwelling was weak.

The consistent 5.1±1.1‰ difference between $\delta^{15}N$ of fresh biomass and $\delta^{15}N_{Chl-a}$ (Sachs et al., 1999, York et al., 2007) is used as a threshold for the effects of diagenesis evaluation: the smaller the Δ (< 5.1±1.1‰) is, the stronger the anoxic diagenetic effect is overprinted on $\delta^{15}N_{sed}$, and vice versa. In figure 6, the areas with Δ<5 are located at the upper slope of Walvis Ridge (18-19ºS) and on the inner shelf at 20-23 ºS, which agree broadly with the locations of OMZs.

Our results highlight that $\delta^{15}N_{sed}$ is only qualified to capture a general variation pattern of isotopic fractionation processes acting on source nitrate, but that it is very

vulnerable to isotopic modification under different redox conditions. In contrast, $\delta^{15}N_{Chl-a}$ is a more reliable marker to record paleoenvironmental signals.

3.4.2 Effects of biological nitrate assimilation on the $\delta^{15}N_{Chl\,a}$ distribution

The extent of nitrate assimilation is determined by plankton growth conditions that include nitrate and phosphorus availability, temperature, irradiance strength in the euphotic zone, and bioavailability of iron, etc. The growth conditions control the efflux rate of the intracellular $^{15}N\text{-}NO_3$ to the ambient nitrate pool (Granger et al., 2004, Karsh et al., 2014), which expresses the fractionation effect on $\delta^{15}N$ of nitrate and further on the $\delta^{15}N_{Chl-a}$. The spatial variability of nitrate assimilation is therefore one factor that contributes to the distribution pattern of the $\delta^{15}N_{Chl-a}$ in surface sediment of the shelf.

The spatial variability of plankton growth conditions in the northern BUS

Isotope fractionation under nitrate-limitations occurs only when residual nitrate concentration is below the half saturation constant (Swart et al., 2014) - a condition never met over the inner shelf in our study area, where sufficient nitrate is provided by upwelling currents. Phosphate concentrations are high and are not limiting primary production in the study area (Nagel et al., 2013). Other phytoplankton growth conditions, like temperature and light (Wada 1980, Granger et al., 2004), are comparatively uniform along the inner shelf from 17°S to 23°S. A putative limitation of bio-available iron should also be uniform in our study area (Sohm et al., 2011, Capone 2014). Therefore, plankton growth conditions differ little between inner shelf stations from 17 °S to 23 °S over the time period represented by the surface layer of sediments, and differences of N-isotope fractionation effects caused by plankton assimilation may be discounted.

The outer shelf waters differ from the inner shelf mainly by the nitrate remaining for assimilation. The surface waters of the outer shelf in the northern sector (17-19ºS) have low nitrate concentrations (Namibia Collection of Bottle dataset), and the nitrate consumption by assimilation progressively lowers its concentration in the surface

layer further ($<\sim 5$ µmol·l^{-1}). With progressive consumption, the remaining nitrate becomes gradually enriched in ^{15}N . This progressive enrichment of ^{15}N in the nitrate pool is reflected in an inshore-offshore gradient of $\delta^{15}N_{Chl-a}$ of 6~7‰ in the northern sector of our study area. However, this onshore-offshore gradient is reversed in the southern sector, which suggests a mechanism that overwhelms nitrate utilization to create the surface distribution of $\delta^{15}N_{Chl-a}$.

The fractionation effect of nitrate assimilation on the spatial ö^{15}N$_{Chl-a}$ distribution

The $\delta^{15}N_{Chl-a}$ (product) is much lower than the δ^{15}N of source nitrate (reactant), and reflects the fractionation factor ε_{ass} of the nitrate assimilation process. A positive ε_{ass} indicates an enrichment of ^{15}N in the reactant. For a system in steady state, i.e. the inner shelf waters with continuous nitrate inputs of uniform δ^{15}N, the apparent ε_{ass} to the reactant equals the difference between $\delta^{15}N_{NO3}$ and $\delta^{15}N_{Chl-a}$ ($\varepsilon_{ass} = \delta^{15}N_{NO3} - \delta^{15}N_{Chl-a}$), while in a closed system with progressive nitrate consumption, i.e. at the surface waters of the outer shelf where nitrate sufficiency are limited, the ε_{ass} follows the Rayleigh fractionation model (Altabet and Francois 1994).

In our study, the lowest $\delta^{15}N_{Chl-a}$ of -4.5‰ coincides with nitrate concentrations of ~ 40 µmol·l^{-1} on the inner shelf at 17°S, near the source of SACW with a $\delta^{15}N_{NO3}$ of 6.1‰ (Nagel et al., 2013, Schukat et al., 2014), so that the ε_{ass} is ~10.6‰. The southward increase of $\delta^{15}N_{Chl-a}$ to a maximum of 4.5‰ on the inner shelf at 22.5°S corresponds to an increase in $\delta^{15}N_{NO_3}$ of up to ~14‰ at 23°S (Nagel et al., 2013), so that the ε_{ass} is there ~9.5‰. Both these estimates of ε_{ass} are in broad agreement with the reported ε_{ass} of 4-10‰ in natural settings (Needoba et al., 2003, Granger et al., 2004). The almost uniform value of ε_{ass} at 17 °and 22.5 °S support our inference that the plankton growth conditions on the inner shelf are uniform, and the spatial difference in fractionation effect on $\delta^{15}N_{Chl-a}$ by nitrate assimilation is negligible.

There are only a few reports on the fractionation effects of nitrate assimilation on $\delta^{15}N_{Chl-a}$ in natural settings. One of them (York et al., 2007) examined the

inter-seasonal $\delta^{15}N_{Chl-a}$ variation along a salinity gradient (0-30 PSU) in an estuary with no existence of water column denitrification, and the NO_3 was consumed progressively from ~50 to ~0 $\mu mol \cdot l^{-1}$. The total range of $\delta^{15}N_{Chl-a}$ in that study was -1.16 to 4.84‰, and thus had a narrower range than our results: the inter-seasonal variation in ε ($\delta^{15}N_{NO3}$ - $\delta^{15}N_{Chl-a}$) exhibited a narrow variance of ±0.78‰ around an annual average of 4.8‰. During the spring season, significant correlations between $\delta^{15}N_{Chl-a}$ and nitrate concentration, and between $\delta^{15}N_{NO3}$ and nitrate concentrations both suggested an apparent fractionation effect of plankton nitrate assimilation on $\delta^{15}N$ of Chl-a (York et al., 2007). Similarly in our study, the progressive nitrate utilization in outer shelf waters of the northern sector is reflected in increasing $\delta^{15}N_{Chl-a}$ of sediments towards the outer shelf waters of the northern sector that are mainly coined by the fractionation effect of nitrate assimilation. If nitrate of SACW provenance and $\delta^{15}N_{NO3}$ of 6.1‰ were upwelled into the photic zone and were assimilated over the inner shelf at 22.5°S, we would expect a $\delta^{15}N_{Chl-a}$ of -4‰ according to an ε_{ass} of ~10‰, which is much lower than our measured $\delta^{15}N_{Chl-a}$ of 4.5‰. The higher $\delta^{15}N_{Chl-a}$ recorded in surface sediments of the inner shelf at 23 °S thus must correspond to a nitrate pool enriched in ^{15}N and can not reflect phytoplankton assimilation alone.

3.4.3 Effects of denitrification process on the $\delta^{15}N_{Chl-a}$ distribution

Denitrification is the other process to significantly modify the $\delta^{15}N_{NO3}$ in upwelling waters and to affect the $\delta^{15}N_{Chl-a}$ distribution over the shelf. Denitrification, together with anammox and other nitrate-cycling processes, occurs intensively in the water column of the northern BUS (Kuypers et al., 2005, Monteiro and van der Plas 2006, Meisel et al., 2011), and significantly raises the $\delta^{15}N_{NO3}$ of residual nitrate (Nagel et al., 2013). This study does not specify the fractionation effects of each process involving nitrate, but considers all the fractionation effects as integrated influences on $\delta^{15}N_{NO3}$, among which denitrification arguably contributes the most to raise $\delta^{15}N_{NO3}$. To illustrate the spatial denitrification intensity, we depict the OMZ intensity over shelf at different water depths (Fig. 3.7) and choose a DO threshold of 20 $\mu mol \cdot l^{-1}$ to

outline the area where denitrification is likely to occur (Kalvelage et al., 2011, Kirkpatrick et al., 2012).
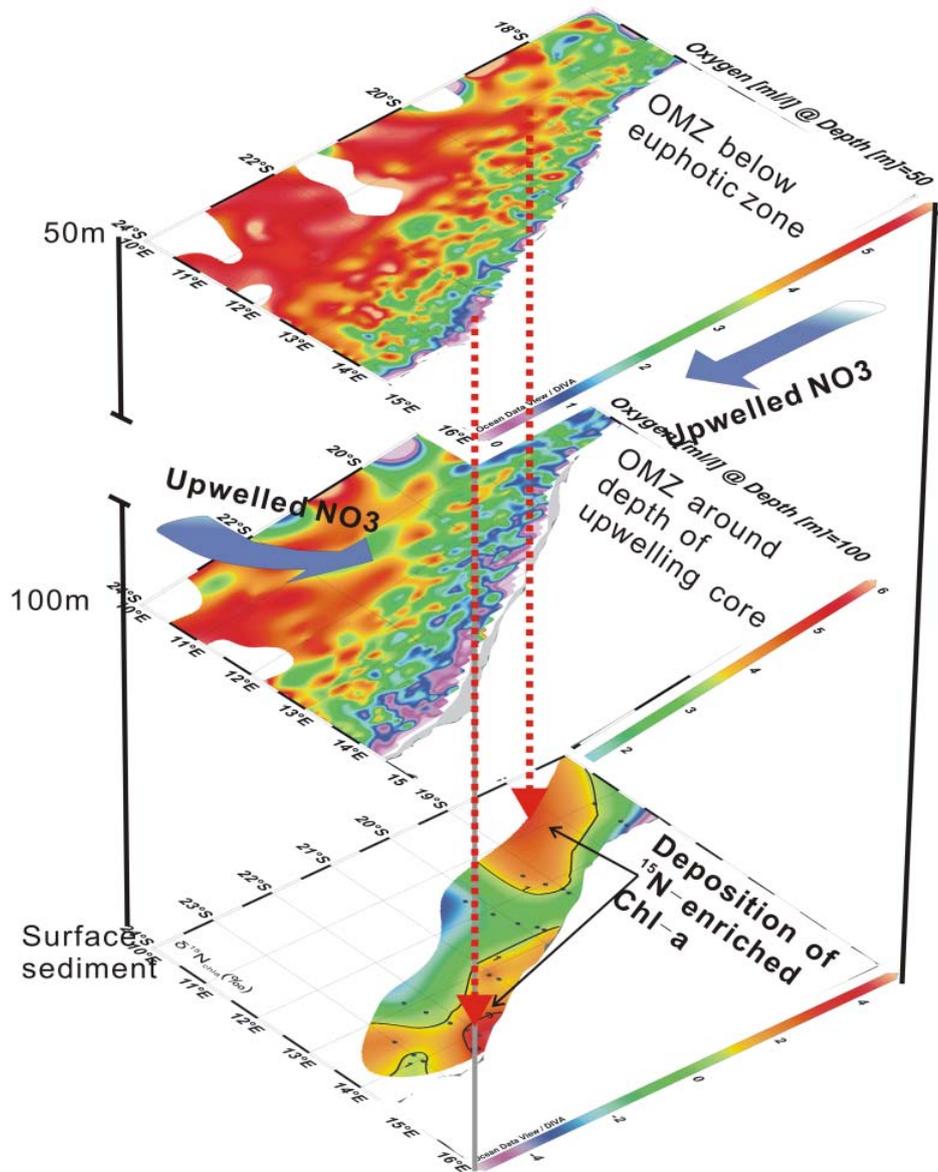
Fig.3.7 A 3-D map to illustrate vertical locations of OMZ and $\delta^{15}N_{Chl-a}$ distributions over the shelf: the solid blue arrow represents the upwelled nitrate of SACW source at a depth of 100 m, downward orange dashed arrow represents the deposition of Chl-a to shelf

The depths of 50m and 100m mark the baseline of the euphotic zone and the depth of thermocline (depth of upwelling core) in the northern BUS. The DO spatial distribution at the two depths (Fig. 3.7) outlines the trajectories through the OMZs where upwelled nitrate has undergone denitrification before it is assimilated by

53

plankton. The location of the OMZ core (DO < 20 µmol·l^{-1}) is located at 22°-23ºS and extends from the inner shelf to the upper continental slope. At a depth of 50m, the OMZ intensifies southward from 17°S and the along-shore increase of $\delta^{15}N_{Chl-a}$ tracks the OMZ intensification. To quantify the spatial OMZ distribution, the OMZ percentage (%) in water columns of each shelf station (cruise M76-2, CTD data) is calculated based on the DO threshold of 20 µmol·l^{-1}, and its significant correlation (R^2=0.65, P<0.0001, Fig. A3.2) with latitude (ºS) suggests a clear pattern of southward OMZ intensification. The $\delta^{15}N_{Chl-a}$ correlates positively with the OMZ percentages (%) as well at these shelf stations (R^2=0.55, P=0.003, Fig. A3.3), which further indicates the impacts of OMZ associated denitrification on the $\delta^{15}N_{Chl-a}$ distribution.

Another area of high $\delta^{15}N_{Chl-a}$ in surface sediments is located between 17.5°-19.5 ºS on the outer shelf, but it corresponds neither to the OMZ distribution at depth of 100m not at depth of 50m (Fig. 3.7). It is likely that the vertical location of the OMZ at depth interval of 50-100m in relation to the trajectory of the upwelled nitrate does not influence $\delta^{15}N$ in the upwelled nitrate pool.

To summarize, the spatial variance of denitrification intensity also plays a role in creating the $\delta^{15}N_{Chl-a}$ distribution pattern over the shelf. The high $\delta^{15}N_{Chl-a}$ in the inner shelf stations of the southern sector is mainly caused by fractionation in the course of the denitrification process. Over the outer shelf in the southern sector, the seaward decreasing $\delta^{15}N_{Chl-a}$ is the result of a weakening denitrification in offshore direction.

3.4.4 Segregating the effects of biological assimilation and denitrification on $\delta^{15}N_{Chl-a}$

In order to segregate the specific effect of assimilation and denitrification on $\delta^{15}N_{Chl-a}$ over the entire studied area, we choose salinity as a qualified tracer to characterize the processes of assimilation and denitrification in coastal waters, for two reasons: i) the nitrate in the northern BUS is supplied mainly by one single water mass, SACW, with fixed salinity, so the variations of salinity in the shelf waters track the upwelling dynamics of SACW and thus nitrate distribution; ii) the salinity gradient corresponds

to the OMZ intensity (R^2=0.50, P=0.013, Fig. A3.4) over the shelf, and thus to the OMZ-associated denitrification intensity. We use the salinity at the 10-20m layer, where the maximal fluorescence (Cruise M76-2 CTD data) indicates the most intensive phytoplankton growth and nitrate assimilation.

3.4.4.1 The correlation of $\delta^{15}N_{Chl\text{-}a}$ and salinity/temperature

The salinity and temperature at 10m (negligible variation down to 20m) of the inner shelf stations show a significant correlation with $\delta^{15}N_{Chl\text{-}a}$ (R^2 0.76 and 0.82, P<0.01, respectively; Fig 3.8a/b). The $\delta^{15}N_{Chl\text{-}a}$ at the furthest offshore stations (bottom depth >300m) also exhibit good correlation with salinity (R^2 0.71, n=7, Fig. 3.9), but are not significantly correlated with temperature (R^2 0.34, n=7) (Fig. A3.5).
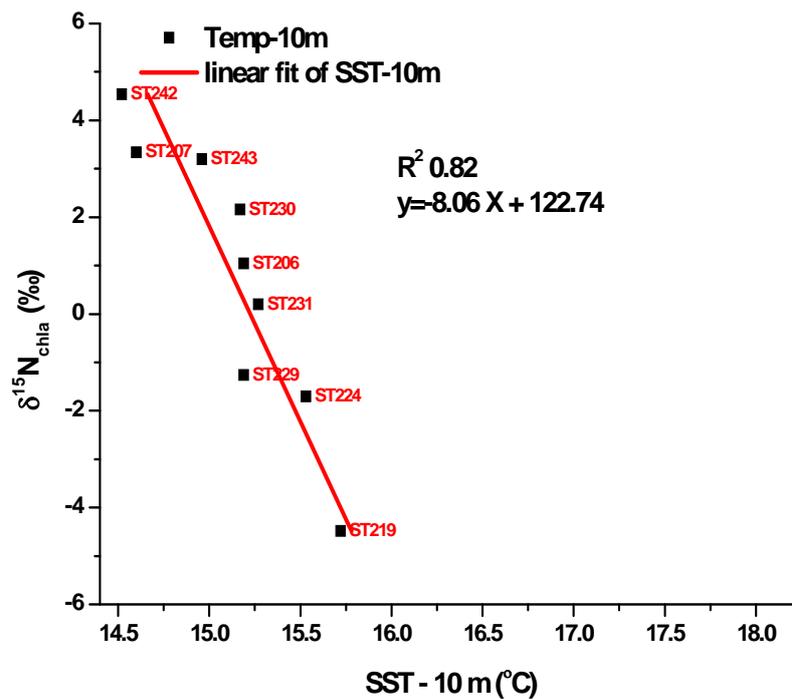
Fig.3.8a Correlation regression of $\delta^{15}N_{Chl\text{-}a}$ (‰) of inner shelf stations and seawater temperature at 10m depth.
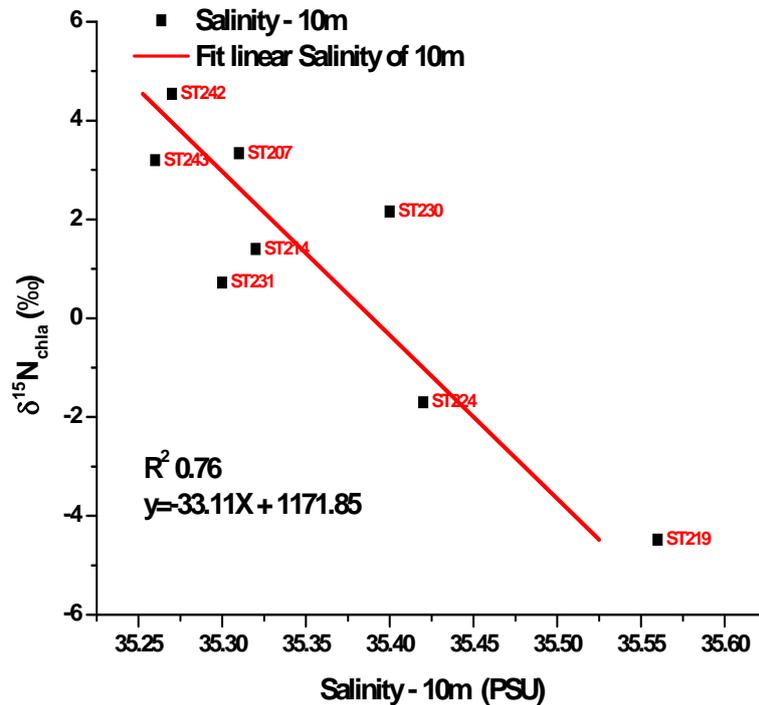
Fig 3.8b Correlation regression of $\delta^{15}N_{Chl-a}$ (‰) of inner shelf stations and seawater salinity at 10m depth

We do not think that spatial variance of SST is the cause for the observed inverse correlation of $\delta^{15}N_{Chl-a}$ and SST. The SST across the inner shelf region varies by only 1.2℃ and in the range of optimal temperature for diatom growth (Sarthou et al., 2005). No conspicuous fractionation effect on ^{15}N is expected when plankton grows under the optimal temperature (Needoba et al., 2003). Instead, we propose that this inverse correlation of $\delta^{15}N_{Chl-a}$-SST/Salinity is created by the co-variation of $\delta^{15}N_{NO_3}$ with upwelling intensity. A stronger upwelling is marked by a lower SST and by an intensified OMZ that causes enhancement of denitrification. As a result, the $\delta^{15}N_{NO3}$ is raised and thus the $\delta^{15}N_{Chl-a}$. A steep slope of the $\delta^{15}N_{Chl-a}$–SST correlation indicates the stronger response of denitrification to the upwelling intensification. Over the inner shelf, the upwelling intensification as expressed by 1 degree of SST decrease would correspond to ~8‰ increase in the surficial $\delta^{15}N_{NO3}$. In the outer shelf waters, a

decrease of 1℃ corresponds to only ~2‰ increase on $\delta^{15}N_{NO3}$. This correlation only provides a yearly-averaged quantification on how much spatial variance in $\delta^{15}N$ of nitrate will be created by upwelling variation across the northern BUS.

A significant correlation of $\delta^{15}N_{Chl-a}$–SST (R^2 0.88, n=5, P<0.001), $\delta^{15}N_{Chl-a}$–salinity (R^2 0.55 n=5, P<0.1) is also observed at 22.5°S (Fig. A3.6). This correlation suggests that a cross-shelf upwelling current exists at 22.5°S, and creates a cross-shelf gradient of SST/salinity and OMZ intensity (Muller et al., 2013). The slope of $\delta^{15}N_{Chl-a}$–SST here implies that 1 ºC decrease of SST reflecting increased upwelling will result in ~1.9‰ positive change in the $\delta^{15}N_{NO3}$ of the nitrate inventory at 22.5°S (refer to Fig. 8 a/b). Other transects in the southern sector of our study area show a similar offshore-onshore increase of $\delta^{15}N_{Chl-a}$, but there is no such conspicuous correlation between physical and isotopic variables.

3.4.4.2 Partitioning of assimilation and denitrification effects on $\delta^{15}N_{Chl-a}$

A regression model (Fig. 3.9) based on the $\delta^{15}N_{Chl-a}$–salinity correlation in station data from the inner shelf (blue solid line) and the outer shelf (red solid line) is the basis for estimating the relative contributions of assimilation and denitrification on the $\delta^{15}N_{Chl-a}$. Over the inner shelf, the difference of $\delta^{15}N_{Chl-a}$ ($\delta^{15}N_{Chl-a\ 23°S}$– $\delta^{15}N_{Chl-a\ 17°S}$) represents the impact of denitrification intensity, while the difference of $\delta^{15}N_{Chl-a}$ between outer and inner shelf stations is a combined effect of both denitrification and phytoplankton assimilation. Their relative contribution varies with latitude. On the ~17°S transect, the difference of $\delta^{15}N_{Chl-a}$ (outer-inner) is mainly caused by the fractionation effect of progressive nitrate assimilation. Further south, denitrification increases gradually and increases the difference in $\delta^{15}N_{Chl-a}$ (outer - inner). At the same time, the contribution of progressive assimilation fractionation is decreasing. On the transect at 22.5°S, the difference of $\delta^{15}N_{Chl-a}$ (outer-inner) is mainly caused by denitrification, which is intensive inshore and decreases in offshore direction, and the assimilation fractionation effect contributes only ~1‰ to this difference.

57
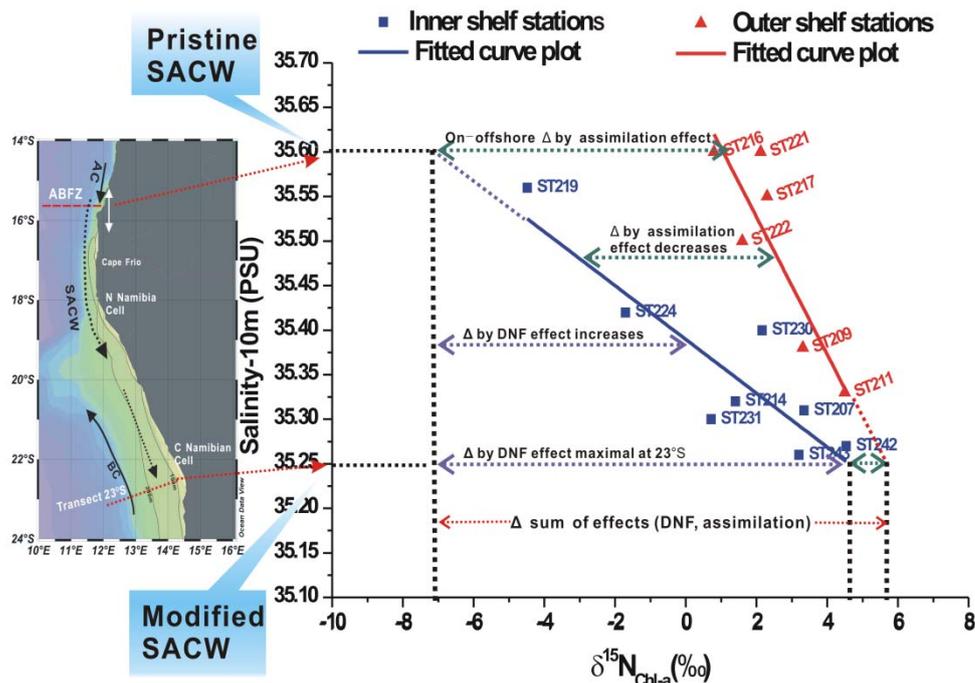
Fig.3.9 A model to discriminate nitrate assimilation and denitrification (DNF) impacts on $\delta^{15}N_{Chl-a}$ over shelf of the northern BUS: the extrapolated dashed line (blue) reaches the salinity of 35.60 characteristic of the pristine SACW, the double-arrow dashed line (green) indicates the on-offshore $\delta^{15}N_{chla}$ discrepancy caused by the plankton assimilation effect, the blue double-arrow dashed line indicates the 17-23ºS $\delta^{15}N_{Chl-a}$ discrepancy caused by denitrification.

Based on this model, the field fractionation effect of nitrate assimilation is calculated as ~9.5‰ and the field fractionation effect of denitrification is ~11.3‰. The latter is the sum of all the fractionation effects of various N-cycling processes involving nitrate, and is an annual average. We exclude possible influences of N_2-fixation that would shift the $\delta^{15}N$ of the nitrate pool to lower the values (Sohm et al., 2011).

3.4.5 Denitrification budget based on spatial $\delta^{15}N_{Chl-a}$

One of the limitations of using the nitrogen isotope composition to investigate nitrogen loss in the ocean is that the co-occurring N-cycling processes with competing isotopic signatures cannot be segregated (Sigman et al., 2009). For example, anammox co-exists with denitrification in OMZs (Kuypers et al., 2005, Jensen et al., 2008, Lavik et al., 2009, Nagel et al., 2013) due to their overlapping oxygen thresholds (Kalvelage et al., 2011). Another concern is that the limited field measurements of $\delta^{15}N_{NO3}$ in nitrate pool on short-term scale (days) are applied to

calculate the N-loss budget that experiences dynamical changes over longer time scales (months to years) (Kirkpatrick et al., 2012). Both the OMZ intensity and the dominant N-loss pathway vary significantly in time and space across the shelf of the BUS, and thus add more complexity to the use of $\delta^{15}N_{NO3}$ for N-loss budget calculations.

In this study, the discrepancy (Δ), $\delta^{15}N_{Chl-a\ 23°S}$ - $\delta^{15}N_{Chl-a\ 17°S}$, represents the $\delta^{15}N_{NO3}$ difference between the pristine SACW at 17°S and that modified by denitrification at 23°S. This $\Delta\ \delta^{15}N_{Chl-a}$ is used here to calculate a denitrification budget along the inner shelf (Eq.1).

$$\delta^{15}N_{reactant} = \delta^{15}N_{initial} + \varepsilon(1-f),\ f = NO_3^-{}_{reactant} / NO_3^-{}_{initial} \quad [1]\ (Mariotti\ et\ al.,\ 1981)$$

The inner shelf is suitable for a steady state model, because it experiences a continuous supply of nitrate by a single water mass (SACW) that is characterized by uniform nitrate concentrations ($\sim$30-40 $\mu mol\cdot l^{-1}$) with a consistent isotopic composition ($\delta^{15}N_{NO3}$= 6.1‰). The inner shelf reservoir (17°S to 23°S) is idealized as a box compartment with a depth of 200m, an average width of 60 km and length of 670 km. The OMZ (DO<20 $\mu mol\cdot l^{-1}$) is set to be located within 50-200m. The initial nitrate concentration is set as 32 $\mu mol\cdot l^{-1}$ according to Mohrholz et al. (2008). 25‰ is accepted for ε of canonical denitrification (Casciotti et al., 2002).

$$\delta^{15}N_{reactant} - \delta^{15}N_{initial} = \varepsilon(1-f),\ \varepsilon = 25\ ‰ \quad [Eq.\ 1]$$

$$NO_{3-initial} = NO_3^-{}_{conc.} \times Reservoir\ Volume\ [Eq.\ 2]$$

$$\delta^{15}N_{reactant} - \delta^{15}N_{initial} = \Delta(\delta^{15}N_{NO3}) = \Delta(\delta^{15}N_{Chl-a}) = 11.3‰ \quad [Eq.\ 3]$$

Denitrification is calculated [Eq. 1] to remove 0.61 Tg of nitrate annually and is comparable with the few published estimates for the northern BUS: 0.25 Tg N·yr^{-1} (Nagel et al., 2013) by using dual isotopic measurements ($\delta^{15}N$, $\delta^{18}O$) on the transect at $\sim$23°S (Walvis bay) and a steady state model; 0.43 Tg N·yr^{-1} (Gutknecht et al., 2013) based on the estimated N-loss rate of 0.38 mol·m^{-2}·yr^{-1} for the whole BUS in a

biogeochemical model developed from field results (22° S ~ 24° S, Walvis Bay). These seemingly comparable results are in fact based on different methods and study areas, i.e. our study covers a broader area from 17-23ºS than the investigations of Nagel et al. (2013) and Gutknecht et al. (2013) and focuses intentionally on the inner shelf where denitrification occurs most intensively.

A few merits of this approach can be easily noticed. Firstly, it presents a yearly-average denitrification budget based on $\delta^{15}N_{Chl-a}$ in surface sediment rather than on short-term field observations of $\delta^{15}N_{NO3}$ over limited coastal regions. Secondly, the $\delta^{15}N_{Chl-a}$ record is a summation of accumulated fractionation effects of various N-cycling processes, and thus the bias of a N-loss budget established on one specific N-cycling process, i.e. canonical denitrification or anammox, is avoided. But, a few concerns should also be taken into account when applying $\delta^{15}N_{Chl-a}$ to calculate a N-loss budget. The pigments extracted from the surface sediment in fact represent 1-2 years of sedimentation on the inner shelf, and ~3-5 years on the outer shelf, thus the $\delta^{15}N_{Chl-a}$ is an average of more than one year, whereas the N-loss intensity is quite dynamical between seasons. It also must be noted that the assimilation fractionation effects on the $\delta^{15}N_{NO3}$ may differs along the nitrate trajectory. A change in the community composition of phytoplankton, variance of irradiance intensity would be possibly cause a spatial differences in fractionation effects of assimilation. The N-loss budget here assumes spatially homogeneous hydrodynamics and parameters for assimilation over the study area, including depth of the euphotic zone and an annually averaged intensity of oxygen minimum zone that are potential errors for this budget.

3.5 Summary and conclusions

This is the first measurement of $\delta^{15}N_{Chl-a}$ in surface sediment of the BUS (17-23°S, 11–14°E). We find that the spatial distribution of $\delta^{15}N_{Chl-a}$ is mainly controlled by the two processes of denitrification and associated isotope fractionation acting on the nitrate pool in upwelling water, and the progressive utilization of nitrate by phytoplankton impacting fractionation on the surface nitrate reservoir. In the northern sector (17-19°S, 11–14°E) of the study area, the offshore-onshore difference (Δ) of

$\delta^{15}N_{Chl-a}$ is mainly explained by assimilation fractionation effects. In the southern sector (20-23°S, 11–14°E), the denitrification process contributes the most to create the offshore-onshore difference (Δ) of $\delta^{15}N_{Chl-a}$. Along the inner shelf (17-23°S) where an intensive OMZ exists, strong upwelling occurs and where the productivity is maximal, the $\delta^{15}N_{Chl-a}$ is found to be inversely correlated with the salinity ($R^2=0.76$, n=9) and temperature ($R^2=0.82$, n=9) at 10 m depth. The southward increase of $\delta^{15}N_{Chl-a}$ along the inner shelf mirrors the continuous denitrification associated with the southward OMZ intensification. The south-north difference of $\delta^{15}N_{Chl-a}$ ($\delta^{15}N_{Chl-a\ 23°S}$ - $\delta^{15}N_{Chl-a17°S}$) is used to calculate an integrated N-loss budget of ~0.6 Tg on annual average, which is in broad agreement with recent reports. This estimate integrates all N-cycling processes in the suboxic water column over the inner shelf. This study shows that the compound specific $\delta^{15}N$ of chlorophyll-a in surface sediments reflects the intensity of denitrification in the OMZ of the northern BUS over periods of years, and that the $\delta^{15}N_{Chl-a}$ is unbiased by diagenetic alteration. In upwelling systems where chlorophyll-a is abundant and low oxygen conditions favor its preservation, the analysis of $\delta^{15}N_{Chl-a}$ in time slices at different locations along the flow path of dominant nitrate source water masses are suitable to establish integrated budgets of anaerobic N-loss.

61

4 Temporal variations of N-loss intensity in the northern Benguela Upwelling System - based on the $\delta^{15}N_{Chlorophyll-a}$ records in a dated sediment core

Abstract

Climate warming is expected to impact the eastern boundary upwelling systems (EBUSs), prompting variations in the upwelling intensity and the extent of oxygen minimum zones (OMZ). As seen in the Benguela Upwelling System (BUS), significant warming is registered in the sea surface at the northern boundary between the northern BUS and the adjacent Atlantic subtropical system. It signals the re-arrangement in the relative proportions of intermediate waters of subtropical Atlantic source in the northern BUS that determines the extent of the OMZ and the associated reactive nitrogen loss via denitrification. Whether this is a directed trend and a reaction to anthropogenic climate change is unknown. To examine the N-loss intensity in response to upwelling fluctuations in the past, we analyzed the alkenone-derived sea surface temperatures and $\delta^{15}N$ of chlorophyll pigment in a dated sediment core located in the core OMZ of the northern BUS. The temperature record reveals a moderate surface warming of ~0.6℃ since the mid-20th century, suggesting a gradual local upwelling relaxation. The $\delta^{15}N_{Chl-a}$ record reveals a considerable change of N-loss that was intensive before 1940 and weakened afterwards. A significant inverse correlation is observed between $U_{37}^{K'}$-SST and $\delta^{15}N_{Chl-a}$ over most of the time period represented by the core, and indicates a $\delta^{15}N_{Chl-a}$ decrease by ~0.5‰ per degree increase of SST. We conclude that the N-loss intensity in the northern BUS varied significantly over the past two centuries, and inversely tracked the upwelling intensity. Differing from older time periods, the decreasing trend of $\delta^{15}N_{Chl-a}$ along with the increasing $U_{37}^{K'}$-SST since 1990 AD suggests that the OMZ is currently weakening in association with upwelling relaxation. These variations in upwelling activity and biogeochemical processes in the northern BUS likely reveal the interactions between the coastal upwelling ecosystem and the remote forcings of

ocean-scale fluctuations under climate warming. But the regional changes as reflected in OMZ weakening and upwelling relaxation in the northern BUS seem to contradict the expected variation trend. Our work proposes that a combined application of $\delta^{15}N_{Chl-a}$ and $U^{K'}_{37}$-SST could interpret the regional variations of N-loss with upwelling intensity at other eastern boundary upwelling systems.

Key words: nitrogen isotope, sediment core, N-loss, oxygen minimum zone, Benguela Upwelling System, $\delta^{15}N$ of chlorophyll pigment

63

4.1 Introduction

The upwelling variations in the major Eastern Boundary Upwelling Systems (EBUSs) have developed in a non-uniform pattern as a response to the global climate warming (McGregor et al., 2007, Belkin 2009, Leduc et al., 2010, Gutiérrez et al., 2011, Monteiro et al., 2011, Pardo et al., 2011). Even within single system, such as the Benguela Upwelling System (BUS, Fig. 4.1), non-uniform, or even antagonistic patterns of upwelling variation had occurred in time and space. Field observations and modeling results have shown enhanced upwelling at the Lüderitz upwelling cell offshore Namibia (Berger et al., 2002, Santos et al., 2012). In contrast, a strong warming trend of ~0.6°C is registered at the Angola-Benguela Frontal Zone (ABFZ) at 17 °S and in the central BUS over the period of 1982-2006 (Monteiro and van der Plas 2006, 2008, 2011). Rouault et al. (2007) detected a uniform warming trend of 0.3-0.4℃ per decade at both the northern and southern boundaries of BUS (ABFZ and Agulhas). Non-uniform upwelling variations in the northern BUS are also evident in SST reconstructions from a series of dated sediment records from the shelf offshore Namibia (Emeis et al., 2009).

The spatially non-uniform upwelling variations in the past imply the re-arrangement of relative proportions in the intermediate water masses that are upwelled to the coastal surface layer. The South Atlantic central water (SACW) and the Eastern SACW (ESACW) are the two major intermediate water masses that compose the upwelling current over the BUS shelves (Mohrholz et al., 2001, Shillington et al., 2006). The SACW originates from the Angola Basin, and is characterized by low oxygen (<90 μmol·l^{-1}) and high nutrient concentration (Lass et al., 2000). The SACW is transported southwards by polarward undercurrent (PUC) at depth of thermocline (Lass et al., 2000, Mohrholz et al., 2001), and it is advected from the Angola Gyre into the northern Benguela across the ABFZ. The ESACW is injected into the BUS via the Benguela Current (BC). Unlike the SACW, the ESACW is typically oxygen-ventilated (~300 μmol·l^{-1}) and nutrient depleted (Mohrholz et al., 2001). Changes in the proportion of SACW / ESACW affect variations in nutrients fluxes

64

and OMZ state in the shelf waters (Mohrholz et al., 2008).
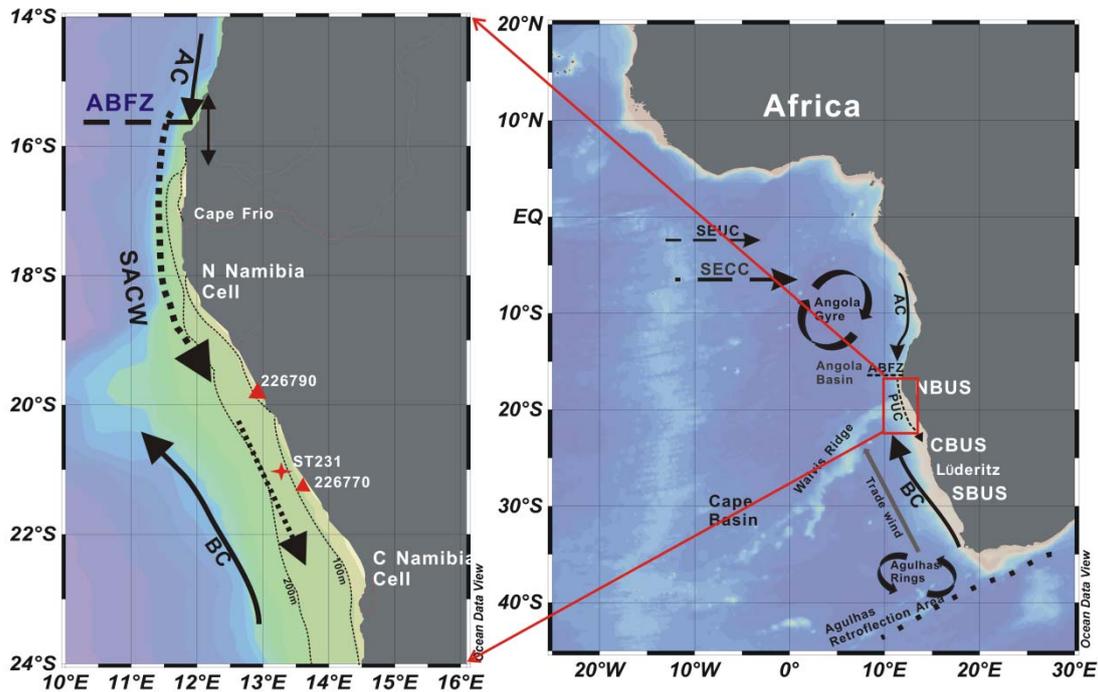
Fig.4.1 Sediment multicore station ST231 (red cross, cruise M76-2,May 2008). Arrows show surface (solid) and subsurface (dashed) hydrographic features. NBUS northern BUS, CBUS central BUS, SBUS southern BUS, ABFZ Angola-Benguela-Frontal Zone, BC Benguela Current, AC Angola Current, PUC Polarward Undercurrent, SEUC South Equatorial Under Current, SECC South Equatorial Counter Current, Two other multicore stations (226770, 226790) from Emeis et al. (2009) are noted as red triangles.

The long-term variation in nitrogen cycling in coastal upwelling systems is complex and difficult to reconstruct (Chavez et al., 2011, Capone and Hutchins 2013). In the case of the northern BUS, two questions are addressed in this study: i) how has the coastal upwelling intensity varied in the past in the northern BUS? ii) what were the variations of OMZ state and the associated N-loss intensity as responses to upwelling variations?

The $\delta^{15}N$ value of sediments ($\delta^{15}N_{sed}$) has been widely employed together with the unsaturation ratio of long chain alkenone (U^{k}_{37}-SST) (Prahl et al., 1988) to investigate the N-loss variation in association with upwelling intensity over different time-periods (Altabet et al., 1999, Altabet 2007, Emeis et al., 2009, Robinson et al., 2012, Deutsch et al., 2014). But the N-loss signal imprinted on $\delta^{15}N_{sed}$ is biased by early diagenesis

65

and post-burial remineralization that change the ^{15}N composition of the bulk organic matter (Lehmann et al., 2002, Meisel and Struck 2011, Schmidt et al., 2011, Robinson et al., 2012).
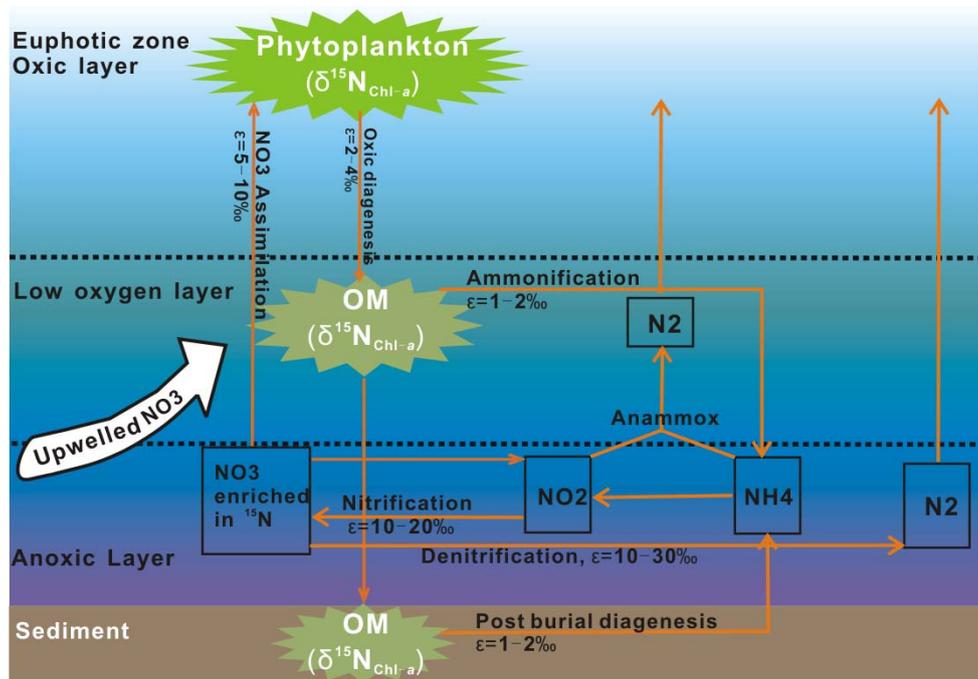
Fig.4.2 The major N-cycling processes (orange arrows) under sub-oxic conditions; the δ^{15}N$_{Chl-a}$ records the ^{15}N signal of co-occurring N-loss in the nitrate pool that is replenished by the upwelling current. The ε of N-cycling processes are from Granger et al (2004) Sigman et al (2009), Kritee et al (2012) and Möbius (2013).

The δ^{15}N of chlorophyll-a (Fig. 4.2) preserved in (shelf) sediments is a suitable proxy that identifies nitrate origin and utilization (Sachs et al., 1999, Higgins. et al., 2011). Differing from δ^{15}N$_{sed}$, the δ^{15}N$_{Chl-a}$ is not altered either during early diagenesis or after being buried in the sediment, unless the molecular skeleton is broken. The δ^{15}N$_{Chl-a}$ integrates the co-occurring isotopic fractionation of biological N-assimilation, and of denitrification associated with the fluctuations of OMZ intensity in shelf waters. Assisted by other proxies ($U^{k'}_{37}$-SST, TOC% etc.), a down-core profile of δ^{15}N$_{Chl-a}$ is able to reflect the variations of past N-loss intensity and its relationship with coastal upwelling intensity.

4.2 Material and Methods

Sediment multi-cores were retrieved during the cruise M76-2 (May, 2008) at station ST231 (Fig. 4.1), which is located on the shelf at 13.25°E, 21°S in a water depth of 131m and under direct coastal upwelling. Upon retrieval, two cores (A and B) were immediately sliced at a resolution of 1 cm and kept in sealed vacuum polyethylene bags at -20 ℃ until freeze drying. Core A was dated and brackets the time from the 18th century to the present and Core B was used for the $\delta^{15}N_{Chl-a}$, $\delta^{15}N_{sed}$ and TN/TOC content (%) analyses that further constrain environmental conditions. SST was reconstructed from the sedimentary record based on the $U_{37}^{k'}$-SST (Prahl et al., 1988) and used to investigate the upwelling intensity and its relationship with fluctuations of $\delta^{15}N_{Chl-a}$ and $\delta^{15}N_{sed}$.

4.2.1 Bulk analyses

Total nitrogen (TN, in wt%) and total organic carbon (TOC, in wt%) were measured in duplicate on a Carlo Erba 1500 CNS Analyser (Milan, Italy).

$(\delta^{15}N=\frac{Rsample - Rstandard}{Rstandard}\times 1000$ [‰]; with $R=\frac{^{15}N}{^{14}N}$ and $R_{standard}$ being the $\frac{^{15}N}{^{14}N}$ ratio of the reference standards, atmospheric N_2 used as the reference)

$\delta^{15}N$ of total N was measured using a Finnigan MAT 252 gas isotope mass spectrometer connected with a Carlo Erba NA-2500 elemental analyzer. Pure tank N_2 calibrated against the reference standards IAEA-N-1 and IAEA-N-2 of the International Atomic Energy Agency. Duplicate measurements of samples resulted in a mean standard deviation of 0.31‰ (Bahlmann et al., 2010).

Unsaturated long-chain alkenone-based Sea Surface Temperature ($U_{37}^{k'}$-SST) was determined following the procedures by Prahl et al. (1988). The reproducibility of the analysis is better than 0.3℃, as determined by repeated measurements.

Sediment ages are determined by dividing the cumulative mass at a given depth by the mass accumulation rate (MAR) that is calculated through the Constant Rate of Supply (CRS) dating model (Appleby and Oldfield 1978, Appleby and Oldfield 1983). The

age-depth model is based on the downcore profile of excess ^{210}Pb determined by gamma spectrometry (Fig. 4.3). The ^{210}Pb excess signal below a depth of 31cm is insignificant and the age model goes back to c.a. 1820, spanning 187 years from the year of 2007.
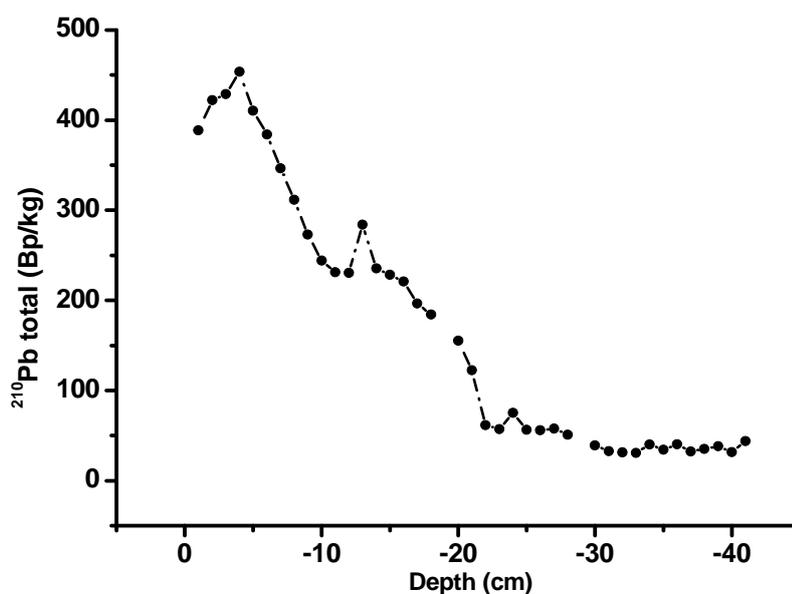
Fig.4.3 Downcore profile of total ^{210}Pb excess (Bp/kg) versus depth (cm) of core ST231.

4.2.2 δ^{15}N measurement of chlorophyll pigment

The chlorophyll pigments were extracted from sediment with a mixture of dichloromethane (DCM) and methanol (9:1) in an ASE 200 (Accelerated Solvent Extraction System, Thermo Fisher Scientific Inc.). Highly pure N_2 gas is used throughout the extraction to prevent the degradation or oxidization of chlorophyll pigments. Chlorophyll pigments were separated by a HPLC procedure modified from Sachs and Repeta (Sachs and Repeta 2000) and Higgins et al (2008, 2011). The separated pigments were identified by chromatography spectra with reference to Chl-a/b standards (Sigma-Aldrich Co.) and cross-checked with published spectra of chlorophyll pigments (Grimm et al., 2006, Roy et al., 2011).

Pigment oxidization

Potassium persulfate ($K_2S_2O_8$) was crystallized 4 times before being dissolved in a NaOH (Semi-conductor grade, Sigma-Aldrich Co.) solution (0.15 mol·l^{-1}) to reach a final concentration of 0.05 mol·l^{-1} (referred to as POR). The purified pigment fraction was dried under a gentle N_2 gas flow in a screw-top quartz tube with a Teflon-lined cap, and 2 ml of POR were added. The quartz tube was sealed and autoclaved at 121℃ for 30 minutes. Then the autoclaved solution was neutralized with H_2SO_4 (10% standard solution, Sigma-Aldrich Co.) to pH 7.0 ± 0.5 for the next step of $\delta^{15}N_{NO3}$ measurement.

Measurement of $\delta^{15}N_{NO3}$

$\delta^{15}N$ of nitrate was determined using the "denitrifier method" (Sigman et al., 2001, Casciotti et al., 2002). The sample solutions were injected into a suspension of Pseudomonas aureofaciens (ATCC#13985). The dissolved nitrate in the samples was quantitatively converted to N_2O gas, which was stripped from the vials by purging with helium, concentrated and purified on a Gas-Bench II, and analyzed on a Delta V mass spectrometer (Thermo Finnigan). Replicate measurements were performed, and two international standards IAEA-N3 ($\delta^{15}N= +4.7‰$) and USGS 34 ($\delta^{15}N= -1.8‰$,), were measured with each batch of samples. For quality assurance of the results, we used an internal potassium nitrate standard that was measured with each batch of samples. Isotope values were corrected using the "bracketing scheme" (Sigman et al., 2009) for the two-point correction referring to IAEA-N3 and USGS34 for $\delta^{15}N_{NO3}$. The standard deviation for international and in-house standards was $0.3‰$ for $\delta^{15}N$ (n $= 6$), deviations for replicate samples were within the same range.

4.3 Results

4.3.1 Down core variations of bulk properties
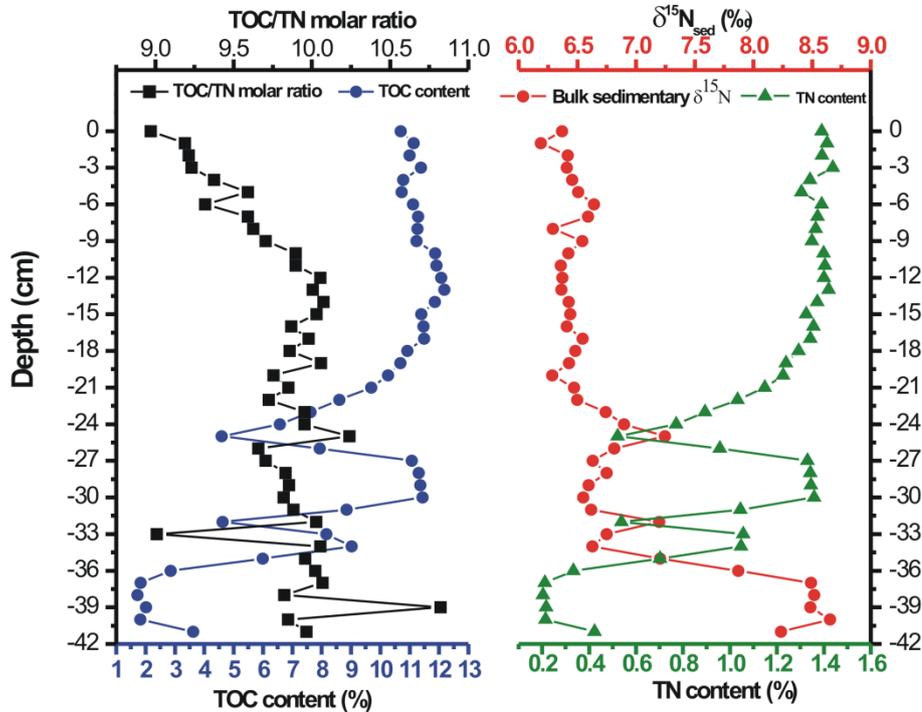
Fig.4.4 Downcore variations of TOC(%) , TN(%) , TOC/TN molar ratio and $\delta^{15}N_{sed}$(‰)

Over the top 20 cm, the TOC and TN contents vary around 11.3% (±0.46%) and 1.4 (±0.048%) respectively. Below the depth of 20 cm, several intensive variations appear at depths of 25 cm and 34 cm (Fig. 4.4). The TOC/TN molar ratio (C/N) increases from 9 to 10 over the top 12 cm of the record and varies around 10 to the depth of 34 cm. The $\delta^{15}N_{sed}$ varies inversely with TN content except revealing a constant value of 6.43±0.10‰ in the top 20 cm of the core, and varies between 6.5‰ and 9‰ to the end of the core.

4.3.2 Variations of U_{37}^{k} -SST and $\delta^{15}N_{Chl-a}$

The variations of U_{37}^{k} -SST (SST in short) and $\delta^{15}N_{Chl-a}$ and other bulk proxies within the dated time period are summarized in figure 4.5. The U_{37}^{k} -SST varies between 16.5-18.5℃. One period of increasing SST by c.a. 0.6℃ is after 1920, compared with the period of 1820-1900, and another is 1990-2007 with the average SST

approximately 0.6℃ higher than that of 1940-1990. Along with increasing SST, the TOC content decreased after 1970. The C/N ratio averages around ~10 before 1970 and does not show apparent association with SST variation, but decreased from 10 to 9 after 1970 in concert with increasing SST.

$\delta^{15}N_{Chl-a}$ ranges over 4‰ (-1.5‰ - +2.5‰) through the core record around a mean value of 0.9‰, and decreases from +2.4‰ to +0.4‰ after ~1960 yr. Among all the proxies, only the $U^{K'}_{37}$-SST shows an inverse variation with the $\delta^{15}N_{Chl-a}$. For the variations of $\delta^{15}N_{sed}$ and $\delta^{15}N_{Chl-a}$, only a vague synchronous fluctuation exists. No apparent co-variation is exhibited between the records of C/N ratio and $\delta^{15}N_{Chl-a}$. Between TN content and $\delta^{15}N_{Chl-a}$, an inverse co-variation is revealed before 1940 but disappears afterwards.

71
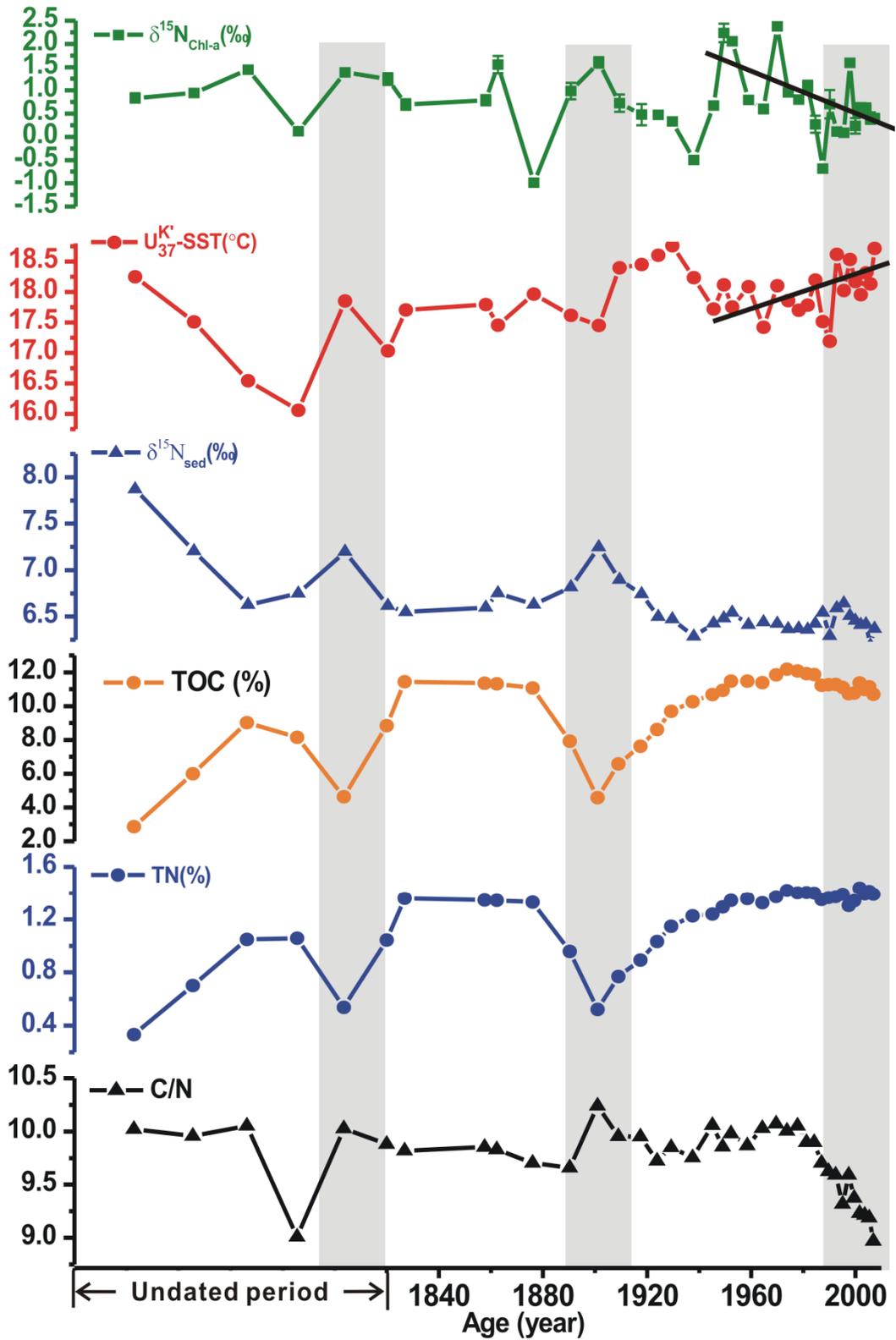
Fig.4.5 Down-core variations of proxies in core ST231, including $U_{37}^{K'}$-SST(℃), $\delta^{15}N_{Chl-a}$ (‰), $\delta^{15}N_{sed}$ (‰), TOC(%), TN(%) and C/N molar ratio. Shaded areas mark time windows when significant variations in N-cycling occurred.

4.4 Discussion

The upwelling intensity in the northern BUS is remotely influenced by the Atlantic subtropic currents system (Mercier et al., 2003, Mohrholz et al., 2008) and locally governed by wind stress curls (Lübbecke et al., 2010, Fennel et al., 2012) and constrained by shelf topography (Monteiro et al., 2008, Jacox and Edwards 2011). Located between the southern subtropic Atlantic and the northern BUS is the ABFZ, which bridges the subtropic intermediate waters to the north and regional coastal upwelling dynamics to the south. The surface warming at ABFZ (Rouault et al., 2007, Rouault et al., 2010) is assumed to change their communication in strength and property, i.e. SACW fluxes or its proportions in the water column. Such a variation has consequences for nutrient delivery and the oxygen budget in the northern BUS that jointly change the biological productivity, the OMZ state and the associated N-loss in shelf waters. Our multicore station (ST231) is located in the middle of the track through which the SACW is advected southward, and the upwelling-favorable wide and shallow shelf helps to clearly express the variations in both hydrodynamic and the upwelling associated biogeochemical processes, which are recorded in the sediment proxies.

In the following sections, I focus on investigating the upwelling variations pattern in the northern BUS (4.4.1), and interpret its impact on N-loss intensity from the $\delta^{15}N_{sed}$ and $\delta^{15}N_{Chl-a}$ records (4.4.2 and 4.4.3) within the dated time period. The difference (Δ) between $\delta^{15}N_{sed}$ and $\delta^{15}N_{Chl-a}$ records is used to evaluate the diagenetic intensity that is closely related with redox conditions (4.4.4). Finally, I tentatively project the future N-loss development in the northern BUS ecosystem (4.4.5).

4.4.1 Variations of upwelling intensity in the northern BUS

The SST in the northern BUS is affected simultaneously by the cold upwelling currents and the atmospheric heating. The cooling signal is possibly offset by the surface heating (Roemmich and McGowan 1995) at coastal locations where the shelf topography is unfavorable for upwelling (Jacox and Edwards 2011). The U^K_{37}-SST

record mirrors the past upwelling variation, but the surface heating can not be ruled out in the interpretation of an increase in $U_{37}^{k'}$-SST that usually indicates an upwelling relaxation. The locations where the $U_{37}^{k'}$-SST record is reconstructed should also be considered for the extent to which the cooling signal of upwelling can be expressed against the surface heating. The shelf topography varies significantly in the northern BUS, thus the $U_{37}^{k'}$-SST records of station ST231 are integrated with previously published data (Fig. 4.6) from two dated cores in the northern BUS (Emeis et al., 2009) to capture the spatial upwelling variation pattern. The SST variation after the mid-20th century is of particular interest, because significant global warming happened since then (Belkin 2009, Leduc et al., 2010).
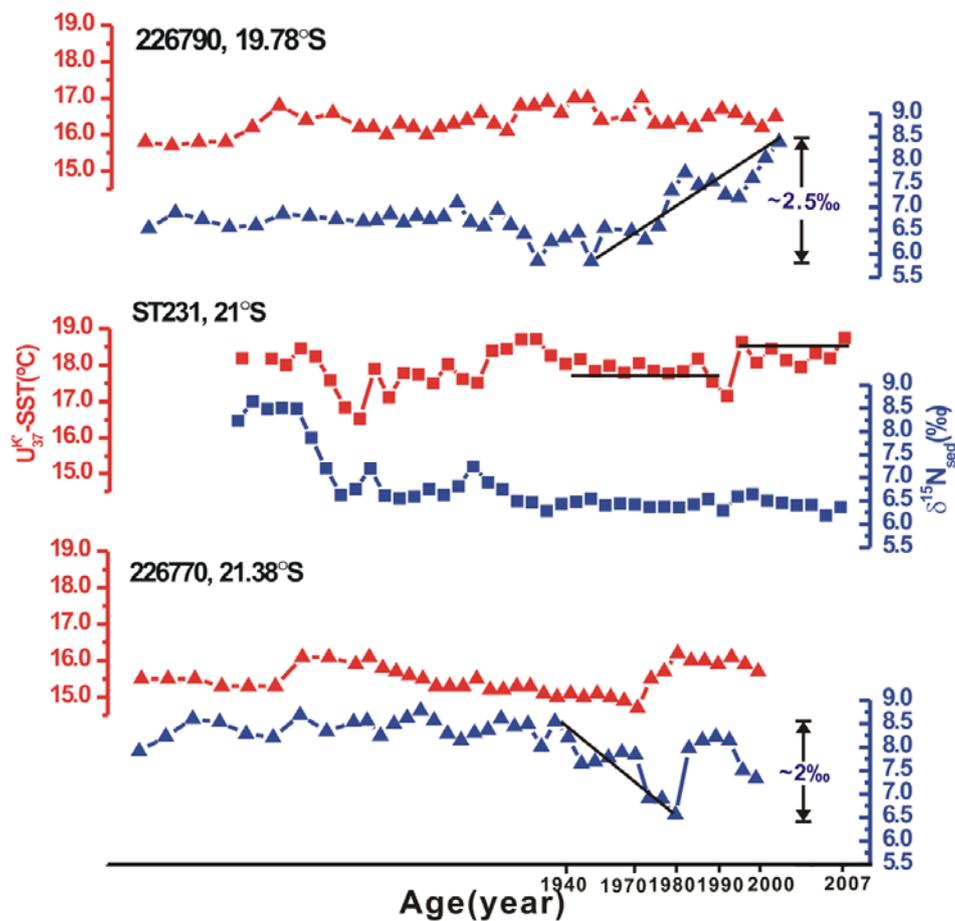
Fig.4.6 A comparison of $U_{37}^{k'}$-SST and $\delta^{15}N_{sed}$ records of 3 inner shelf stations in the northern BUS: ST231 from this study, and 226770, 226790 from Emeis et al (2009).

Similar to the recent SST increase at ST231, there is an obvious surface warming of over 1℃ during the past 30 years (~1970-2000) at station 226770. But the SST record at the station 226790, 2 degree north of ST231, reveals no clear trend of either warming or cooling and varies randomly by ~1 ℃. The SST records of three inner shelf stations together suggest that the upwelling in the northern BUS exhibits non-uniform variations (Emeis et al., 2009), and that the increase of SST is significant at 21ºS, implying a weakening in local upwelling intensity.

Compared with SST variation, the annual average of coastal atmospheric temperatures at 21ºS (World Bank Data) exhibits an increase of only 0.2℃ from the period 1960-1990 to 1990-2009. So, the SST increase of 0.6 ℃ registered at ST231 cannot be exclusively attributed to atmospheric heating, but is mainly explained by the upwelling relaxation. Lower organic matter input is expected in tandem with upwelling relaxation: the decreasing TOC after 1990 with synchronously increasing SST (Fig. A4.1 and Fig. A4.2) both are in live with the upwelling relaxation after 1990. A similar increase in SST at 226770 suggests an upwelling relaxation since ~1970, but this is not reflected by the TOC variations. In contrast, an upwelling intensification can be recognized in the time interval of 1980-2000 in tandem with increasing TOC inputs at 226790 (Fig. A4.1).

Such a non-uniform pattern of upwelling variation in the northern BUS is possibly caused by the re-organization of upwelling cells that is driven by the changing wind stress curl (Emeis et al. 2009; Fennel et al. 2013). But I argue that it is the shelf topography plus the surface atmospheric heating that jointly resulted in the different upwelling variations. Similar non-uniform variations in upwelling within one single coastal upwelling system have been reported in the offshore of northern and central California (Di Lorenzo et al., 2005, Chhak and Di Lorenzo 2007, García-Reyes and Largier 2010, Dufois et al., 2012, García-Reyes and Largier 2012) and Chile (Aravena et al., 2014), where the shelf topography is proposed as an important factor to constrain upwelling activity. The cooling signal of upwelling is more significantly expressed over a shallow shelf (Jacox and Edwards 2011), i.e. 20-23ºS, than the

75

steeper shelf, i.e. 17-19ºS. Thus, the surface warming at 21ºS mainly tracks the upwelling relaxation.

Overall, a spatially heterogeneous pattern is observed in the upwelling variation as reconstructed from the U_{37}^{K}-SST records in the northern BUS, but the upwelling variations are only broadly coupled with TOC proxies. The surface warming could offset the cooling signal of upwelling due to the constraining effect of shelf topography, and could thus obscure the relationship between upwelling intensity, SST and TOC proxies.

4.4.2 N-loss variation based on $\delta^{15}N_{sed}$ records

Both denitrification and anammox are active N-loss processes in the northern BUS (Kuypers et al., 2005, Emeis et al., 2009, Lam and Kuypers 2011, Nagel et al., 2013). The increase in $\ddot{o}^{15}N$ of the nitrate pool is thereby attributed to the joint effects of these two processes (Kirkpatrick et al., 2012). The $\delta^{15}N_{sed}$ downcore variation should correspond to the N-loss intensity in the OMZ in shelf waters. That is, an increasing $\delta^{15}N_{sed}$ indicates intensified N-loss, and vice versa.

The $\delta^{15}N_{sed}$ at ST231 suggests a broadly decreasing trend of N-loss intensity over the time period covered by the core (Fig. 4.6). But its fluctuation after 1940 is too small to specify any N-loss variation trend. A decreasing trend of N-loss is also recognized from the overall $\delta^{15}N_{sed}$ records at 226770, where a significant decrease in $\delta^{15}N_{sed}$ by 1-2‰ occurred after 1940. In contrast, the $\delta^{15}N_{sed}$ record at 226790 implies intensified N-loss by a distinct increase of ~2.5‰ after 1940. Apparently, the $\delta^{15}N_{sed}$ records from 3 different coastal stations together suggest the same non-uniform variation pattern in N-loss intensity as in upwelling intensity in the northern BUS.
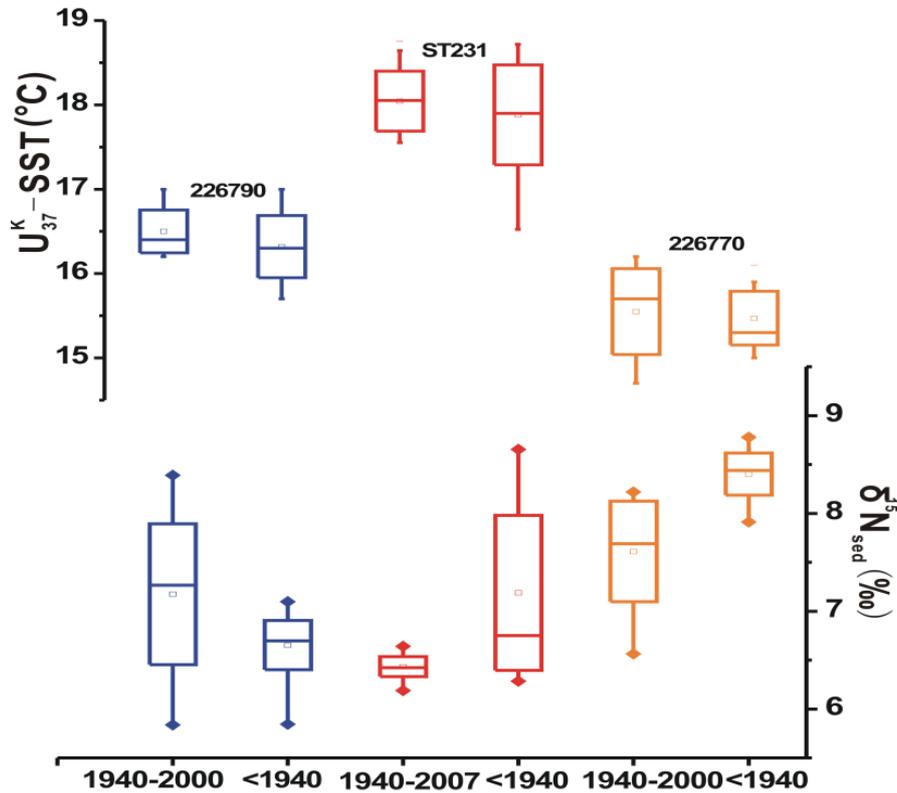
Fig.4.7 Box charts of the $\delta^{15}N_{sed}$ and $U_{37}^{K'}$-SST at 3 shelf stations (ST231 in this study, 226770 and 226790 from Emeis et al (2009). The box size spans the standard deviation, horizontal solid line in the box is the average value, empty rectangle is median value, solid diamond is the max-min value.).

However, the two processes seem uncoupled since no significant correlation between the $\delta^{15}N_{sed}$ and SST is seen at either of the three stations (Fig. 4.6). But an inverse co-variation between the $\delta^{15}N_{sed}$ and $U_{37}^{K'}$-SST before and after 1940 yr can be observed at all the three stations (Fig. 4.7, T-test is run for statistical significance examinations by SPSS 19.0. Results are summarized in table A4.2), indicating that the N-loss variations is inversely related to upwelling intensity. Moreover, the N-loss intensity responded differently to upwelling variation at these three stations. Over the same time period, i.e. after 1940, the $\delta^{15}N_{sed}$ varied to upwelling change by ~0.7 ‰/℃ at ST231, while at 226770 and 226790, the $\delta^{15}N_{sed}$ varied by ~2 and ~4 per mil/℃ respectively. This different response in N-loss as seen in $\delta^{15}N_{sed}$ to upwelling variations could be attributed to either the non-uniform fluctuation of upwelling

intensity in space and time, or the variations in OMZ and the associated N-loss intensity, or a combination of the two. Diagenetic overprinting could also shift the $\delta^{15}N_{sed}$ from the original N-loss signal that was imprinted on, which is discussed in section 4.4.4.

To summarize, the $\delta^{15}N_{sed}$ records at three coastal multicore stations reveal a non-uniform development in N-loss intensity in the northern BUS. The lack of significant correlation in $\delta^{15}N_{sed}$-SST prevents solid conclusions on the N-loss development in response to upwelling intensity variation. But the data does suggest that the N-loss intensity relaxed at 21ºS and enhanced at 19.78ºS during the recent time period.

4.4.3 N-loss variation based on the $\delta^{15}N_{Chl-a}$ record

The overall fluctuation in the course of $\delta^{15}N_{Chl-a}$ mirrors the variability of N-loss intensity in the water column, and a decreasing trend of $\delta^{15}N_{Chl-a}$ after ~1990 (Fig. 4.5) indicates a decrease in the intensity of N-loss. The significant correlation of the $\delta^{15}N_{Chl-a}$ with SST (R^2 0.68, p<0.001), rather than with other bulk proxies, suggests that the $\delta^{15}N_{Chl-a}$ is a more sensitive tracer than $\delta^{15}Nsed$ to capture the upwelling-induced N-loss intensity. A high value of $\delta^{15}N_{Chl-a}$ represents an intense OMZ during the high phase of upwelling (lower SST) that invokes intensive N-loss, and vice versa. This co-variation is also found in the spatial distributions of $\delta^{15}N_{Chl-a}$ and SST over the inner shelf of the northern BUS (chapter 3, Fig. 3.8a), where a gradient of southward increasing $\delta^{15}N_{Chl-a}$ corresponds to a decreasing SST that indicates a gradually-enhanced upwelling.
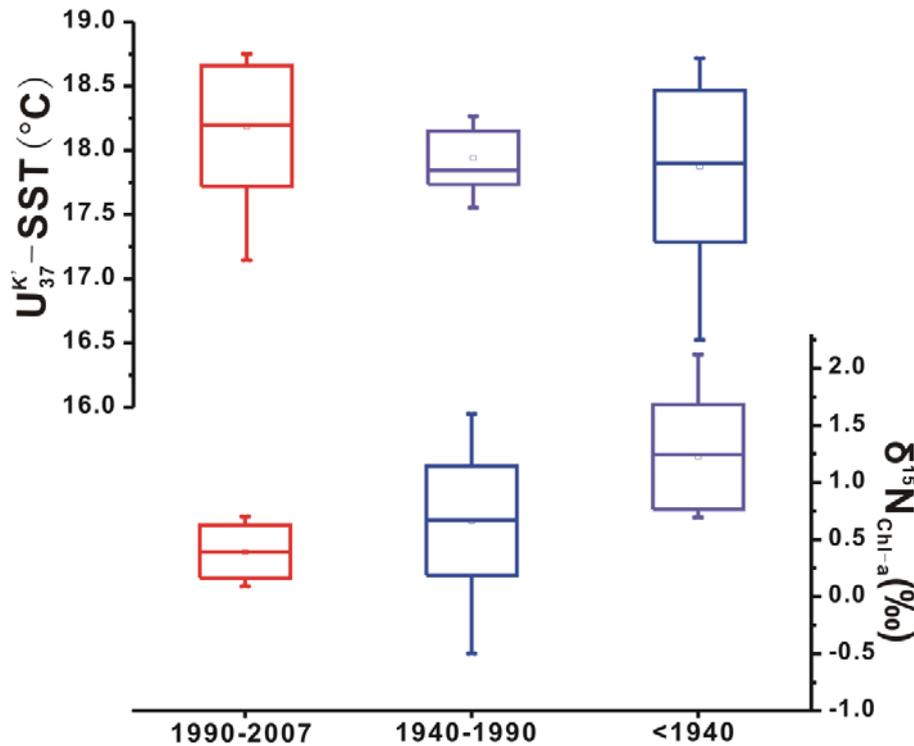
Fig.4.8 Box plots of $U_{37}^{K'}$-SST (℃) and $\delta^{15}N_{Chl-a}$ (‰) in different time periods at ST231. T-test is run for statistical significance examinations. Results are summarized in supplementary material table 2

The co-variation between the N-loss intensity (reconstructed from $\delta^{15}N_{Chl-a}$) and upwelling intensity (reconstructed from SST) is also observed at different time periods (Fig. 4.8), during which a gradual decrease in $\delta^{15}N_{Chl-a}$ is seen with increasing sea surface temperature. This co-variation may express different slope of the $\delta^{15}N_{Chl-a}$-SST correlation at different time periods that are represented by depth intervals of a sediment core. We thus examine the slope of the $\delta^{15}N_{Chl-a}$-SST paired data based on the assumption that at high (low) phases of upwelling, one degree (℃) change of upwelling intensity caused different responses of the N-loss activity by $\delta^{15}N$ increase/decrease in chlorophyll. We demarcate the time intervals by referring to the major climate development phases: (i) the period since 1940 when significant global atmospheric warming occurred; (ii) the period before 1940. These two periods correspond to the core depth intervals of 0-20 cm and 21-42cm, respectively.

79
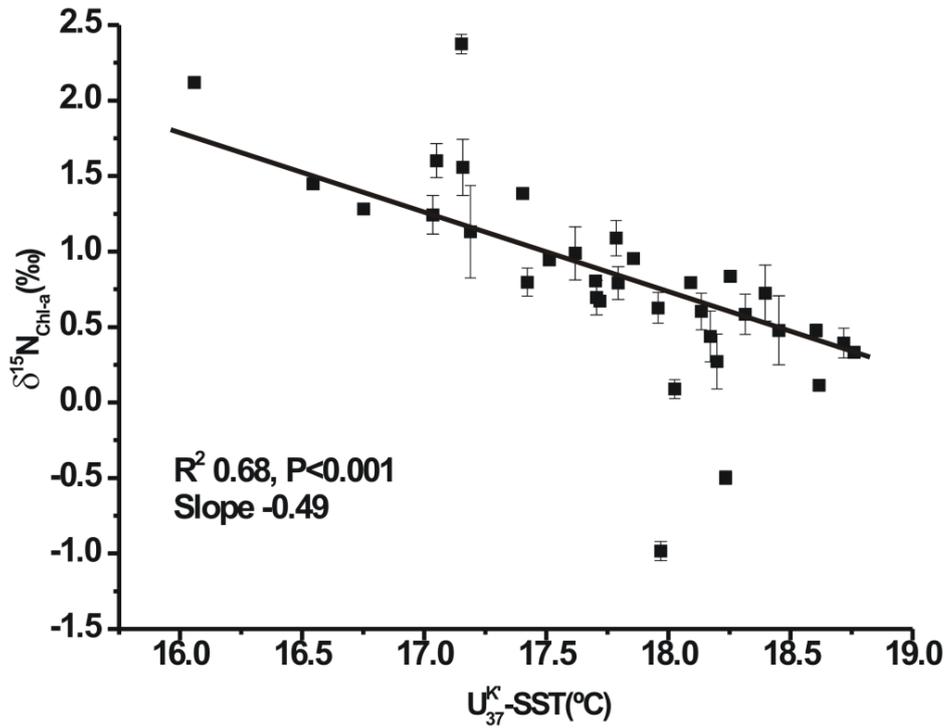
Fig.4.9a The correlation between $\delta^{15}N_{Chl-a}$(‰) and U^{k}_{37}-SST(℃) of core ST231(time interval 1820-2007 A.D.).
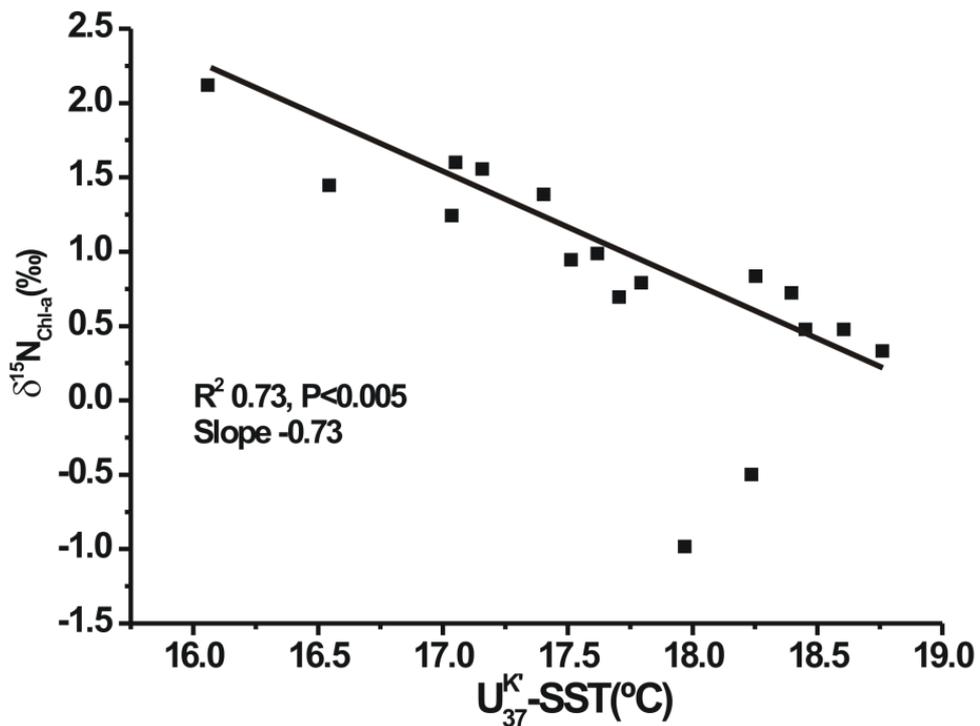
Fig.4.9b The correlation between $\delta^{15}N_{Chl-a}$ (‰) and U^{k}_{37}-SST(℃) of core ST231 (before 1940 AD), core interval 21-42 cm.

In the depth interval of 21-42cm, the slope of $\delta^{15}N_{Chl-a}$ - SST is -0.70 (R^2 0.73, p<0.005, Fig. 4.9b), and -0.39 (R^2 0.24, P<0.05) in the top 20cm, in comparison with -0.49 for the whole core record (R^2 0.68, P<0.001, Fig. 4.9a). A steeper slope implies a stronger N-loss intensity in response to upwelling intensity. Thus, this slope variation suggests intensified N-loss existed before 1940, and a slight weakening occurred afterwards in concert with local upwelling relaxation.

Bakun (1990) hypothesized that the coastal upwelling intensifies as the result of atmospheric warming. In such case, the N-loss is expected to occur more actively on the condition that intensified upwelling promotes coastal productivity and OMZ intensification. Apparently, the data here do not support the above scenario. Instead, I argue that N-loss decreased at the studied site, and that OMZ relaxation in association with decreasing SACW invasion should be the plausible explanation. The decreasing SACW upwelling is indicated by the increasing SST and a synchronous decline of organic matter (OM) inputs after 1990 (Fig. A4.2). The extent to which OM flux decreased at ST231 is too small to significantly weaken the magnitude of denitrification (Kalvelage et al., 2013). Therefore, the weakening of N-loss can not be attributed to reduced OM input, and the weakened OMZ intensity in the water column is the only conceivable mechanism.

Other N-cycling processes could as well result in a lower $\delta^{15}N$ of nitrate and a decreasing $\delta^{15}N_{Chl-a}$. The $\delta^{15}N$ in the local nitrate pool could be depleted by either exogenic advection of a N-source with lower $\delta^{15}N$ of nitrate from adjacent seas, or a local contribution by N-fixation ($\delta^{15}N$=-1-2‰), or atmospheric wet/dry N-deposition ($\delta^{15}N$=~0-1‰) (Sigman et al., 2009). However, there are no indications in past research (Capone et al., 2005, Moore et al., 2009) or latest reports (Sohm et al., 2011, Capone 2014) to suggest either of these processes in the northern BUS. Therefore, the only explanation for the decreasing $\delta^{15}N_{Chl-a}$ is the declining N-loss intensity.

4.4.4 Diagenetic intensity variations

The narrow variance of $\delta^{15}N_{sed}$ (0.1‰) and TN content (0.048%) within the top 20 cm at ST231 seems to suggest that a steady organic nitrogen input (Pichevin et al., 2004),

81

or a consistent diagenetic intensity, or a combination of both may play a role. It is suspected that the early diagenesis in the water column and sedimentary remineralization together modify both the organic N content and $\delta^{15}N$ of planktonic biomass, the isotopic precursor of $\delta^{15}N_{sed}$ (Lehmann et al., 2002, Gaye-Haake et al., 2005). In the following, the paired $\delta^{15}N$ proxies are used to evaluate the diagenesis effect on the organic matter and its co-variation with the upwelling intensity.
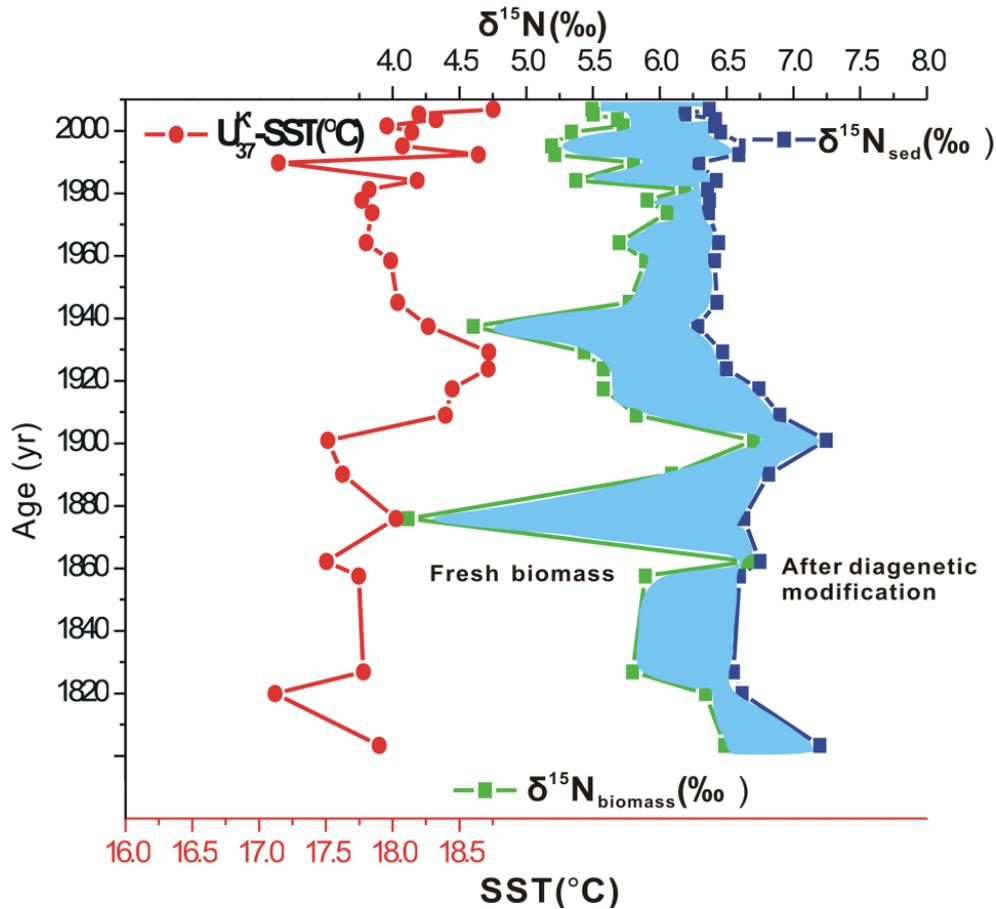
Fig.4.10 An illustration of the post deposition diagenetic intensity of bulk-biomass by the $\Delta(\delta^{15}N_{sed} - \delta^{15}N_{biomass})$, and its variation with SST(℃). Blue shaded area indicates the variation of diagenetic intensity.

A positive correlation (R^2=0.53, P<0.001, Fig. A4.3) between the $\delta^{15}N_{sed}$ and $\delta^{15}N_{Chl-a}$ over the whole core record is related to the same origin and $\delta^{15}N$ nitrate, from which the N_{Chl-a} and N_{sed} are produced. But the paired $\delta^{15}N$ proxies reveal no correlation (R^2=0.06, P=0.96, Fig. A4.3) within the top 20 cm (~1940-2007), which is probably caused by the diagenetic processes that compromised the isotopic linkage between

them. Diagenetic ^{15}N-enrichment under oxic conditions is well established in sinking particles and surface sediments (Freudenthal et al., 2001, Gaye-Haake et al., 2005). But under anoxic condidtions, different mechanisms have been reported as either depleting the organic nitrogen through the selective degradation of ^{15}N-rich amino acid/proteins-N (Calleja et al., 2013), or enriching the organic matter by releasing ^{15}N-depleted ammonium (Meisel and Struck 2011, Möbius 2013).

Besides the assimilation effects imprinted on both of the proxies, the $\delta^{15}N_{sed}$ integrates two sets of signals, diagenesis and N-loss, while the $\delta^{15}N_{Chl-a}$ bears only the N-loss signal. It is therefore assumed that the Δ value of ($\delta^{15}N_{sed}$-$\delta^{15}N_{biomass}$) corresponds to the intensity of diagenetic alteration on the $\delta^{15}N$ of bulk biomass. The $\delta^{15}N_{biomass}$ increases by 2-4‰ through oxic degradation (Lehmann et al., 2002). But under anoxic conditions, the fractionation effect of diagenesis is much smaller (<2‰) than under the oxic conditions (Alkhatib et al., 2012, Möbius 2013). The original $\delta^{15}N_{biomass}$ is thus modified by the diagenesis under oxic-anoxic oscillating, and the imprinted signal of N-loss on $\delta^{15}N_{biomass}$ is gradually erased while the $\delta^{15}N$ of Chl-a keeps the isotopic signal intact.

Sachs et al (1999) found a consistent difference of 5.1±1.1‰ between $\delta^{15}N_{Chl-a}$ and pristine $\delta^{15}N_{biomass}$, which is used to reconstruct the $\delta^{15}N_{biomass}$ based on the core record of $\delta^{15}N_{Chl-a}$ (Fig. 4.10). The $\Delta(\delta^{15}N_{sed}$-$\delta^{15}N_{Chl-a})$ correlates positively (R^2=0.52, p<0.001) with SST, indicating that the diagenesis intensity is closely associated with the upwelling intensity. That is, during low phase of upwelling (+SST), better ventilation enables oxic diagenesis that increases the $\delta^{15}N$ of biomass, while it lowers $\delta^{15}N_{Chl-a}$ due to weakened N-loss, during which a higher $\Delta(\delta^{15}N_{sed}$-$\delta^{15}N_{Chl-a})$ is produced. We further propose that the $\Delta(\delta^{15}N_{sed}$-$\delta^{15}N_{Chl-a})$ could represent the diagenetic fractionation effect on $\delta^{15}N$ of biomass. The fractionation effect of diagenesis on $\delta^{15}N$ of OM in core ST231 varied from 0.2-2.5‰, with an average of 0.9‰, implying that low oxygen conditions existed over most of the dated period at station ST231 in association with anoxic diagenetic processes. The fractionation factor (ε) of sedimentary remineralization was reported to correlate significantly

(R^2=0.73, P<0.005) with in-situ redox conditions (Alkhatib et al., 2012). The more severe the anoxic condition is, the weaker the fractionation effect becomes. The diagenetic intensity at ST231 was highly variable in the past and was closely correlated with redox conditions that were driven by the local upwelling intensity. There is a slight trend to better oxygen ventilation after 1980 AD that was associated with the increasing SST.

4.4.5 Implications to the N-cycling in the northern BUS

Our study indicates that a weakening OMZ coincided with relaxed upwelling activity at ST231. One possible cause would be a decreasing proportion of SACW in the water column. It is postulated that the surface warming at ABFZ could cause a reduction of SACW advection into the northern BUS, which requires an increasing compensation by oxygen-rich ESACW carried by the northward BC, so that a relaxation in both OMZ intensity and the associated N-loss ensued. But this hypothesis needs more examinations.

4.5 Summary and conclusions

Climate-driven fluctuations in the depth of the thermocline/nutricline largely control the nutrients fluxes and primary production along subtropical coastal upwelling zones. The upwelling intensity in the northern BUS has undergone a spatially non-uniform variation. A conspicuous warming trend has occurred at ABFZ since ~1980s (Rouault et al., 2007) and is likely to affect the nitrate supply to the northern BUS by restricting the advection of SACW. My investigation of the past variability in upwelling (SST) and N-loss ($\delta^{15}N_{sed}$, $\delta^{15}N_{Chl-a}$) associated with suboxic processes in the OMZ on the shelf off Namibia leads to the following conclusions on past variations in upwelling and OMZ intensity and denitrification.

1. The upwelling intensity has varied in a spatially non-uniform pattern in the northern BUS. The U_{37}^{K}-SST record at 21 ºS suggest a mild surface warming of

~0.6℃ since 1990 AD, and this increase of SST is mainly caused by decreasing local upwelling intensity.

2. The vague correlation between $U_{37}^{K'}$-SST and $\delta^{15}N_{sed}$ is caused by the diagenesis and remineralization processes. The variation of N-loss intensity cannot be clearly filtered out from the $\delta^{15}N_{sed}$ records. In contrast, the $\delta^{15}N_{Chl-a}$ record reveals considerable variations in N-loss intensity, and is significantly associated with upwelling activity as seen in the $\delta^{15}N_{Chl-a} - U_{37}^{K'}$-SST correlation.

3. The $\Delta(\delta^{15}N_{sed} - \delta^{15}N_{biomass})$ represents the diagenetic bias on the $\delta^{15}N$ of bulk organic matter, and its variation is closely coupled with redox conditions that are locked to variations in upwelling intensity.

4. A slope of -0.49 in the $\delta^{15}N_{Chl-a} - U_{37}^{K'}$-SST correlation through out the core implies that SST changes by 1 ℃ correspond to ~0.5‰ changes in the $\delta^{15}N$ of the nitrate pool due to stronger or weaker denitrification. The slope of $\delta^{15}N_{Chl-a} - U_{37}^{K'}$-SST has steepened since 1940 AD, suggesting that the OMZ weakened and denitrification decreased after 1940.

I conclude that the upwelling at ST231 weakened over the past few decades, which was associated with a decreasing effect of denitrification on $\delta^{15}N$ of assimilated nitrate. This means that the intensity and/or the extent of the OMZ has decreased.

Although, this study is based on only one sediment multicore, it is the first attempt to link the N-loss intensity in an OMZ with the variations of upwelling intensity in an eastern boundary upwelling system. The downcore $\delta^{15}N_{Chl-a}$-SST variation is very promising to be applied widely at other EBUSs as well.

5 Conclusions and Outlook

5.1 Major conclusions

The following conclusions can be drawn from this thesis:

1, A two-step HPLC method was established for thorough separation of chlorophyll pigments that are extracted from coastal sediments. The recrystallized $K_2S_2O_8$ used to oxidize phaeopigments in this study has a small source of contamination and has a depleted $\delta^{15}N$ value of -15‰. The $\delta^{15}N$ of the recrystallized $K_2S_2O_8$ would bias the $\delta^{15}N$ value of pigment samples at nanomolar masses. The overall measurement of $\delta^{15}N_{pigment}$ has an average analytical precision better than ±0.5‰ (1σ).

2, The spatial distribution pattern of $\delta^{15}N_{Chl-a}$ in surficial sediment reveals that the plankton assimilation and denitrification in OMZ are the two major processes to modify the $\delta^{15}N$ in the upwelled nitrate in the northern BUS. The on-shelf upwelling dynamics control the relative contribution of the plankton assimilation and the denitrification to produce distinct north-south and offshore-onshore gradients in surficial $\delta^{15}N_{Chl-a}$. The inner shelf (17°S to 23°S) stations outline a southward increase of 11.3‰ in $\delta^{15}N_{Chl-a}$ that mirrors an increase of $\delta^{15}N_{NO3}$, from which an annual N-loss of ~0.6 Tg·yr^{-1} is calculated.

3, A dated core record of $\delta^{15}N_{Chl-a}$ exhibits a clear variation of denitrification intensity that associated significantly with upwelling intensity and associated cooling or warming of sea surface temperature ($U^{K'}_{37}$-SST). The slope of $\delta^{15}N_{Chl-a}–U^{K'}_{37}$-SST correlation at different depth intervals (time intervals) indicates the variance of denitrification intensity in response to upwelling fluctuation. On the inner shelf at 21ºS, the denitrification became weakened after 1990 yr, in concert with a mild surface warming that was mainly caused by upwelling relaxation. It is speculated that the reduced upwelling of SACW is the possible explanation for OMZ mitigation and the weakening denitrification intensity.

This thesis is based on $\delta^{15}N_{Chl-a}$ in limited numbers of samples of surficial sediment and one sediment multicore. All the conclusions and speculations need corroboration

based on more sediment sample analyses. But the results illustrate the application of pigment-based proxies to reconstruct the N-loss intensity in the ocean and its co-variance with the development of upwelling and OMZ intensity in the northern BUS. The surficial and downcore $\delta^{15}N_{Chl-a}$-SST correlation is very promising to be widely applied in other eastern boundary upwelling systems.

5.2 Outlooks for N-cycling in the northern BUS

5.2.1 The non-uniform upwelling variations at multi-decadal scale
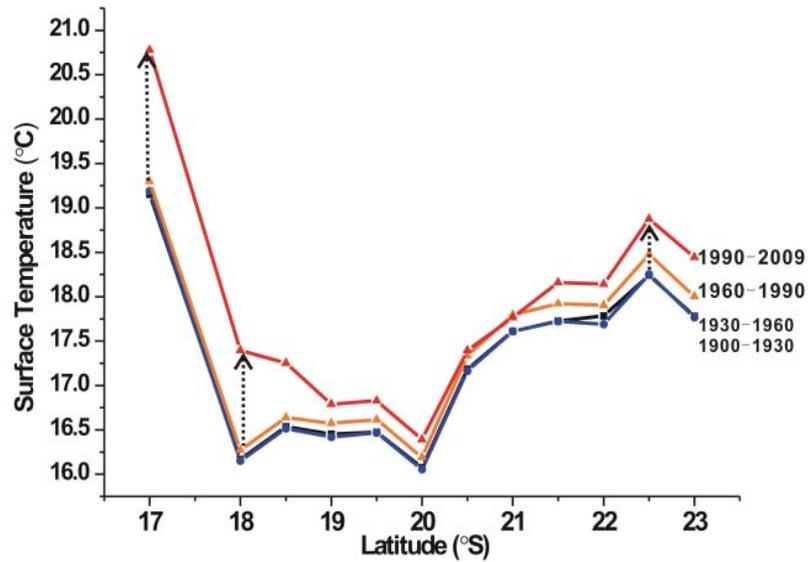
Fig.5.1a The annual average of coastal atmospheric temperature in the northern BUS (data sets are from World Bank).
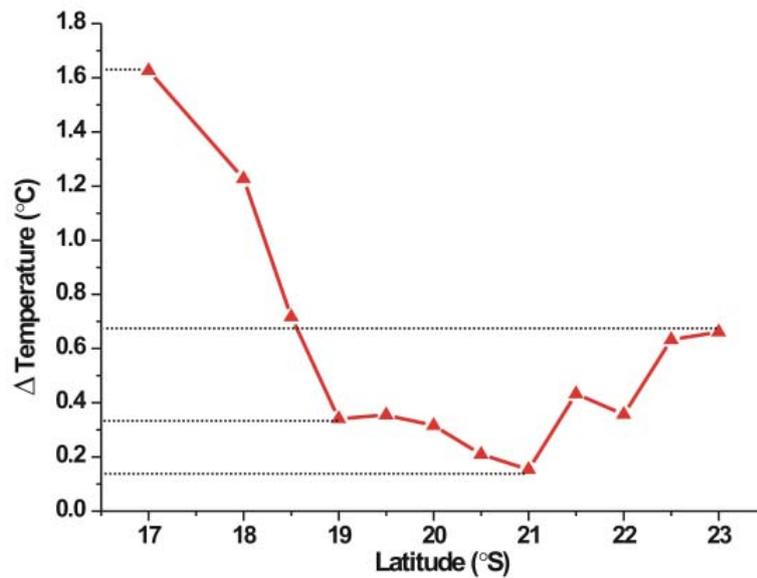
Fig.5.1b The increase in coastal atmospheric temperature from 1900-1930 to 1990-2009 in the northern BUS (Data sets are from World Bank).

The coastal upwelling in the northern BUS is experiencing a non-uniform variation that was clearly exhibited by the coastal atmospheric temperature variations at different latitudinal locations over the last century (Fig. 5.1a/b). Both the northern boundary (17ºS) and the central Namibia (23ºS) exhibit significant warming trends. The SST at the northern boundary increased ~1.6℃ over the past four decades, which is double the ~0.7℃ increase at 23ºS. But at 21ºS, the SST increased only ~0.2℃ over the same time period. This conspicuously inhomogeneous variation pattern of coastal atmospheric temperature in the northern BUS is believed to result from the non-uniform development of upwelling intensity in space. However, the lack of long-term field data or finer scales and possibly unrecognized hydrodynamic processes severely limit our capability to forecast the development of the BUS ecosystem in response to present-day global ocean warming (Belkin 2009, Levitus et al., 2009).

5.2.2 Meso-scale processes in coastal upwelling zones

The spatially non-uniform SST variation in the northern BUS in fact signals the changes in communications between intermediate waters and surface waters, which are controlled by different on-shelf hydrodynamic processes. Besides upwelling and Ekman transportation, the sub-/mesoscale eddies and filaments have received increasing attention for their significant impact on both the cross-pycnocline heat and mass exchange and the biogeochemical processes (Klein and Lapeyre 2009, Pietri et al., 2013, Echevin et al., 2014).

Eddies is a characteristic feature of eastern boundary coastal upwelling zones (Morales et al., 2012, Hormazabal et al., 2013, Stramma et al., 2013). The eddies could harbor anaerobic denitrifying process and act as an important hotspot for loss of fixed nitrogen (Altabet et al., 2012). The downwelling filaments on the other hand could re-ventilate the hypoxic subsurface layer with DO-rich upper layer water (Mahadevan 2014), and simultaneously relieve high productivity at inner shelf by transporting residual nutrients and organic matter across thermocline towards the open sea (Gruber et al., 2011). How these hydrodynamic processes affect the spatial

89

variation in upwelling intensity in the northern BUS, shape the OMZ intensity, and influence the N-cycling processes emerges as a challenging question.

5.3 Future research

The $\delta^{15}N_{Chl-a}$-SST correlation is promising tool to capture the variation of denitrification and upwelling intensity over time periods of a few hundreds of years. Similar research should be carried out at other shelf locations (i.e. 17, 19, 21 and 23ºS), where the non-uniform upwelling variations are most significantly exhibited (Fig.1a/b). Submesoscale processes should also be considered in the analysis of spatial upwelling variations. A comparing study on the $\delta^{15}N_{Chl-a}$–SST correlations in space is able to establish the variation pattern of OMZ state and the associated N-loss intensity in response to upwelling development in the northern BUS, and would significantly enhance our understanding on the development of eastern boundary upwelling ecosystems under climate-driven perturbations.

References

Alkhatib, M., M. Lehmann and P. d. Giorgio (2012). The nitrogen isotope effect of benthic remineralization-nitrification-denitrification coupling in an estuarine environment. Biogeosciences 9(5), 1633-1646.

Altabet, M. A. (2007). Constraints on oceanic N balance/imbalance from sedimentary ^{15}N records. Biogeosciences 4(1), 75-86.

Altabet, M. A. and R. Francois (1994). Sedimentary nitrogen isotopic ratio as a recorder for surface ocean nitrate utilization. Global Biogeochemical Cycles 8(1), 103-116.

Altabet, M. A., C. Pilskaln, R. Thunell, C. Pride, D. Sigman, F. Chavez and R. Francois (1999). The nitrogen isotope biogeochemistry of sinking particles from the margin of the Eastern North Pacific. Deep Sea Research Part I: Oceanographic Research Papers 46(4), 655-679.

Altabet, M. A., E. Ryabenko, L. Stramma, D. W. R. Wallace, M. Frank, P. Grasse and G. Lavik (2012). An eddy-stimulated hotspot for fixed nitrogen-loss from the Peru oxygen minimum zone. Biogeosciences 9(12), 4897-4908.

Appleby, P. and F. Oldfield (1978). The calculation of lead-210 dates assuming a constant rate of supply of unsupportedc ^{210}Pb to the sediment. Catena 5(1), 1-8.

Appleby, P. and F. Oldfield (1983). The assessment of ^{210}Pb data from sites with varying sediment accumulation rates. In Paleolimnology, volume 15, ed. J. Merilainen, P. Huttunen and R. W. Battarbee, Springer Netherlands: pp. 29-35.

Aravena, G., B. Broitman and N. C. Stenseth (2014). Twelve Years of Change in Coastal Upwelling along the Central-Northern Coast of Chile: Spatially Heterogeneous Responses to Climatic Variability. PLoS ONE 9(2), e90276.

Arhan, M., H. Mercier and Y.-H. Park (2003). On the deep water circulation of the eastern South Atlantic Ocean. Deep Sea Research Part I: Oceanographic Research Papers 50(7), 889-916.

Aydin, N., S. Daher and F. O. Gülaçar (2003). On the sedimentary occurrence of chlorophyllone a. Chemosphere 52(5), 937-942.

Bahlmann, E., S. M. Bernasconi, S. Bouillon, M. Houtekamer, M. Korntheuer, F. Langenberg, C. Mayr, M. Metzke, J. J. Middelburg and B. Nagel (2010). Performance evaluation of nitrogen isotope ratio determination in marine and lacustrine sediments: an inter-laboratory comparison. Organic Geochemistry 41(1), 3-12.

Bailey, G. and P. Chapman (1991). Short-term variability during an anchor station study in the southern Benguela upwelling system: Chemical and physical oceanography. Progress in Oceanography 28(1), 9-37.

Bakun, A. (1973). Coastal upwelling indices, west coast of North America, 1946-71, US Department of Commerce, National Oceanic and Atmospheric Administration, National Marine Fisheries Service, pp.1-23.

Bakun, A. (1990). Global climate change and intensification of coastal ocean upwelling. Science 247(4939), 198-201.

Bakun, A., D. B. Field, A. Redondo-Rodriguez and S. J. Weeks (2010). Greenhouse gas, upwelling-favorable winds, and the future of coastal ocean upwelling ecosystems. Global Change Biology 16(4), 1213-1228.

Belkin, I. M. (2009). Rapid warming of Large Marine Ecosystems. Progress in Oceanography 81(1–4), 207-213.

Berger, W. H., C. B. Lange and G. Wefer (2002). Upwelling history of the Benguela–Namibia system: a synthesis of Leg 175 results. Proceedings of the Ocean Drilling Program, Scientific Results, 1-103.

Bidigare, R. R., M. C. Kennicutt, W. L. Keeney-Kennicutt and S. A. Macko (1991). Isolation and purification of chlorophylls a and b for the determination of stable carbon and nitrogen isotope compositions. Analytical Chemistry 63(2), 130-133.

Bohlen, L., A. Dale, S. Sommer, T. Mosch, C. Hensen, A. Noffke, F. Scholz and K. Wallmann (2011). Benthic nitrogen cycling traversing the Peruvian oxygen

minimum zone. Geochimica et Cosmochimica Acta 75(20), 6094-6111.

Bremner, J. (1981). Shelf morphology and surficial sediment off central and northern South West Africa (Namibia). Geo-Marine Letters 1(2), 91-96.

Brüchert, V., B. Currie, K. R. Peard, U. Lass, R. Endler, A. Dübecke, E. Julies, T. Leipe and S. Zitzmann (2006). Biogeochemical and physical control on shelf anoxia and water column hydrogen sulphide in the Benguela coastal upwelling system off Namibia. and Present Marine Water Column Anoxia, edited by Neretin, NL, Jørgensen, BB, and Murray, JW, Springer, Berlin, Springer: 161-193.

Brüchert, V., B. Currie and K. R. Peard (2009). Hydrogen sulphide and methane emissions on the central Namibian shelf. Progress in Oceanography 83(1), 169-179.

Brunner, B., S. Contreras, M. F. Lehmann, O. Matantseva, M. Rollog, T. Kalvelage, G. Klockgether, G. Lavik, M. S. Jetten and B. Kartal (2013). Nitrogen isotope effects induced by anammox bacteria. Proceedings of the National Academy of Sciences 110(47), 18994-18999.

Buick, R. (2007). Did the Proterozoic 'Canfield Ocean' cause a laughing gas greenhouse? Geobiology 5(2), 97-100.

Bulow, S. E., J. J. Rich, H. S. Naik, A. K. Pratihary and B. B. Ward (2010). Denitrification exceeds anammox as a nitrogen loss pathway in the Arabian Sea oxygen minimum zone. Deep Sea Research Part I: Oceanographic Research Papers 57(3), 384-393.

Calleja, M. L., F. Batista, M. Peacock, R. Kudela and M. D. McCarthy (2013). Changes in compound specific δ^{15}N amino acid signatures and d/l ratios in marine dissolved organic matter induced by heterotrophic bacterial reworking. Marine Chemistry 149(0), 32-44.

Capone, D. G. (2014). An iron curtain in the Atlantic Ocean forms a biogeochemical divide. Proceedings of the National Academy of Sciences 111(4), 1231-1232.

Capone, D. G., J. A. Burns, J. P. Montoya, A. Subramaniam, C. Mahaffey, T.

Gunderson, A. F. Michaels and E. J. Carpenter (2005). Nitrogen fixation by Trichodesmium spp.: An important source of new nitrogen to the tropical and subtropical North Atlantic Ocean. Global Biogeochemical Cycles 19(2), GB2024.

Capone, D. G. and D. A. Hutchins (2013). Microbial biogeochemistry of coastal upwelling regimes in a changing ocean. Nature Geoscience 6(9), 711-717.

Carr, M.-E. and E. J. Kearns (2003). Production regimes in four Eastern Boundary Current systems. Deep Sea Research Part II: Topical Studies in Oceanography 50(22–26), 3199-3221.

Casciotti, K. L. (2009). Inverse kinetic isotope fractionation during bacterial nitrite oxidation. Geochimica et Cosmochimica Acta 73(7), 2061-2076.

Casciotti, K. L., D. M. Sigman, M. G. Hastings, J. K. Böhlke and A. Hilkert (2002). Measurement of the oxygen isotopic composition of nitrate in seawater and freshwater using the denitrifier method. Analytical Chemistry 74(19), 4905-4912.

Chapman, P. and L. Shannon (1987). Seasonality in the oxygen minimum layers at the extremities of the Benguela system. South African Journal of Marine Science 5(1), 85-94.

Chavez, F. P., M. Messié and J. T. Pennington (2011). Marine primary production in relation to climate variability and change. Annual Review of Marine Science 3, 227-260.

Chhak, K. and E. Di Lorenzo (2007). Decadal variations in the California Current upwelling cells. Geophysical Research Letters 34(14), L14604.

Clayson, C. H. (2000). Sensing of nitrate concentration by UV absorption spectrophotometry. Chemical Sensors in Oceanography. Gordon and Breach, London, 107-121.

Codispoti, L., J. A. Brandes, J. Christensen, A. Devol, S. Naqvi, H. W. Paerl and T. Yoshinari (2001). The oceanic fixed nitrogen and nitrous oxide budgets: Moving targets as we enter the anthropocene? Scientia Marina 65(S2), 85-105.

Dähnke, K. and B. Thamdrup (2013). Nitrogen isotope dynamics and fractionation during sedimentary denitrification in Boknis Eck, Baltic Sea. Biogeosciences 10(5), 3079-3088.

Den Camp, O., B. Kartal, D. Guven, L. Van Niftrik, S. Haaijer, W. Van Der Star, K. Van De Pas-Schoonen, A. Cabezas, Z. Ying and M. Schmid (2006). Global impact and application of the anaerobic ammonium-oxidizing(anammox) bacteria. Biochemical Society Transactions 34(1), 174-178.

Deutsch, C., W. Berelson, R. Thunell, T. Weber, C. Tems, J. McManus, J. Crusius, T. Ito, T. Baumgartner, V. Ferreira, J. Mey and A. van Geen (2014). Centennial changes in North Pacific anoxia linked to tropical trade winds. Science 345(6197), 665-668.

Di Lorenzo, E., A. J. Miller, N. Schneider and J. C. McWilliams (2005). The warming of the California Current System: Dynamics and ecosystem implications. Journal of Physical Oceanography 35(3), 336-362.

Dufois, F., P. Penven, C. Peter Whittle and J. Veitch (2012). On the warm nearshore bias in Pathfinder monthly SST products over Eastern Boundary Upwelling Systems. Ocean Modelling 47(0), 113-118.

Echevin, V., A. Albert, M. Lévy, M. Graco, O. Aumont, A. Piétri and G. Garric (2014). Intraseasonal variability of nearshore productivity in the Northern Humboldt Current System: The role of coastal trapped waves. Continental Shelf Research 73(0), 14-30.

Emeis, K.-C., V. Brüchert, B. Currie, R. Endler, T. Ferdelman, A. Kiessling, T. Leipe, K. Noli-Peard, U. Struck and T. Vogt (2004). Shallow gas in shelf sediments of the Namibian coastal upwelling ecosystem. Continental Shelf Research 24(6), 627-642.

Emeis, K.-C., U. Struck, T. Leipe and T. G. Ferdelman (2009). Variability in upwelling intensity and nutrient regime in the coastal upwelling system offshore Namibia: results from sediment archives. International Journal of Earth Sciences 98(2), 309-326.

Fennel, W., T. Junker, M. Schmidt and V. Mohrholz (2012). Response of the Benguela upwelling systems to spatial variations in the wind stress. Continental Shelf Research 45(0), 65-77.

Freudenthal, T., T. Wagner, F. Wenzhöfer, M. Zabel and G. Wefer (2001). Early diagenesis of organic matter from sediments of the eastern subtropical Atlantic: evidence from stable nitrogen and carbon isotopes. Geochimica et Cosmochimica Acta 65(11), 1795-1808.

Fulton, J. M., M. A. Arthur and K. H. Freeman (2012). Black Sea nitrogen cycling and the preservation of phytoplankton δ^{15}N signals during the Holocene. Global Biogeochemical Cycles 26(2), GB2030.

García-Reyes, M. and J. Largier (2010). Observations of increased wind-driven coastal upwelling off central California. Journal of Geophysical Research 115(C4), C04011.

García-Reyes, M. and J. Largier (2012). Seasonality of coastal upwelling off central and northern California: new insights, including temporal and spatial variability. Journal of Geophysical Research: Oceans (1978–2012) 117(C3).

Gaye-Haake, B., N. Lahajnar, K. C. Emeis, D. Unger, T. Rixen, A. Suthhof, V. Ramaswamy, H. Schulz, A. L. Paropkari, M. V. S. Guptha and V. Ittekkot (2005). Stable nitrogen isotopic ratios of sinking particles and sediments from the northern Indian Ocean. Marine Chemistry 96(3–4), 243-255.

Gaye, B., B. Nagel, K. Dähnke, T. Rixen and K.-C. Emeis (2013). Evidence of parallel denitrification and nitrite oxidation in the ODZ of the Arabian Sea from paired stable isotopes of nitrate and nitrite. Global Biogeochemical Cycles 27(4), 1059-1071.

Godfrey, L. V. and J. B. Glass (2011). The geochemical record of the ancient nitrogen cycle, nitrogen isotopes, and metal cofactors. In: Research on Nitrification and Related Processes (Part A), Methods in Enzymology 486, ed. M. G. Klotz, Academic Press. pp. 483-506.

Granger, J., M. G. Prokopenko, D. M. Sigman, C. W. Mordy, Z. M. Morse, L. V.

Morales, R. N. Sambrotto and B. Plessen (2011). Coupled nitrification-denitrification in sediment of the eastern Bering Sea shelf leads to ^{15}N enrichment of fixed N in shelf waters. Journal of Geophysical Research 116(C11), C11006.

Granger, J., D. M. Sigman, J. A. Needoba and P. J. Harrison (2004). Coupled nitrogen and oxygen isotope fractionation of nitrate during assimilation by cultures of marine phytoplankton. Limnology and Oceanography 49, 1763-1773.

Grimm, B., R. J. Porra, W. Rüdiger and H. Scheer (2006). Chlorophylls and bacteriochlorophylls: biochemistry, biophysics, functions and applications, Springer Science & Business Media, pp. 27-37.

Gruber, N., Z. Lachkar, H. Frenzel, P. Marchesiello, M. Munnich, J. C. McWilliams, T. Nagai and G.-K. Plattner (2011). Eddy-induced reduction of biological production in eastern boundary upwelling systems. Nature Geoscience 4(11), 787-792.

Güven, D., A. Dapena, B. Kartal, M. C. Schmid, B. Maas, K. van de Pas-Schoonen, S. Sozen, R. Mendez, H. J. O. den Camp and M. S. Jetten (2005). Propionate oxidation by and methanol inhibition of anaerobic ammonium-oxidizing bacteria. Applied and Environmental Microbiology 71(2), 1066-1071.

Gutiérrez, D., I. Bouloubassi, A. Sifeddine, S. Purca, K. Goubanova, M. Graco, D. Field, L. Méjanelle, F. Velazco, A. Lorre, R. Salvatteci, D. Quispe, G. Vargas, B. Dewitte and L. Ortlieb (2011). Coastal cooling and increased productivity in the main upwelling zone off Peru since the mid-twentieth century. Geophysical Research Letters 38(7), L07603.

Gutknecht, E., I. Dadou, P. Marchesiello, G. Cambon, B. L. Vu, J. Sudre, V. Garçon, E. Machu, T. Rixen and A. Kock (2013). Nitrogen transfers off Walvis Bay: a 3-D coupled physical/biogeochemical modeling approach in the Namibian upwelling system. Biogeosciences 10(6), 4117-4135.

Hagen, E. and R. Schemainda (1987). On the zonal distribution of South Atlantic Central Water (SACW) along a section off Cape Blanc, Northwest Africa.

Oceanologica Acta, 61-70.

Hannig, M., G. Lavik, M. Kuypers, D. Woebken, W. Martens-Habbena and K. Jürgens (2007). Shift from denitrification to anammox after inflow events in the central Baltic Sea. Limnology and Oceanography 52(4), 1336-1345.

Higgins, R. S. Robinson, S. J. Carter and A. Pearson (2010). Evidence from chlorin nitrogen isotopes for alternating nutrient regimes in the Eastern Mediterranean Sea. Earth and Planetary Science Letters 290(1–2), 102-107.

Higgins, M. B., R. S. Robinson, S. J. Carter and A. Pearson (2010). Evidence from chlorin nitrogen isotopes for alternating nutrient regimes in the Eastern Mediterranean Sea. Earth and Planetary Science Letters 290(1), 102-107.

Higgins, M. B., R. S. Robinson, K. L. Casciotti, M. R. McIlvin and A. Pearson (2008). A method for determining the nitrogen isotopic composition of porphyrins. Analytical Chemistry 81(1), 184-192.

Higgins., F. Wolfe-Simon, R. S. Robinson, Y. Qin, M. A. Saito and A. Pearson (2011). Paleoenvironmental implications of taxonomic variation among $\delta^{15}N$ values of chloropigments. Geochimica et Cosmochimica Acta 75(22), 7351-7363.

Higginson, M. J., J. R. Maxwell and M. A. Altabet (2003). Nitrogen isotope and chlorin paleoproductivity records from the Northern South China Sea: remote vs. local forcing of millennial-and orbital-scale variability. Marine Geology 201(1), 223-250.

Holmes, E., G. Lavik, G. Fischer, M. Segl, G. Ruhland and G. Wefer (2002). Seasonal variability of $\delta^{15}N$ in sinking particles in the Benguela upwelling region. Deep Sea Research Part I: Oceanographic Research Papers 49(2), 377-394.

Hormazabal, S., V. Combes, C. E. Morales, M. A. Correa-Ramirez, E. Di Lorenzo and S. Nuñez (2013). Intrathermocline eddies in the coastal transition zone off central Chile (31–41° S). Journal of Geophysical Research: Oceans 118(10), 4811-4821.

Jacox, M. G. and C. A. Edwards (2011). Effects of stratification and shelf slope on nutrient supply in coastal upwelling regions. Journal of Geophysical Research:

Oceans 116(C3), C03019.

Jensen, M. M., M. M. Kuypers, G. Lavik and B. Thamdrup (2008). Rates and regulation of anaerobic ammonium oxidation and denitrification in the Black Sea. Limnology and Oceanography 53(1), 23.

Junium, C. K. (2010). Nitrogen biogeochemistry and ancient oceanic anoxia, Ph.D. thesis, Pennsylvania State University, pp. 103-138.

Kalvelage, T., M. M. Jensen, S. Contreras, N. P. Revsbech, P. Lam, M. Günter, J. LaRoche, G. Lavik and M. M. Kuypers (2011). Oxygen sensitivity of anammox and coupled N-cycle processes in oxygen minimum zones. PLoS ONE 6(12), e29299.

Kalvelage, T., G. Lavik, P. Lam, S. Contreras, L. Arteaga, C. R. Loscher, A. Oschlies, A. Paulmier, L. Stramma and M. M. M. Kuypers (2013). Nitrogen cycling driven by organic matter export in the South Pacific oxygen minimum zone. Nature Geoscience 6(3), 228-234.

Karsh, K. L., J. Granger, K. Kritee and D. M. Sigman (2012). Eukaryotic assimilatory nitrate reductase fractionates N and O isotopes with a ratio near unity. Environmental Science & Technology 46(11), 5727-5735.

Karsh, K. L., T. W. Trull, D. M. Sigman, P. A. Thompson and J. Granger (2014). The contributions of nitrate uptake and efflux to isotope fractionation during algal nitrate assimilation. Geochimica et Cosmochimica Acta 132(0), 391-412.

Kirkpatrick, J. B., C. A. Fuchsman, E. Yakushev, J. T. Staley and J. W. Murray (2012). Concurrent activity of anammox and denitrifying bacteria in the Black Sea, Frontiers in Microbiology, 3, 256. doi:10.3389/fmicb.2012.00256.

Klein, P. and G. Lapeyre (2009). The oceanic vertical pump induced by mesoscale and submesoscale turbulence. Annual Review of Marine Science 1, 351-375.

Kritee, K., D. M. Sigman, J. Granger, B. B. Ward, A. Jayakumar and C. Deutsch (2012). Reduced isotope fractionation by denitrification under conditions relevant to the ocean. Geochimica et Cosmochimica Acta 92(0), 243-259.

Kuenen, J. G. (2008). Anammox bacteria: from discovery to application. Nature

Reviews Microbiology 6(4), 320-326.

Kuypers, M. M., A. O. Sliekers, G. Lavik, M. Schmid, B. B. Jørgensen, J. G. Kuenen, J. S. S. Damsté, M. Strous and M. S. Jetten (2003). Anaerobic ammonium oxidation by anammox bacteria in the Black Sea. Nature 422(6932), 608-611.

Kuypers, M. M. M., G. Lavik, D. Woebken, M. Schmid, B. M. Fuchs, R. Amann, B. B. Jørgensen and M. S. M. Jetten (2005). Massive nitrogen loss from the Benguela upwelling system through anaerobic ammonium oxidation. Proceedings of the National Academy of Sciences 102(18), 6478-6483.

Lam, P. and M. M. M. Kuypers (2011). Microbial nitrogen cycling processes in oxygen minimum zones. Annual Review of Marine Science 3(1), 317-345.

Lam, P., G. Lavik, M. M. Jensen, J. van de Vossenberg, M. Schmid, D. Woebken, D. Gutiérrez, R. Amann, M. S. Jetten and M. M. Kuypers (2009). Revising the nitrogen cycle in the Peruvian oxygen minimum zone. Proceedings of the National Academy of Sciences 106(12), 4752-4757.

Lass, H. U., M. Schmidt, V. Mohrholz and G. Nausch (2000). Hydrographic and Current Measurements in the Area of the Angola–Benguela Front. Journal of Physical Oceanography 30(10), 2589-2609.

Lavik, G., T. Stuhrmann, V. Bruchert, A. Van der Plas, V. Mohrholz, P. Lam, M. Mussmann, B. M. Fuchs, R. Amann, U. Lass and M. M. Kuypers (2009). Detoxification of sulphidic African shelf waters by blooming chemolithotrophs. Nature 457(7229), 581-584.

Leduc, G., C. T. Herbert, T. Blanz, P. Martinez and R. Schneider (2010). Contrasting evolution of sea surface temperature in the Benguela upwelling system under natural and anthropogenic climate forcings. Geophysical Research Letters 37(20), L20705.

Lehmann, M. F., S. M. Bernasconi, A. Barbieri and J. A. McKenzie (2002). Preservation of organic matter and alteration of its carbon and nitrogen isotope composition during simulated and in situ early sedimentary diagenesis. Geochimica et Cosmochimica Acta 66(20), 3573-3584.

Levitus, S., J. Antonov and T. Boyer (2005). Warming of the world ocean, 1955–2003. Geophysical Research Letters 32(2), L02604.

Levitus, S., J. Antonov, T. Boyer, R. Locarnini, H. Garcia and A. Mishonov (2009). Global ocean heat content 1955–2008 in light of recently revealed instrumentation problems. Geophysical Research Letters 36(7).

Lübbecke, J. F., C. W. Böning, N. S. Keenlyside and S. P. Xie (2010). On the connection between Benguela and equatorial Atlantic Niños and the role of the South Atlantic Anticyclone. Journal of Geophysical Research: Oceans (1978–2012) 115(C9).

Mack, J. and J. R. Bolton (1999). Photochemistry of nitrite and nitrate in aqueous solution: a review. Journal of Photochemistry and Photobiology A: Chemistry 128(1), 1-13.

Macko, S. A. and M. L. Estep (1984). Microbial alteration of stable nitrogen and carbon isotopic compositions of organic matter. Organic Geochemistry 6, 787-790.

Mahadevan, A. (2014). Ocean science: Eddy effects on biogeochemistry. Nature 506(7487), 168-169.

Mariotti, A., J. Germon, P. Hubert, P. Kaiser, R. Letolle, A. Tardieux and P. Tardieux (1981). Experimental determination of nitrogen kinetic isotope fractionation: some principles; illustration for the denitrification and nitrification processes. Plant and soil 62(3), 413-430.

McGregor, H., M. Dima, H. Fischer and S. Mulitza (2007). Rapid 20th-century increase in coastal upwelling off northwest Africa. Science 315(5812), 637-639.

Meisel, S., K.-C. Emeis, U. Struck and I. Kristen (2011). Nutrient regime and upwelling in the northern Benguela since the middle Holocene in a global context-a multi-proxy approach. Fossil Record 14(2), 171-193.

Meisel, S. and U. Struck (2011). The potential distortion of sedimentary $\delta^{15}N$ and Corg/N ratios by NH_4^+ and the effects of pre-analysis sample treatment. Fossil

Record 14(2), 141-152.

Mercier, H., M. Arhan and J. R. Lutjeharms (2003). Upper-layer circulation in the eastern Equatorial and South Atlantic Ocean in January–March 1995. Deep Sea Research Part I: Oceanographic Research Papers 50(7), 863-887.

Ming-Yi, S., C. Lee and R. C. Aller (1993). Laboratory studies of oxic and anoxic degradation of chlorophyll-*a* in Long Island Sound sediments. Geochimica et Cosmochimica Acta 57(1), 147-157.

Möbius, J. (2013). Isotope fractionation during nitrogen remineralization (ammonification): Implications for nitrogen isotope biogeochemistry. Geochimica et Cosmochimica Acta 105(0), 422-432.

Mohrholz, V., C. H. Bartholomae, A. K. van der Plas and H. U. Lass (2008). The seasonal variability of the northern Benguela undercurrent and its relation to the oxygen budget on the shelf. Continental Shelf Research 28(3), 424-441.

Mohrholz, V., M. Schmidt and J. Lutjeharms (2001). The hydrography and dynamics of the Angola-Benguela Frontal Zone and environment in April 1999. South African Journal of Science 97(5/6), 199-208.

Monteiro, P., A. Van Der Plas, J.-L. Melice and P. Florenchie (2008). Interannual hypoxia variability in a coastal upwelling system: Ocean–shelf exchange, climate and ecosystem-state implications. Deep Sea Research Part I: Oceanographic Research Papers 55(4), 435-450.

Monteiro, P. and A. K. van der Plas (2006). 5 Low oxygen water (LOW) variability in the Benguela system: key processes and forcing scales relevant to forecasting. Large Marine Ecosystems 14, 71-90.

Monteiro, P. M., B. Dewitte, M. I. Scranton, A. Paulmier and A. K. van der Plas (2011). The role of open ocean boundary forcing on seasonal to decadal-scale variability and long-term change of natural shelf hypoxia. Environmental Research Letters 6(2), 025002.

Monteiro, P. M., G. Nelson, A. van der Plas, E. Mabille, G. W. Bailey and E. Klingelhoeffer (2005). Internal tide-shelf topography interactions as a forcing

factor governing the large-scale distribution and burial fluxes of particulate organic matter (POM) in the Benguela upwelling system. Continental Shelf Research 25(15), 1864-1876.

Monteiro, P. M. S., A. van der Plas, V. Mohrholz, E. Mabille, A. Pascall and W. Joubert (2006). Variability of natural hypoxia and methane in a coastal upwelling system: Oceanic physics or shelf biology? Geophysical Research Letters 33(16), L16614.

Moore, C. M., M. M. Mills, E. P. Achterberg, R. J. Geider, J. LaRoche, M. I. Lucas, E. L. McDonagh, X. Pan, A. J. Poulton and M. J. Rijkenberg (2009). Large-scale distribution of Atlantic nitrogen fixation controlled by iron availability. Nature Geoscience 2(12), 867-871.

Morales, C. E., S. Hormazabal, M. Correa-Ramirez, O. Pizarro, N. Silva, C. Fernandez, V. Anabalón and M. L. Torreblanca (2012). Mesoscale variability and nutrient–phytoplankton distributions off central-southern Chile during the upwelling season: The influence of mesoscale eddies. Progress in Oceanography 104(0), 17-29.

Muller, A. A., V. Mohrholz and M. Schmidt (2013). The circulation dynamics associated with a northern Benguela upwelling filament during October 2010. Continental Shelf Research, 63, 59-68.

Nagel, B., K. C. Emeis, A. Flohr, T. Rixen, T. Schlarbaum, V. Mohrholz and A. Plas (2013). N-cycling and balancing of the N-deficit generated in the oxygen minimum zone over the Namibian shelf-An isotope-based approach. Journal of Geophysical Research: Biogeosciences, 118(1), 361-371.

Narayan, N., A. Paul, S. Mulitza and M. Schulz (2010). Trends in coastal upwelling intensity during the late 20th century. Ocean Science 6(3), 815-823.

Needoba, J. A., N. Waser, P. Harrison and S. Calvert (2003). Nitrogen isotope fractionation in 12 species of marine phytoplankton during growth on nitrate. Marine Ecology Progress Series 255, 81-91.

Nydahl, F. (1978). On the peroxodisulphate oxidation of total nitrogen in waters to

nitrate. Water Research 12(12), 1123-1130.

Pardo, P. C., X. A. Padín, M. Gilcoto, L. Farina-Busto and F. F. Pérez (2011). Evolution of upwelling systems coupled to the long-term variability in sea surface temperature and Ekman transport. Climate Research 48, 1123-1130.

Pichevin, L., P. Bertrand, M. Boussafir and J.-R. Disnar (2004). Organic matter accumulation and preservation controls in a deep sea modern environment: an example from Namibian slope sediments. Organic Geochemistry 35(5), 543-559.

Pietri, A., P. Testor, V. Echevin, A. Chaigneau, L. Mortier, G. Eldin and C. Grados (2013). Finescale Vertical Structure of the Upwelling System off Southern Peru as Observed from Glider Data. Journal of Physical Oceanography 43(3).

Poole, R. and M. Tomczak (1999). Optimum multiparameter analysis of the water mass structure in the Atlantic Ocean thermocline. Deep Sea Research Part I: Oceanographic Research Papers 46(11), 1895-1921.

Prahl, F. G., L. A. Muehlhausen and D. L. Zahnle (1988). Further evaluation of long-chain alkenones as indicators of paleoceanographic conditions. Geochimica et Cosmochimica Acta 52(9), 2303-2310.

Richter, I., S. K. Behera, Y. Masumoto, B. Taguchi, N. Komori and T. Yamagata (2010). On the triggering of Benguela Niños: Remote equatorial versus local influences. Geophysical Research Letters 37(20), L20604.

Robinson, R. S., M. Kienast, A. Luiza Albuquerque, M. Altabet, S. Contreras, R. De Pol Holz, N. Dubois, R. Francois, E. Galbraith, T.-C. Hsu, T. Ivanochko, S. Jaccard, S.-J. Kao, T. Kiefer, S. Kienast, M. Lehmann, P. Martinez, M. McCarthy, J. Möbius, T. Pedersen, T. M. Quan, E. Ryabenko, A. Schmittner, R. Schneider, A. Schneider-Mor, M. Shigemitsu, D. Sinclair, C. Somes, A. Studer, R. Thunell and J.-Y. Yang (2012). A review of nitrogen isotopic alteration in marine sediments. Paleoceanography 27(4), PA4203, 1-13.

Roemmich, D. and J. McGowan (1995). Climatic warming and the decline of zooplankton in the California Current. Science 267, 1324-1326.

Rogers, J. and J. Bremner (1991). The Benguela ecosystem: 7. Marine-geological aspects. Oceanography and Marine Biology: An Annual Review 29, 1-85.

Roman, M., R. Dovi, R. Yoder, F. Dias and B. Warden (1991). Determination by ion chromatography and spectrophotometry of the effects of preservation on nitrite and nitrate. Journal of Chromatography A 546, 341-346.

Rouault, M., S. Illig, C. Bartholomae, C. J. C. Reason and A. Bentamy (2007). Propagation and origin of warm anomalies in the Angola Benguela upwelling system in 2001. Journal of Marine Systems 68(3–4), 473-488.

Rouault, M., B. Pohl and P. Penven (2010). Coastal oceanic climate change and variability from 1982 to 2009 around South Africa. African Journal of Marine Science 32(2), 237-246.

Roy, S., C. A. Llewellyn, E. S. Egeland and G. Johnsen (2011). Phytoplankton pigments: characterization, chemotaxonomy and applications in oceanography, Cambridge University Press, pp. 675-822.

Sachs, J. P. and D. J. Repeta (2000). The purification of chlorins from marine particles and sediments for nitrogen and carbon isotopic analysis. Organic Geochemistry 31(4), 317-329.

Sachs, J. P., D. J. Repeta and R. Goericke (1999). Nitrogen and carbon isotopic ratios of chlorophyll from marine phytoplankton. Geochimica et Cosmochimica Acta 63(9), 1431-1441.

Santos, F., M. Gomez-Gesteira, M. deCastro and I. Alvarez (2012). Differences in coastal and oceanic SST trends due to the strengthening of coastal upwelling along the Benguela current system. Continental Shelf Research 34(0), 79-86.

Sarthou, G., A. R. Baker, S. Blain, E. P. Achterberg, M. Boye, A. R. Bowie, P. Croot, P. Laan, H. J. W. de Baar, T. D. Jickells and P. J. Worsfold (2003). Atmospheric iron deposition and sea-surface dissolved iron concentrations in the eastern Atlantic Ocean. Deep Sea Research Part I: Oceanographic Research Papers 50(10–11), 1339-1352.

Sarthou, G., K. R. Timmermans, S. Blain and P. Tréguer (2005). Growth physiology

and fate of diatoms in the ocean: a review. Journal of Sea Research 53(1), 25-42.

Schmid, M. C., N. Risgaard‑Petersen, J. Van De Vossenberg, M. M. Kuypers, G. Lavik, J. Petersen, S. Hulth, B. Thamdrup, D. Canfield and T. Dalsgaard (2007). Anaerobic ammonium-oxidizing bacteria in marine environments: widespread occurrence but low diversity. Environmental Microbiology 9(6), 1476-1484.

Schmidt, F., B. P. Koch, M. Elvert, G. Schmidt, M. Witt and K.-U. Hinrichs (2011). Diagenetic transformation of dissolved organic nitrogen compounds under contrasting sedimentary redox conditions in the Black Sea. Environmental Science & Technology 45(12), 5223-5229.

Schukat, A., H. Auel, L. Teuber, N. Lahajnar and W. Hagen (2014). Complex trophic interactions of calanoid copepods in the Benguela upwelling system. Journal of Sea Research 85(0), 186-196.

Shillington, F., C. Reason, C. Duncombe Rae, P. Florenchie and P. Penven (2006). 4 Large scale physical variability of the Benguela Current Large Marine Ecosystem (BCLME). Large Marine Ecosystems 14, 49-70.

Sigman, D., K. Kash and K. Casciotti (2009). Ocean process tracers: nitrogen isotopes in the ocean. Encyclopedia of Ocean Science, 2nd edn. Elsevier, Amsterdam, pp. 4138-4153.

Sigman, D. M., K. L. Casciotti, M. Andreani, C. Barford, M. Galanter and J. K. Böhlke (2001). A bacterial method for the nitrogen isotopic analysis of nitrate in seawater and freshwater. Analytical Chemistry 73(17), 4145-4153.

Sohm, J. A., J. A. Hilton, A. E. Noble, J. P. Zehr, M. A. Saito and E. A. Webb (2011). Nitrogen fixation in the South Atlantic Gyre and the Benguela upwelling system. Geophysical Research Letters 38(16), L16608.

Sohm, J. A., E. A. Webb and D. G. Capone (2011). Emerging patterns of marine nitrogen fixation. Nature Reviews Microbiology 9(7), 499-508.

Stramma, L., H. W. Bange, R. Czeschel, A. Lorenzo and M. Frank (2013). On the role

of mesoscale eddies for the biological productivity and biogeochemistry in the eastern tropical Pacific Ocean off Peru. Biogeosciences 10(11), 7293-7306.

Struck, U., A. V. Altenbach, K.-C. Emeis, J. Alheit, C. Eichner and R. Schneider (2002). Changes of the upwelling rates of nitrate preserved in the δ^{15}N-signature of sediments and fish scales from the diatomaceous mud belt of Namibia. Geobios 35(1), 3-11.

Swart, P. K., S. Evans, T. Capo and M. A. Altabet (2014). The fractionation of nitrogen and oxygen isotopes in macroalgae during the assimilation of nitrate. Biogeosciences. 11(5), 6909-6943.

Thamdrup, B., T. Dalsgaard, M. M. Jensen, O. Ulloa, L. Farías and R. Escribano (2006). Anaerobic ammonium oxidation in the oxygen-deficient waters off northern Chile. Limnology and Oceanography 51(5), 2145.

Tyler, J., Y. Kashiyama, N. Ohkouchi, N. Ogawa, Y. Yokoyama, Y. Chikaraishi, R. A. Staff, M. Ikehara, C. Bronk Ramsey, C. Bryant, F. Brock, K. Gotanda, T. Haraguchi, H. Yonenobu and T. Nakagawa (2010). Tracking aquatic change using chlorin-specific carbon and nitrogen isotopes: The last glacial-interglacial transition at Lake Suigetsu, Japan. Geochemistry, Geophysics, Geosystems 11(9), Q09010.

Vink, S. and C. I. Measures (2001). The role of dust deposition in determining surface water distributions of Al and Fe in the South West Atlantic. Deep Sea Research Part II: Topical Studies in Oceanography 48(13), 2787-2809.

Wada, E. (1980). Nitrogen isotope fractionation and its significance in biogeochemical processes occurring in marine environments. Isotope marine chemistry, 375-398.

Ward, B., A. Devol, J. Rich, B. Chang, S. Bulow, H. Naik, A. Pratihary and A. Jayakumar (2009). Denitrification as the dominant nitrogen loss process in the Arabian Sea. Nature 461(7260), 78-81.

Waser, N., P. Harrison, B. Nielsen, S. Calvert and D. Turpin (1998). Nitrogen isotope fractionation during the uptake and assimilation of nitrate, nitrite, ammonium,

and urea by a marine diatom. Limnology and Oceanography 43(2), 215-224.

Wasmund, N., G. Nausch and A. Hansen (2014). Phytoplankton succession in an isolated upwelled Benguela water body in relation to different initial nutrient conditions. Journal of Marine Systems 140, 163-174.

Wenk, C. B., J. Blees, J. Zopfi, M. Veronesi, A. Bourbonnais, C. J. Schubert, H. Niemann and M. F. Lehmann (2013). Anaerobic ammonium oxidation (anammox) bacteria and sulfide-dependent denitrifiers coexist in the water column of a meromictic south-alpine lake. Limnology and Oceanography 58(1), 1-12.

Wright, S., S. Jeffrey and R. Mantoura (1997). High-resolution HPLC system for chlorophylls and carotenoids of marine phytoplankton. Phytoplankton pigments in oceanography: guidelines to modern methods. ed. S.W. Jeffrey, R.F.C. Mantoura and S.W. Wright. Paris: UNESCO Publishing, pp. 327-341.

York, J. K., G. Tomasky, I. Valiela and D. J. Repeta (2007). Stable isotopic detection of ammonium and nitrate assimilation by phytoplankton in the Waquoit Bay estuarine system. Limnology and Oceanography 52(1), 144-155.

Appendix

A 1 Figures, tables and abbreviations

A 1.1 List of figure captions

112

116

A 1.2 List of table captions

A 1.3 List of abbreviations

ABFZ   Angola Benguela Frontal Zone

AC   Angola Current

ACS   American Chemical Society'

Anammox   anaerobic ammonium oxidization

ASE   accelerated solvent extraction system

BC   Benguela Current

BUS   Benguela Upwelling System

CBUS   central Benguela Upwelling System

Chl-a   chlorophyll a

C/N   molar ratio of total organic carbon to total nitrogen

CRS   constant rate of supply

CTD   conductivity, temperature, depth

DCM   dichloromethane

DO   dissolved oxygen

ε fractionation factor

ESACW   Eastern South Atlantic Central Water

ETSP   Eastern Tropical South Pacific

GC-FID   gas chromatography with flame ionization detector

HPLC   High-performance liquid chromatography

HZG   Helmholtz-Zentrum Geesthacht

IAEA   International Atomic Energy Agency

JGOFS   Joint Global Ocean Flux Study

NBUS   northern Benguela Upwelling System

N_{sed} total nitrogen in sediment

MAR   mass accumulation rate

OM   organic matter

OMZ	oxygen minimum zone
PN	particulate nitrogen
PON	particulate organic nitrogen
POR	persulfate (potassium) oxidizing reagent
PTFE	polytetrafluoroethylene
PUC	polarward undercurrent
SACW	South Atlantic Central Water
SBUS	southern Benguela Upwelling System
SECC	South Equatorial Counter-Current
SEUC	South Equatorial Under Current
TN	total nitrogen
TOC	total organic carbon
$U_{37}^{K\prime}$-SST	unsaturated alkenone derived sea surface temperature
USGS	United States Geological Survey
UV-Vis	ultraviolet-visible spectrophotometry

A2 A two-step HPLC separation of chlorophyll pigment in sediments and the δ^{15}N measurement

A2.1 General Procedures

Before the experiments, all the glass volumetric pipettes, vials, PTFE-lined septa (Polytetrafluoroethylene) and quartz tubes were soaked in a 10% hydrochloric acid (HCl) bath overnight. Then, all of them were rinsed thoroughly with Milli-Q water and dried in a designated clean space. The glass vials and quartz tubes were heated in a Fisher Scientific Iso-temp Muffle Furnace overnight at 450˚C. The volumetric bottle and caps were treated with the acid-bath and rinsed thoroughly with Milli-Q water.

Reagents and Standards

Milli-Q water used to prepare all solutions was produced by a Millipore Q-water system (Millipore Corp., Bedford, MA). HPLC grade methanol (MeOH), acetone (ACE), dichloromethane (DCM), and ethyl acetate (EE) were purchased from VWR. All the organic solvents were re-distilled, 1000× concentrated and checked for purity by GC-FID.

Chl-a and Chl-b standards (purity>95%) were purchased from Sigma-Aldrich Co.. Concentrated hydrochloric acid (37%, Reagent Grade, VWR) was used to prepare the 10% acid bath. Unless otherwise noted, all chemicals used in this project were reagent grade from VWR.

A2.2 UV-Vis method for aqueous nitrate measurement

UV-Vis spectrum at the Soret band has been widely applied to measure the nitrate concentration in natural water systems (Clayson 2000). The adsorption at 210 nm wavelength gives concentration of nitrate based on Beer's Law. We established the UV-Vis method for a quick and accurate measurement of the nitrate concentration in samples. It is found out that the SO_4, which decomposed from $K_2S_2O_8$, has absorbance at 210 nm. The 0.05 $mol \cdot l^{-1}$ $K_2S_2O_8$ will produce 0.1 $mol \cdot l^{-1}SO_4$ in the post-oxidization solution. 0.1 $mol \cdot l^{-1}$ SO_4 (in Milli-Q) has an absorbance of 0.016 at 210 nm, and drops to 0.11 with the addition of 80 µl H_2SO_4 (2 $mol \cdot l^{-1}$). This strong absorbance background of HSO_4/SO_4 overestimated the N-blank of POR (~3 $µmol \cdot l^{-1}$), while in fact the POR contains 1.4-1.8 $µmol \cdot l^{-1}$ N as measured by an auto-analyzer (Bran&Lübbe AA3). Therefore, this UV-Vis method is modified by using 0.1 $mol \cdot l^{-1}$ Na_2SO_4 Milli-Q solution instead of Milli-Q to establish the nitrate calibration curve. As shown in figure 1 a/b, the nitrate calibration curve of two different aqueous systems shows different slopes and intercepts that refer to different absorbance background. The N-nitrate in N-blank of POR and post-oxidization Chl-a standard is measured by this calibrated UV-Vis curve (Fig.1b) and agrees well with the result that is measured by a nutrient auto-analyzer (Fig. 2).
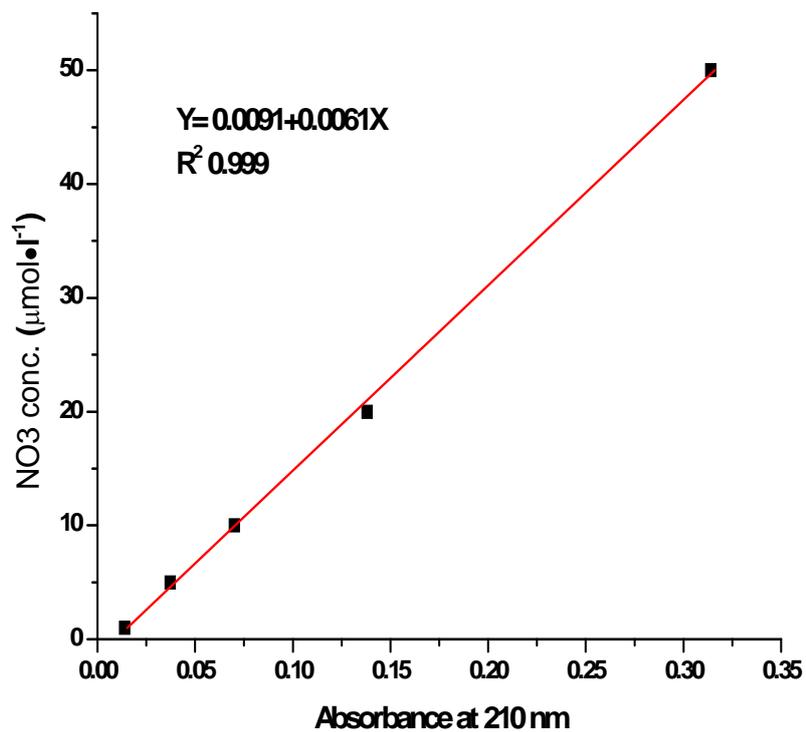
Fig. A2.1a Calibration curve (0.5, 1.0, 2.0, 5.0, 10.0, 20.0, and 50.0 $\mu M \cdot l^{-1}$ NO_3 in Milli-Q)
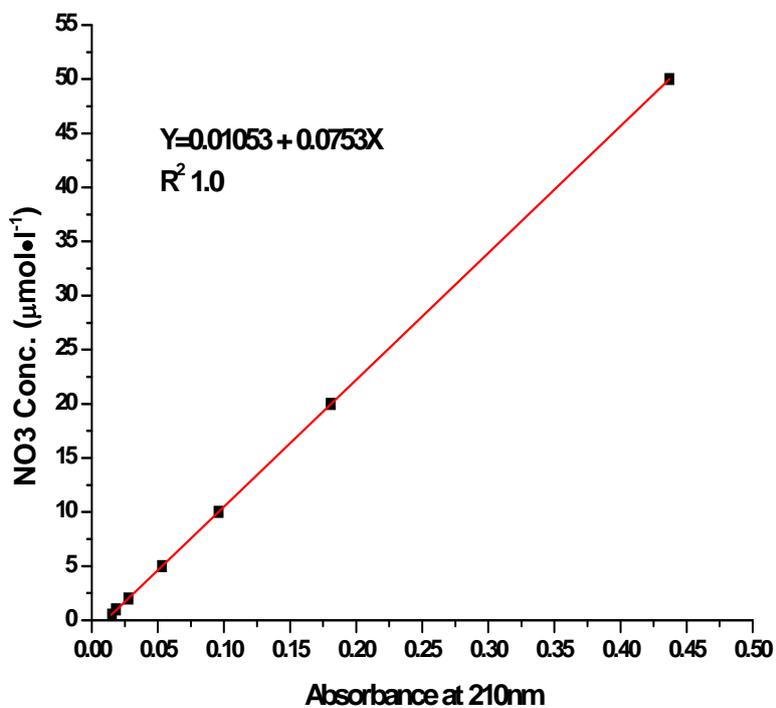
Fig. A2.1b Modified calibration curve (NO_3 in 0.1mol·l^{-1} Na_2SO_4 Milli-Q solution, with 80 μl

H$_2$SO$_4$ added)
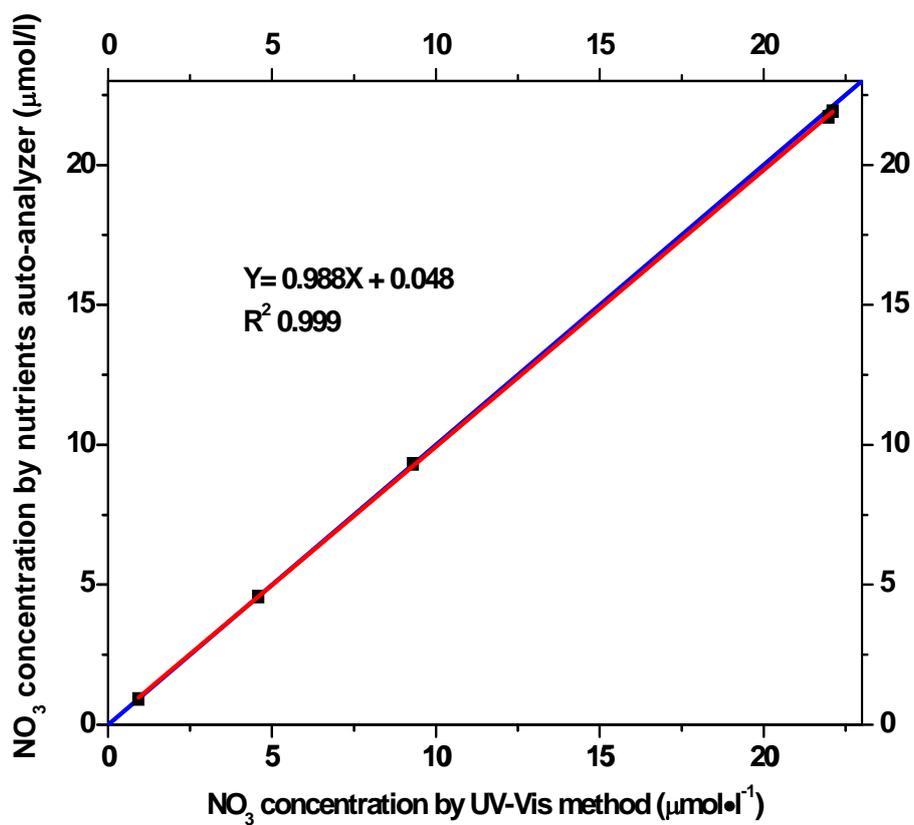
Fig. A2.2 Nitrate concentrations in post-oxidization Chl-a standard that are measured separately by UV-Vis method (X-axis) and nutrient auto-analyzer (y-axis): red line is the regression fitting; blue line is the 1:1 ratio.

A2.3 N-blank in POR solution

A quartz tube instead of normal glass tube (Glasgerätebau Ochs, GL45) is used in POR oxidization. The replicate results of oxidization treatment indicate good reproducibility and a consistent N-blank in the stock of re-crystallized $K_2S_2O_8$ that is stored over long periods of time.

To prevent freshly-made $K_2S_2O_8$ crystals from adsorbing air-borne nitrogen (Nydahl 1978), the saturated solution of $K_2S_2O_8$ (at 20℃, in fresh Milli-Q water) is prepared in a Duran bottle (GL45 Premium) sealed with a PTFE-coated cap after the 4th re-crystallization. Each time when POR solution is prepared, the saturated solution of $K_2S_2O_8$ is diluted by freshly-made NaOH aqueous solution (0.15 mol·l^{-1} in Milli-Q).

Table A2.1 Nitrate blank in autoclaved POR measured by UV-Vis method

04 Sept.2013		
Sample ID	Absorbance(210nm)	NO$_3$ conc.(μmol·l^{-1})
POR-1	0.023	1.67
POR-2	0.024	1.80
POR-3	0.023	1.67
POR-4	0.024	1.80
POR-5	0.02	1.27
POR-6	0.021	1.40
POR-7	0.022	1.53
AVG	0.022	1.59
STD	0.002	0.20
5th Sept.2013		
POR-1	0.024	1.80
POR-2	0.021	1.40
POR-3	0.023	1.67
AVG	0.023	1.62
STD	0.002	0.20

124

A2.4 Oxidization efficiency

Five replicates of Chl-a standard were oxidized by POR solution. The nitrate concentration in the autoclaved solution was measured by UV-Vis method, and the oxidization efficiency was calculated based on aqueous nitrate concentration against the molar N in the Chl-a standard.

Table A2.2 The oxidization efficiency of Chl-a standard

Sample ID	Pigment-N Conc. ($\mu mol \cdot ml^{-1}$)	NO3 Conc. ($\mu mol \cdot ml^{-1}$) by UV-Vis method	Oxidization efficiency (%)
POR		1.93	
Chla-1	8.82	8.69	98.5
Chla-2	8.82	9.09	103.0
Chla-3	8.82	8.53	96.7
Chla-4	8.82	9.06	102.7
Chla-5	8.82	9.19	104.2
AVG		8.91	101.0
STD		0.29	3.3

A2.5 N-blank in organic solvents and HPLC columns

The nitrate blank of redistilled organic solvent was examined by the following steps: the redistilled solvent is first concentrated to enrich the N contained, then it is oxidized to nitrate by POR, and at last it is measured by the UV-Vis method. The acetone shows comparatively high N contamination, which is estimated to be ~0.2 nmol·ml^{-1}.

Table A2.3 N-blank of organic solvents

	Blank-MilliQ (80μl H$_2$SO$_4$)	POR	EE (4ml)	DCM (6ml)	MeOH (10ml)	ACE (6ml)	ACE-NO3 conc.(nmol· ml^{-1})
1	0.004	0.03	0.031	0.029	0.033	0.04	0.2
2		0.03	0.034	0.03	0.031	0.037	0.2
3		0.03	0.031	0.031	0.029	0.039	0.2
4		0.029	0.03	N.a.	0.03	0.038	0.2
AVG		0.03	0.03	0.03	0.03	0.04	0.2
STD		0.00	0.00	0.00	0.00	0.00	0.03

The N-blank of all the HPLC-columns involved in separation were also examined. It is indicated that after careful washing, there is no N content released from the columns used in this study. The normal phase analytical column used in another HPLC may be slightly contaminated due to its long-time service, which made the N-background higher than that of the other normal phase analytical columns.

Table A2.4 Summary of N-blank in HPLC columns

Columns type	Quantity	Conclusions
LiChrospher RP-18 9.4mmx250mm, 10μr Merck KGaA	1	No N-content released
LiChrospher RP-18e 4.0mmx250mm, 5ur Merck KGaA	3	No N-content released
Lichrospher Si-60 9.4mm×250mm, 10 μr Merck KGaA	1	No N-content released
Lichrospher Si-60, 4.6mm×250mm, 5 μr Merck KGaA	2	No N-content released

Table A2.5 The detailed results of N-blank in HPLC columns

Replicates	Blank-MilliQ	POR	Semi-RP
1	0.005	0.046	0.043
2		0.047	0.046
3		0.049	0.048
AVG±STD		0.047±0.002	0.046±0.003
	Blank-MilliQ	**POR**	**Anal-RP**
1	0.003	0.042	0.042
2		0.042	0.044
3		0.039	0.046
4			0.042
		0.041±0.002	0.044±0.002
	Blank-MilliQ	**POR**	**Semi-NP**
1	0.003	0.03	0.033
2		0.03	0.034
3		0.03	0.033
		0.03	0.033±0.001
	Blank-MilliQ	**POR**	**HPLC-NP anal column**
1		0.03	0.033
2	0.003	0.029	0.035
3		0.03	0.034
4			0.032
		0.030±0.001	0.034±0.001
		POR	**LC-MS Anal column**
1		0.037	0.041
2		0.036	0.04
3		0.037	0.041
4			0.042
		0.037±0.001	0.041±0.001

A2.6 Identification of pheophytin-a by RP-HPLC

For the demetallated chlorins, the two most prominent λ-max (the wavelength with maximal absorbance) are at 420 and 660nm. Because the ultraviolet end of the spectrum is generally more affected by contamination than the infrared end, the absorption at 660 (the red band), rather than at 420 nm (the Soret band), is used to monitor the separation of pigment mixtures.
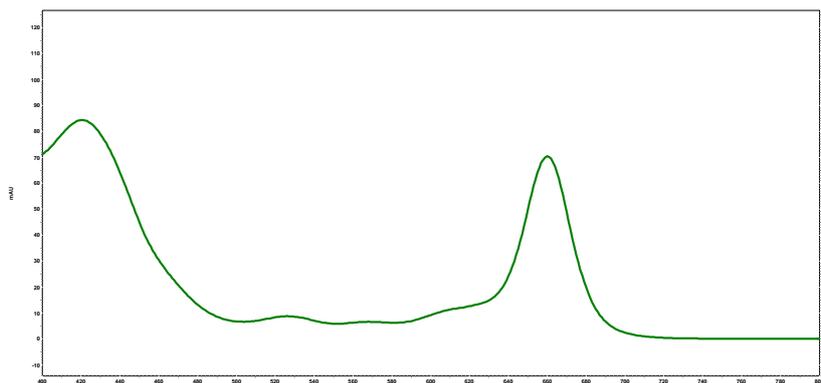
Fig. A2.3 The UV-Vis spectrum of the target pigment in this study.(the difference between their spectra is the presence of 3 small bumps in the 500 nm range which are distinctive for pheophytin a)
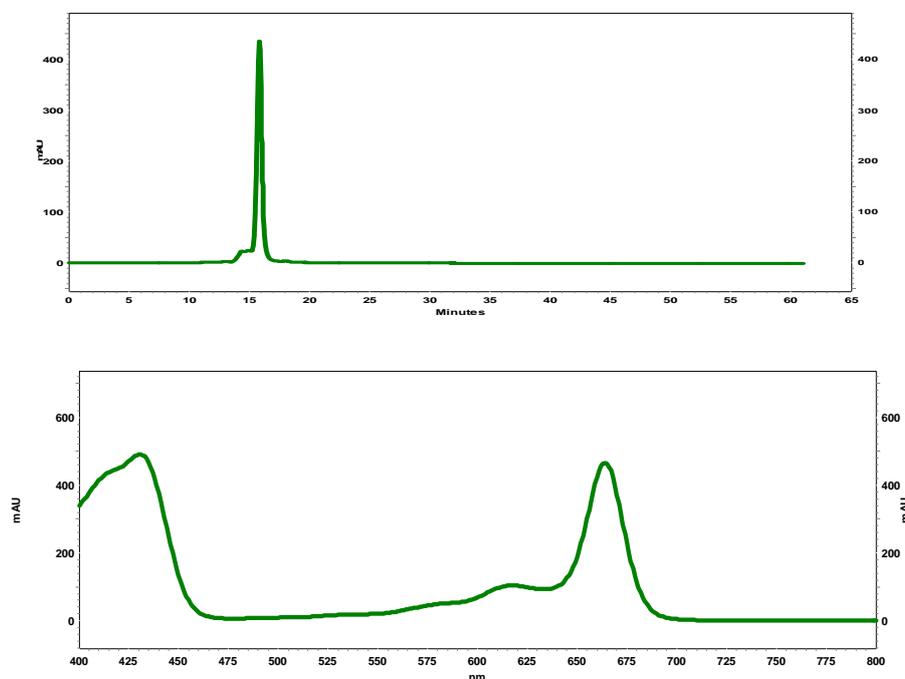

Fig. A2.4 Chromatography and spectrum of Chl-a on HPLC (Semi-RP column, 24 Oct. 2012)

128
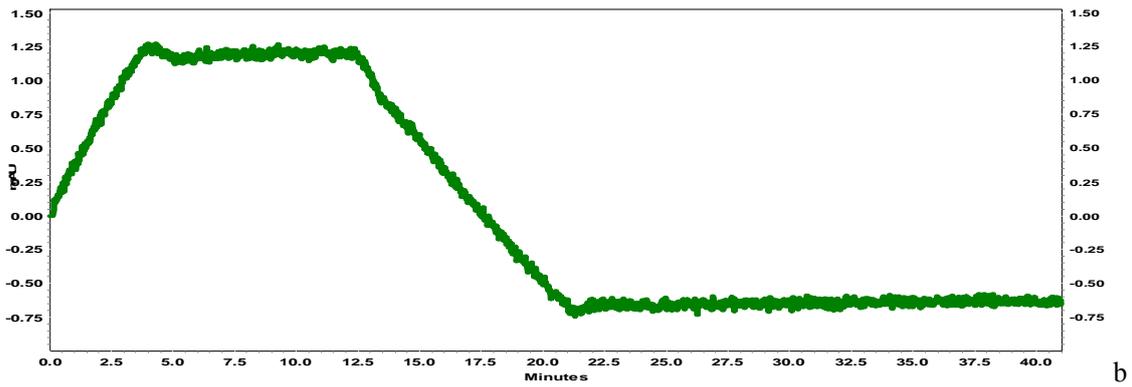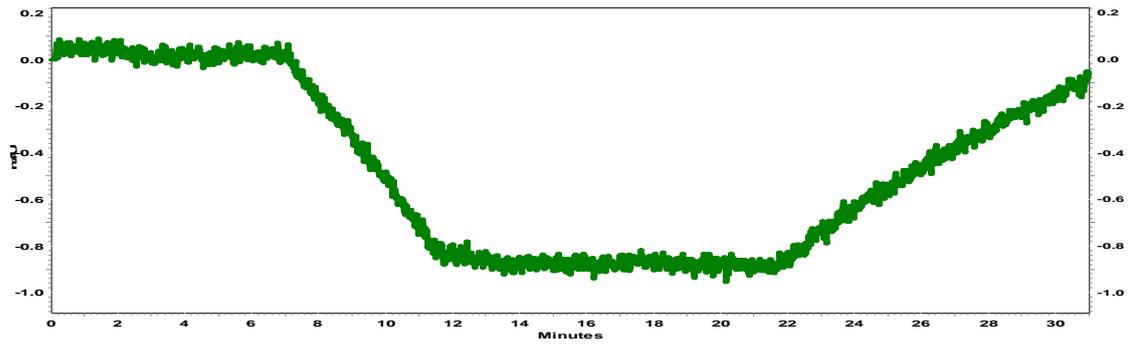
Fig. A2.5 The baseline chromatography after repeated washing (upper panel is semi-prep RP column, lower panel is analytical RP column). Wavelength is set at 660 nm.

A2.7 Running sequences for $\delta^{15}N$ measurement of chlorophyll pigment

An optimized running sequence for $\delta^{15}N$ measurement of chlorophyll pigment was established (Table 6). The chlorophyll-a standard is used as an internal standard. Seven pigment samples can be measured in duplicate within one round of measurement.

Table A2.7 An example of the running sequence for $\delta^{15}N$ measurement of pigment

Vial No.	Sample ID	Injection Volume (ml)	Vial No.	Sample ID	Injection Volume (ml)
1	Bacteria culture blank	0	....	Chl-a standard	1.0
2	IAEA-N3 10 μmol	1.0	29	Chl-a standard	1.0
3	POR-spiked IAEA	1.0	30	Chl-a standard	1.0
4	IAEA-N3 10 μmol	1.0	31	USGS 34 10 μmol	1.0
5	POR-spiked IAEA	1.0	32	POR-spiked USGS 34	1.0
6	IAEA-N3 10 μmol	1.0	33	USGS 34 10 μmol	1.0
7	POR-spiked IAEA	1.0	34	POR-spiked USGS 34	1.0
....	Pigment sample	1.0	35	USGS 34 10 μmol	1.0
....	Pigment sample	1.0	36	POR-spiked USGS 34	1.0

A 3 Spatial distribution of $\delta^{15}N_{Cholorophyll\text{-}a}$ in surface sediment of the northern Benguela Upwelling System

Table A3.1 Basic information of surface sediment stations of cruise M6-2 (mean of duplicate measurement is given here.)

Station	Latitude(ºS)	Longitude(ºE)	Depth (m)	TC (%)	TIC (%)	TOC (%)	TN (%)	$\delta^{15}N_{sed}$ (‰)	$\delta^{15}N_{Chl\text{-}a}$ (‰)
ST203	22.9990	13.4985	233.5	12.75	7.61	5.14	0.60	6.28	2.5
ST205	23.0005	13.8660	144.7	14.94	2.82	12.12	1.56	5.74	0.49
ST206	22.9978	14.0492	130.7	5.53	0.75	4.77	0.83	3.46	1.04
ST207	22.1667	14.0833	64	6.47	0.00	6.47	0.86	8.89	3.34
ST209	21.1947	12.6698	365	11.10	8.13	2.97	0.34	5.72	3.3
ST210	21.1140	12.9227	273	10.31	4.66	5.65	0.65	5.95	0.38
ST211	21.0443	13.1083	129	1.68	0.28	1.40	0.17	6.27	4.5
ST214	21.0078	13.2530	122	11.41	1.49	9.92	1.33	6.15	1.40
ST216	17.4207	11.0310	1509	3.16	0.51	2.65	0.34	5.18	0.8
ST217	17.4263	11.3672	302	1.30	0.58	0.72	0.07	5.45	2.3
ST218	17.4217	11.5348	150	1.53	0.26	1.27	0.17	4.32	0.4
ST219	17.4195	11.6525	93	3.82	0.37	3.45	0.49	4.04	-4.5
ST221	19.2227	11.6887	339	10.68	6.37	4.31	0.52	5.09	2.12
ST222	19.1223	12.0113	236	5.46	0.82	4.64	0.66	4.51	1.6
ST224	19.0160	12.3435	97	4.90	0.47	4.43	0.70	5.18	-1.71
ST225	19.0167	12.2290	119	3.17	0.02	3.15	0.461	4.92	2.5
ST226	20.1827	11.6672	739	10.49	5.70	4.79	0.55	5.38	-2.7
ST227	20.1000	12.1078	307	12.95	5.83	7.12	0.85	5.53	-0.66
ST228	19.9848	12.4592	171	10.19	3.80	6.39	0.86	5.55	-1.17
ST229	19.8445	12.6748	120	7.66	0.92	6.74	0.93	6.33	-1.3

ST230	19.8138	12.7728	99.7	11.95	1.25	10.70	1.39	6.29	2.2
ST231	21.0078	13.2533	102.7	11.95	1.25	10.70	1.39	6.37	0.72
ST239	22.3235	12.9092	325	11.46	9.22	2.24	0.27	6.36	-1.8
ST240	22.2408	13.2430	228	13.28	8.35	4.93	0.57	6.08	0.80
ST241	22.1582	13.6183	134	13.97	2.66	11.31	1.52	6.14	0.53
ST242	22.0560	14.0512	56	2.89	0.26	2.63	0.33	8.43	4.54
ST243	22.0957	13.8615	102.7	9.33	0.95	8.38	1.20	7.61	3.20

132

Figure A3.1 The correlation between OMZ percentage (%) and Δ ($\delta^{15}N_{sed}$-$\delta^{15}N_{Chl\text{-}a}$, in ‰) in surface sediment of the northern BUS (M76-2).

OMZ is defined by dissolved oxygen concentration <20 $\mu mol \cdot l^{-1}$, the OMZ percentage is calculated by the thickness of the OMZ interval (m) divided by the bottom depth of sampling station (m).
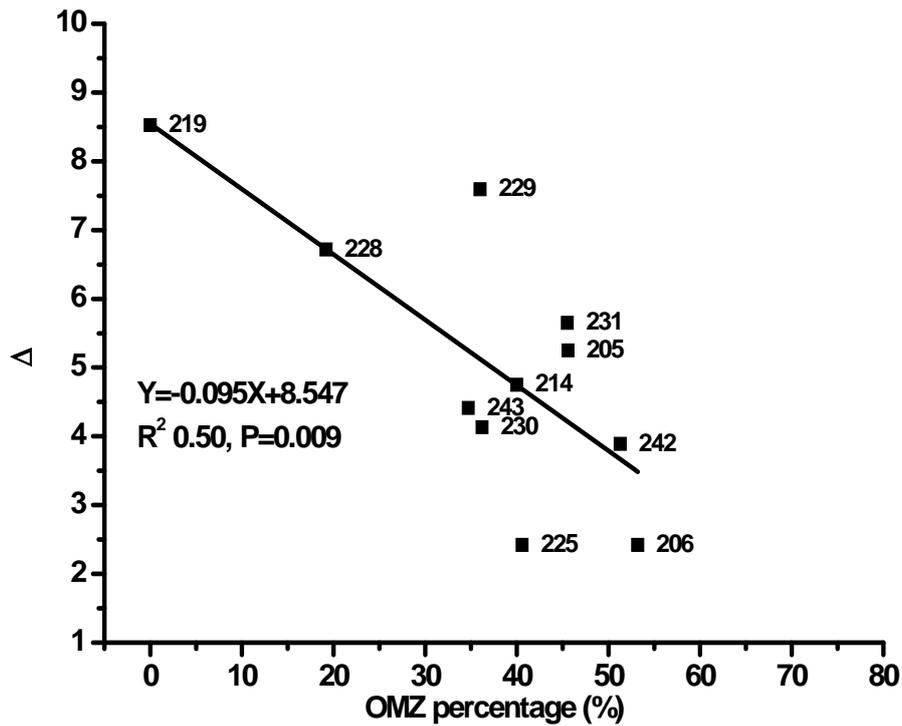
Fig. A3.1 The correlation between OMZ proportions (%) and GAP ($\delta^{15}N_{sed}$-$\delta^{15}N_{Chl\text{-}a}$, in ‰).

Figure A3.2 The correlation between $\delta^{15}N_{Chl-a}$ (‰) and OMZ percentage (%) at shelf stations (M76-2)

OMZ is defined by dissolved oxygen concentration <20 µmol·l^{-1}, the OMZ percentage is calculated by the thickness of the OMZ interval (m) divided by the bottom depth of sampling station (m).
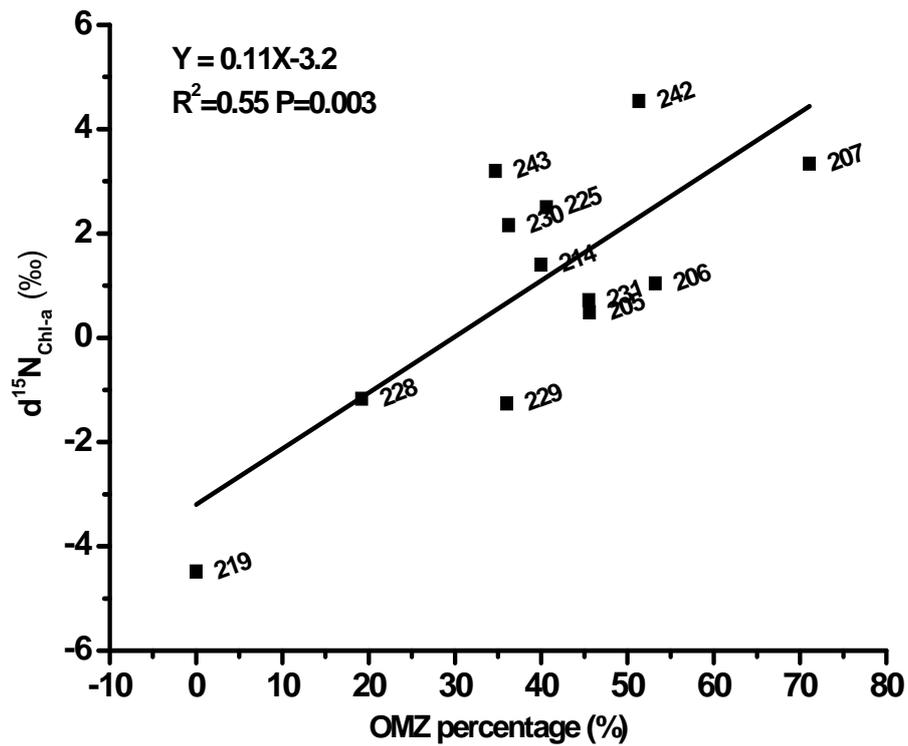
Fig. A3.2 The correlation between $\delta^{15}N_{Chl-a}$ (‰) and OMZ percentage (%) of shelf stations (M76-2).

Figure A3.3 The correlation between OMZ percentage (%) and the latitude (^{0}S) of sampling station in M76-2
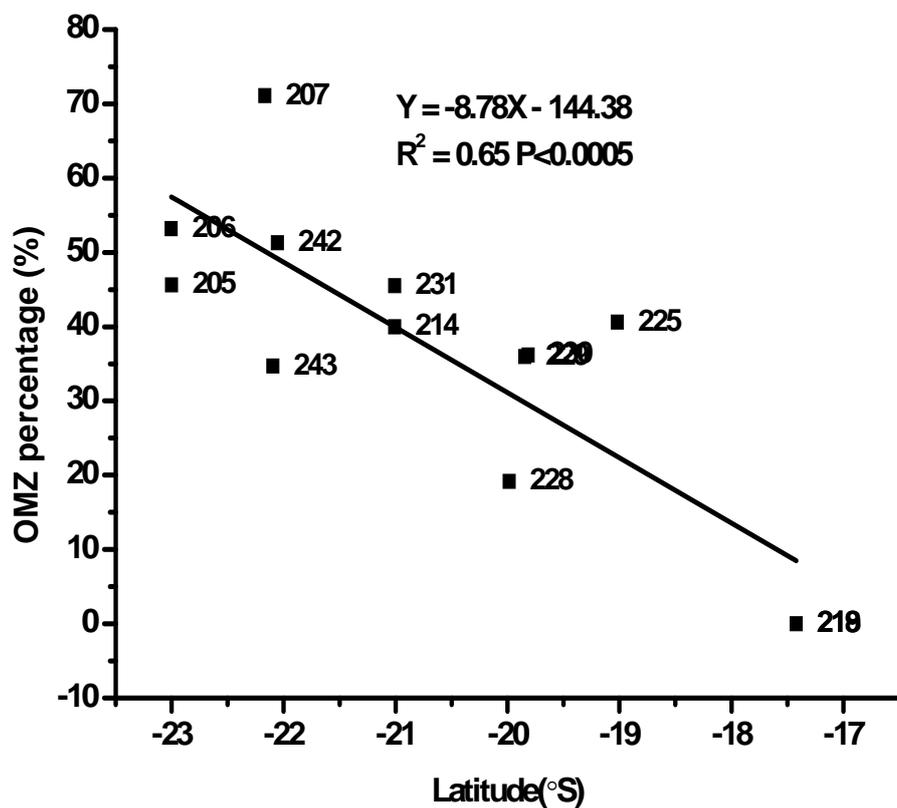
Fig. A3.3 The correlation between OMZ proportion (%) and the latitude (ºS) of the stations in M76-2.

Figure A3.4 The correlation between DO concentration (μmol·l⁻¹) and salinity (PSU) in the thermocline layer. Dataset is from cruise M76-2, May, 2008.
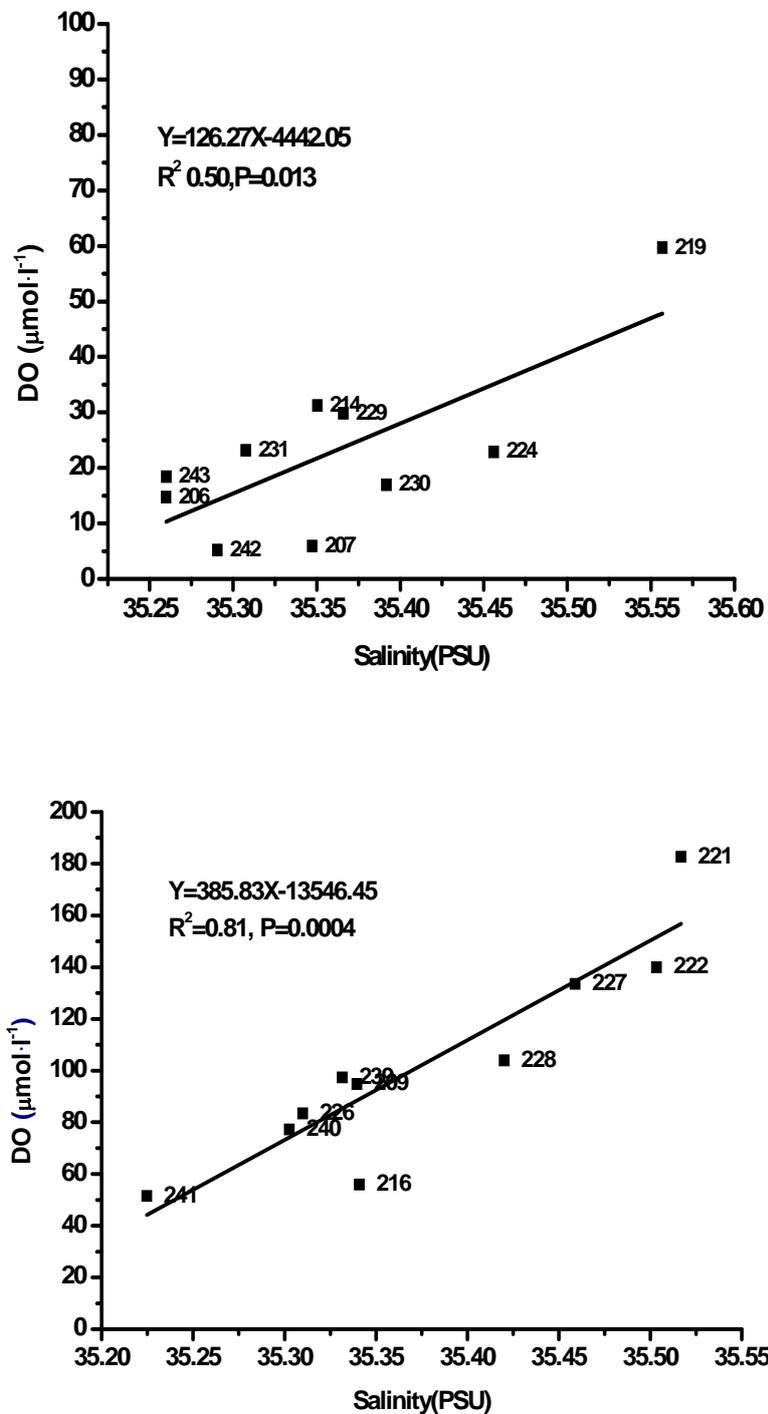
Fig. A3.4 The correlation between DO concentration (μmol·l⁻¹) and salinity (PSU) in the thermocline layer: upper panel is for inner shelf stations, lower panel is for the outer shelf stations).

Figure A3.5 The correlation between $\delta^{15}N_{Chl-a}$ (‰) and sea surface temperature at 10 m depth (℃) over the outer shelf stations.
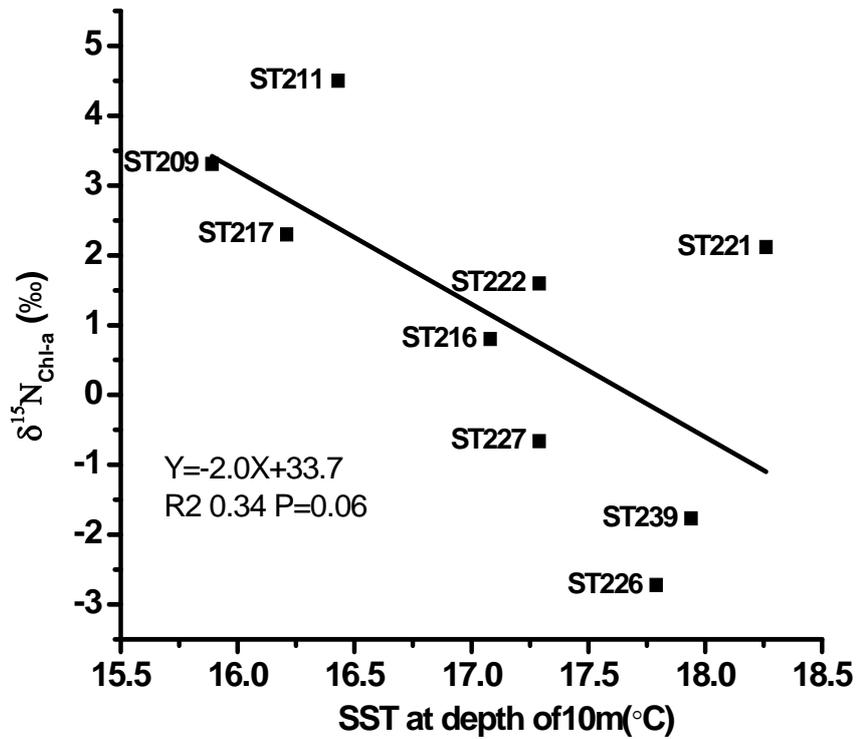
Fig. A3.5 The correlation between $\delta^{15}N_{Chl-a}$ (‰) and sea surface temperature at 10 m epth (℃) over the outer shelf stations.

Figure A3.6 The correlation between $\delta^{15}N_{\text{Chl-a}}$ and seawater temperature (℃) and salinity (PSU) at depth of 10m across the transect at ~22.5°S.
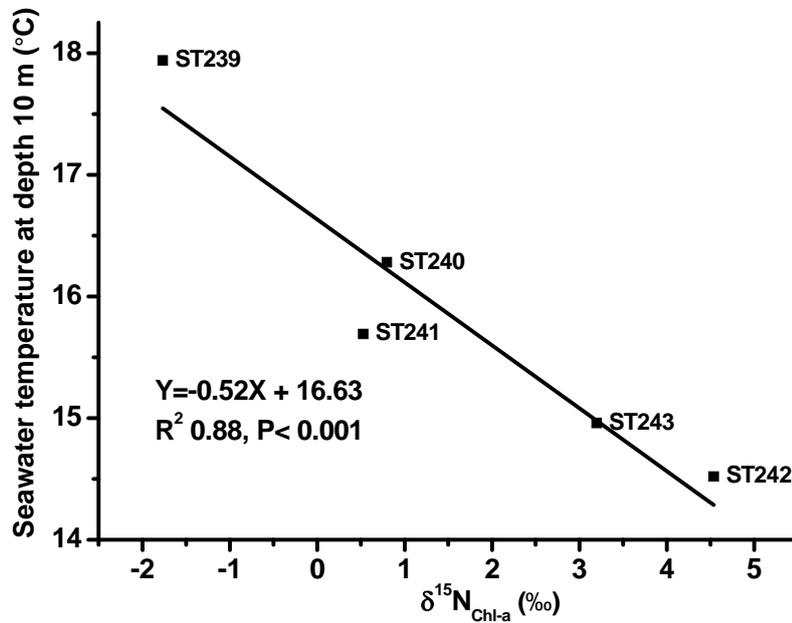
Fig. A3.6a The correlation between the $\delta^{15}N_{\text{Chl-a}}$ and seawater temperature (℃) at depth of 10m. Stations are located at the transect of ~22.5°S.
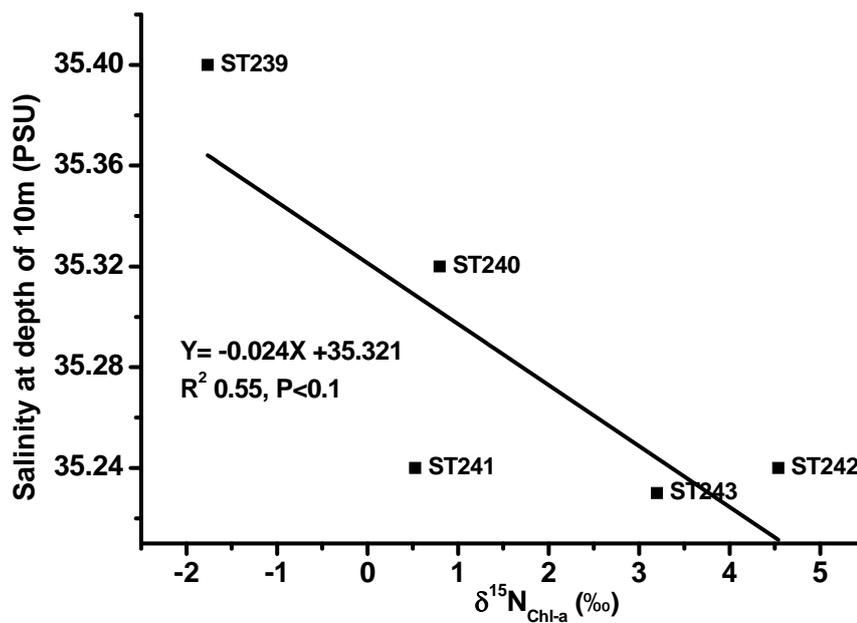

Fig. A3.6b The correlation between the $\delta^{15}N_{\text{Chl-a}}$ and seawater salinity (PSU) at depth of 10m. Stations are located at the transect of ~22.5°S.

A 4 Temporal variations of N-loss intensity in the northern Benguela Upwelling System - based on the $\delta^{15}N_{Chlorophyll-a}$ records in a dated sediment core

Table A4.1 Data set of all the proxies measured in multicore ST231

Depth (cm)	Dated age (Yr)	TN (%)	C_{org} (%)	C/N molar	$U^{k'}_{37}$-SST	$\delta^{15}N_{sed}$ (‰)	$\delta^{15}N_{Chl-a}$ (‰)	Error (duplicate)	$\Delta(\delta^{15}N_{sed}-\delta^{15}N_{Chl-a})$
0-1	2007	1.4	10.7	9.0	18.7	6.4	0.4	0.1	6.0
1-2	2005	1.4	11.1	9.2	18.1	6.2	0.4	0.1	5.8
2-3	2004	1.4	11.0	9.2	18.3	6.4	0.6	0.1	5.8
3-4	2002	1.4	11.4	9.2	18.0	6.4	0.6	0.1	5.8
4-5	2000	1.3	10.8	9.4	18.2	6.5	0.2	0.2	6.2
5-6	1997	1.3	10.7	9.6	18.5	6.5	1.6	0.1	4.9
6-7	1995	1.4	11.1	9.3	18.0	6.6	0.1	0.1	6.6
7-8	1992	1.4	11.3	9.6	18.6	6.6	0.1	0.0	6.5
8-9	1990	1.4	11.3	9.6	17.2	6.3	0.7	0.3	5.6
9-10	1987	1.3	11.2	9.7	17.5	6.5	1.3	0.0	4.2
10-11	1984	1.4	11.9	9.9	18.2	6.4	0.3	0.2	6.2
11-12	1981	1.4	11.9	9.9	17.8	6.4	1.1	0.1	5.3
12-13	1978	1.4	12.1	10.1	17.7	6.4	0.8	0.0	5.6
13-14	1974	1.4	12.2	10.0	17.9	6.4	1.0	0.0	5.4
14-15	1970	1.4	11.9	10.1	18.1	6.4	2.4	0.1	4.1
15-16	1964	1.3	11.4	10.0	17.4	6.4	0.6	0.1	5.8

16-17	1958	1.4	11.5	9.9	18.1	6.4	0.8	0.0	5.6
17-18	1952	1.3	11.5	10.0	17.8	6.5	2.1	0.0	4.5
18-19	1949	1.3	10.9	9.9	18.1	6.5	2.2	0.2	4.2
19-20	1945	1.2	10.7	10.1	17.7	6.4	0.7	0.0	5.8
20-21	1937	1.2	10.3	9.8	18.2	6.3	-0.5	0.0	6.8
21-22	1929	1.1	9.7	9.8	18.8	6.5	0.3	0.0	6.1
22-23	1924	1.0	8.6	9.7	18.6	6.5	0.5	0.0	6.0
23-24	1917	0.9	7.6	10.0	18.5	6.7	0.5	0.2	6.3
24-25	1909	0.8	6.6	10.0	18.4	6.9	0.7	0.2	6.2
25-26	1901	0.5	4.6	10.2	17.5	7.2	1.6	0.1	5.6
26-27	1890	1.0	7.9	9.7	17.6	6.8	1.0	0.2	5.8
27-28	1876	1.3	11.1	9.7	18.0	6.6	-1.0	0.1	7.6
28-29	1862	1.3	11.3	9.8	17.5	6.8	1.6	0.2	5.2
29-30	1858	1.3	11.4	9.9	17.8	6.6	0.8	0.1	5.8
30-31	1827	1.4	11.4	9.8	17.7	6.6	0.7	0.1	5.9
31-32	1820	1.0	8.8	9.9	17.0	6.6	1.2	0.1	5.4
32-33	32cm	0.5	4.6	10.0	17.9	7.2	1.4	0.0	5.8
33-34	33cm	1.1	8.2	9.0	16.1	6.7	2.1	n.a.	4.6
34-35	34cm	1.0	9.0	10.1	16.5	6.6	1.4	n.a.	5.2
35-36	35cm	0.7	6.0	10.0	17.5	7.2	0.9	n.a.	6.3
36-37	36cm	0.3	2.9	10.0	18.3	7.9	0.8	0.1	7.0

Core slices at depth of 32-36 cm are not dated due to the undetected ^{210}Pb excess. Error bar is not available for the data at depth interval of 33-35 cm, because the pigment extractions are insufficient for duplicate measurements. The $\delta^{15}N_{sed}$ is mean value of duplicates.

140

Table A4.2 The results of student's T-test of $\delta^{15}N_{Chl\text{-}a}$ (‰), $\delta^{15}N_{sed}$(‰), TOC (%), SST (℃) in different time intervals**.**

SPSS 19.0 is used for T-test examinations. The "√" means that the data between the time intervals passes T-test and is statistically different (95 % confidence intervals); and the "×" means that the data between the time intervals fails T-test, but no further examinations by other statistical methods are carried out.

$\delta^{15}N_{Chl\text{-}a}$ (‰)	1980-2007	1940-1980	1940-1980	<1940
ST231[*]	√		√	
Bulk $\delta^{15}N_{sed}$(‰)				
226790	√		√	
226770	×		√	
ST231[*]	×		√	
TOC (%)				
226790	√		×	
226770	×		√	
ST231[*]	√		√	
SST (℃)				
226790	√		√	
226770	√		√	
ST231[*]	√		×	

ST231[*]: the time intervals are demarcated as 1990-2007, 1940-1990, <1940 for better statistical robustness.

Figure A4.1 Box analyses of SST and TOC variations of three shelf stations in different time periods.

Data of 226790, 266770 are from Emeis et al (2009), data of ST231 is from this study. Global warming is considered to become obvious after 1940, and Rouault et al (2007, 2010) reported a significant warming trend at the northern boundary of ABFZ since 1982. Thus, the 3 time periods are marked accordingly. Because the data of 226790, 266770 within 1990-2000 are too few for a robust statistical analysis, the periods are demarcated as 1980-2000, 1940-1980, <1940. There is a broadly inverse trend between SST and TOC at ST 231 and 226790, which indicates that upwelling promotes biological production. But this trend is not observed at 226770, where the TOC averages 3% throughout the core record except in the period of 1980-1990.
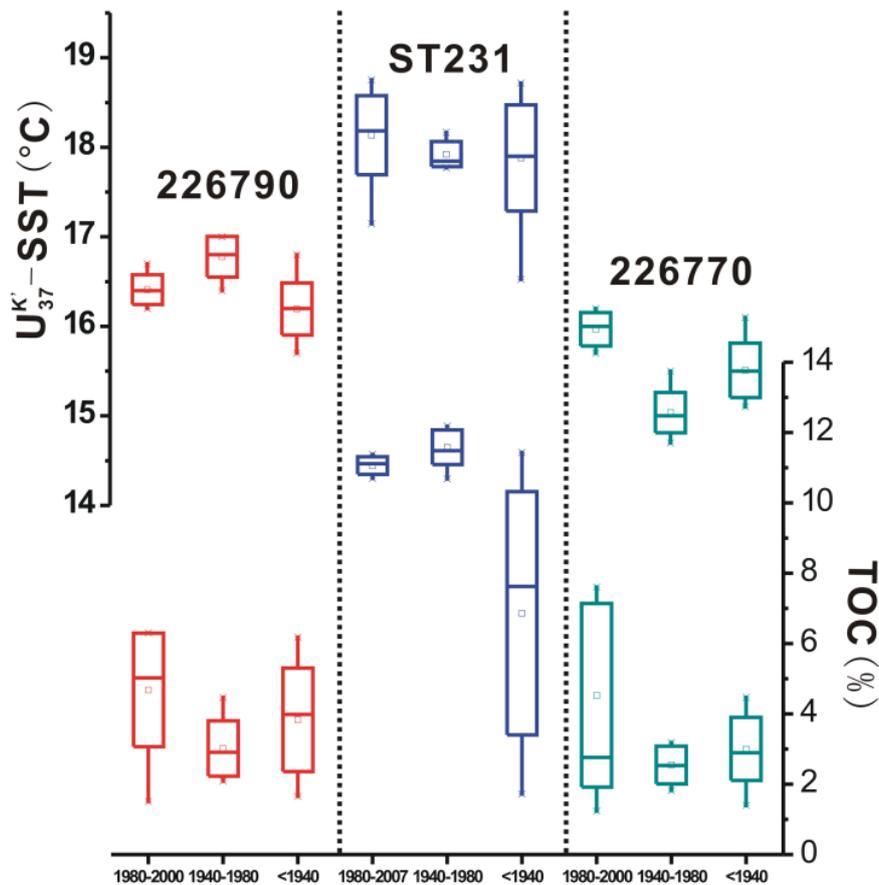

Fig. A4.1 Box analyses of SST (℃) and TOC (%) at three shelf stations in those time intervals

Figure A4.2 Box charts of SST, TOC and $\delta^{15}N_{sed}$ at ST231 in different time periods

There is an obvious decreasing trend in $\delta^{15}N_{Chl\text{-}a}$ since 1990. In order to obtain the broad variation trend between SST, TOC, and $\delta^{15}N_{sed}$ over the dated time period, we mark 3 stages: 1990-2007 (ABFZ warming), 1940-1990 (global warming), and before 1940 (without significant global warming).
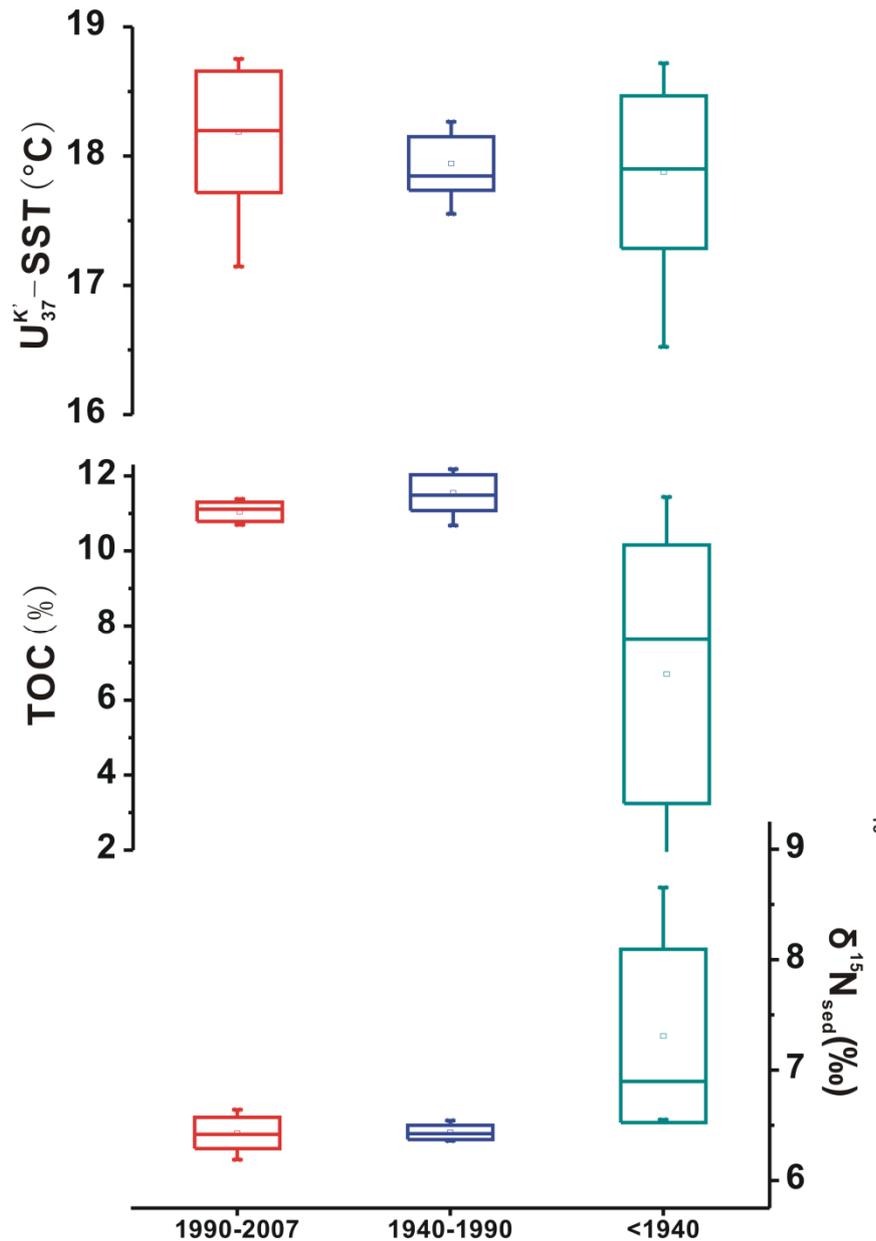

Fig. A4.2 Box charts of SST (℃), TOC (%) and $\delta^{15}N_{sed}$ (‰) at ST231 in different time periods

Figure A4.3: The correlation between $\delta^{15}N_{Chl-a}$ (‰) and $U^{K\prime}_{37}$SST (℃) at station ST231 over the time period of 1940-2007.
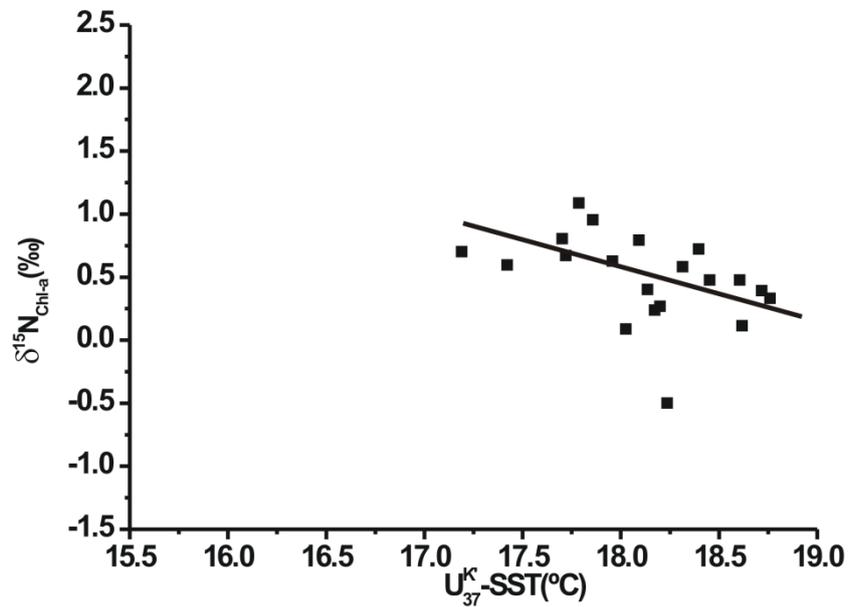
Fig.A4.3: The correlation between $\delta^{15}N_{Chl-a}$ and $U^{K\prime}_{37}$SST (℃) at station ST231 over the time period of 1940-2007 that is reconstructed from core records of 0-20 cm.. . .

Figure A4.4 The correlation between $\delta^{15}N_{Chl-a}$ and $\delta^{15}N_{sed}$ (‰) at station ST231. The upper panel is the correlation of whole core records, and the lower panel is the correlation of the depth interval of 0-20 cm.
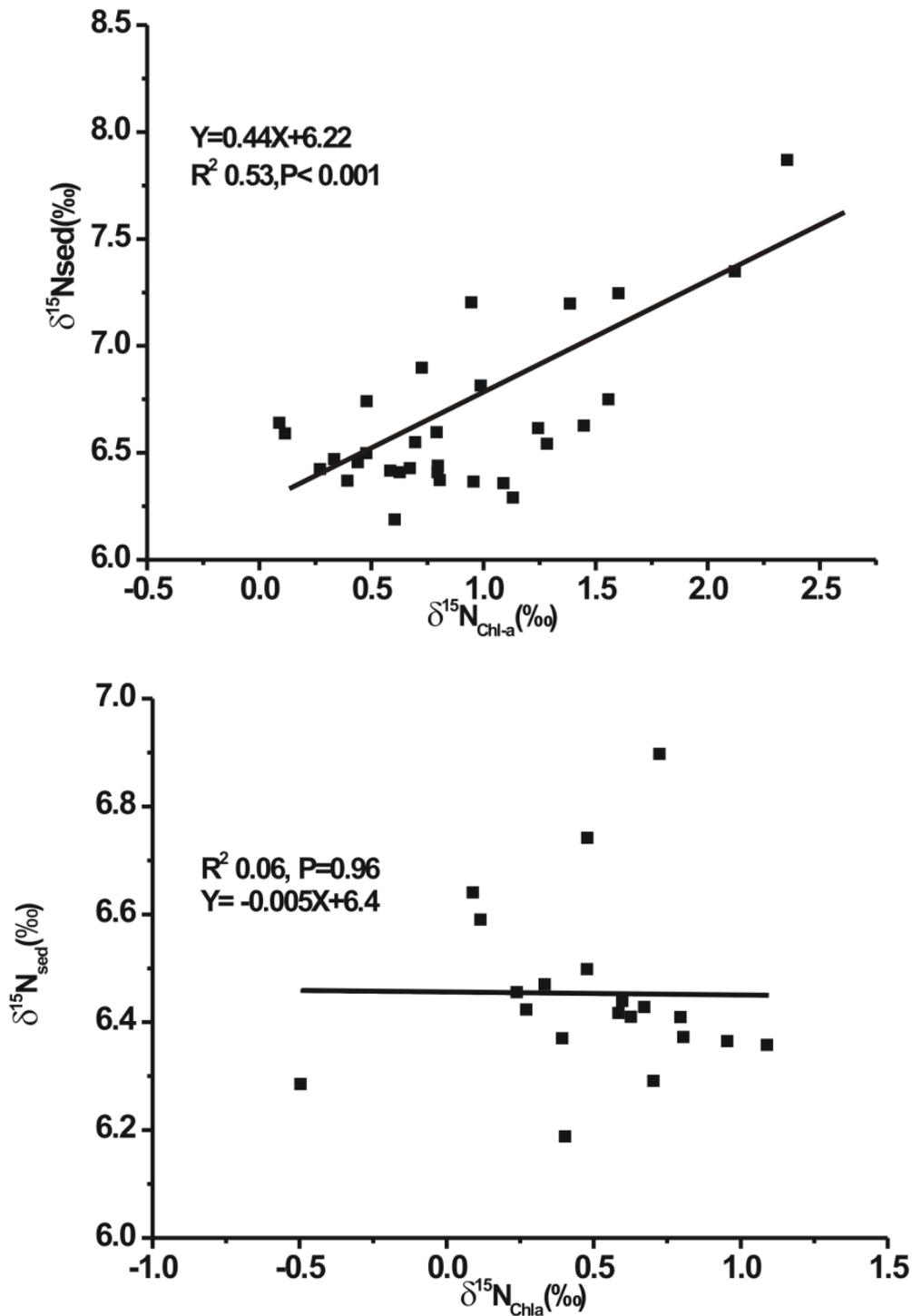
Fig. A4.4 The correlation between $\delta^{15}N_{Chl-a}$ and $\delta^{15}N_{sed}$ (‰) at station ST231. The upper panel is the correlation of whole core records, and the lower panel is the correlation at the depth interval of 0-20 cm.

Acknowledgement

This is the last part I write for my thesis. In the past four years, I had so many people to whom I owned hearty thanks that are beyond the capability of my words.

My parents are the first that jump in my minds. When I decided to study abroad by giving up my career as an administration staff at Ocean University of China, they chose to stand by my side affirmatively, supporting me without a single moment of hesitation. I think, the accomplishment of my thesis is the best reward to them. My fiancée, Ms. Shi Jing, was a DAAD scholarship holder that I happened to meet in a DAAD-organized re-union activity. She attracted me all of a sudden. At last, she became my fiancée and waited me patiently in China for almost two years. Whenever I was in bad mood or frustrated, she was there for me.

My colleagues in Geomatikum are really nice persons. They helped me a great deal whenever I had difficulties either in experiment or in personal issues. Mrs. Sabine Beckmann trained me well for the experimental skills that I almost forgot. She is such a capable technician that I realized how important an excellent technician is for a well-running lab. Mrs. Frauke Langenberg is another excellent person I want to thank. She measured my samples with precise and satisfactory results that provided solid foundation to my thesis. Dr. Kirstin Dähnke is so kind to help me to develop the method for measuring the nitrogen isotope of pigment samples. Mr. Markus Ankele is thanked for his contributions to measurement of the N-blank in chemical reagent. Other colleagues like Dr. Niko Lahajnar, Dr. Jürgen Möbius, Dr. Philip Menzel, Dr. Anna Böll are all equally thanked for their kindness and generous help to my experiment and discussions in my thesis writing.

My colleagues in Ocean University of China are grateful for their consistent support by sharing with me the latest development in marine science in China, and helped me to build up my career plan upon my graduation. Most of my friends in Hamburg are majoring in physical oceanography. Their academic background greatly helped me in understanding the hydrodynamic processes in upwelling system.

DAAD is so grateful for its financial support during the past three years and eight

months. It is this organization that gives me this valuable chance to let me study and experience my life in Germany.

Last but not the least, my supervisors, Prof. Kay Christian-Emeis and Dr. Richard Seifert, are the person I own so much. Prof. Emeis offered me the opportunity in May 2010 to change my life. I remembered clearly that night when he agreed on my application. Dr. Richard Seifert was such a kind person who owns very sharp vision on scientific problems and social issues. Quite often, his remarks and suggestions help me to make the decisions.

Without these people, I can barely reach the final step of my thesis. I will remember their kindness and virtues deeply in the bottom of my heart.

Hamburg, Nov. 2014 _____

Eidesstattliche Erklärung 1

Hiermit versichere ich, XIN Yu, geboren am 06. November 1979 in Shan Dong/China, an Eides statt, dass ich die vorgelegte Dissertation mit dem Titel:

Nitrogen cycling in the northern Benguela Upwelling System based on the $\delta^{15}N$ of chlorophyll pigment

Abgesehen durch die Beratung meiner Betreuer selbständig ausgearbeitet und verfasst habe und keine anderen Quellen und Hilfsmittlel als die angegebenen verwendet habe bzw. Die benutzten Quellen als soche kenntlich gemacht habe. Ich habe die vorliegende Arbeit weder gänzlich noch in Teilen einem anderen Fachbereich im In- oder Ausland im Rahmen eines Prüfungsverfahrens vorgelegt.

Hamburg den

————————————————

XIN Yu

Eidesstattliche Erklärung 2

Hiermit versichere ich, XIN Yu, geboren am 06. November 1979 in Shan Dong, China, an Eides statt, dass ich die am 28.01.2015 gehaltene Disputation mit dem Titel:

N-cycling in the northern Benguela Upwelling System (BUS) based on the $\delta^{15}N$ of chlorophyll pigment

erstmalig gehalten habe. Dies war, sowohl im Inland als auch im Ausland, meine erste mündliche Verteidigung mit der Absicht einen Doktortitel zu erlangen.

Hamburg, den   _____

                                    XIN Yu

149